Article:
El-Deen, N.A., DeFilippis, R., Abdel-Aziz, A.K. et al. (15 more authors) (2025) Structural Optimization and MD Simulation Study of Benzimidazole Derivatives as Potent Mutant FLT3 Kinase Inhibitors Targeting AML. Archiv der Pharmazie, 358 (5). e70002. ISSN 0365-6233

https://doi.org/10.1002/ardp.70002

WILEY-VCH

Archiv der Pharmazie

Structural Optimization and MD Simulation Study of Benzimidazole Derivatives as Potent Mutant FLT3 Kinase Inhibitors Targeting AML

Nada Alaa El-Deen[1,†], RosaAnna DeFilippis[2,†], Amal Kamal Abdel-Aziz[3,4], Sandra N. Milik[1,5], Suhana Patel[2], Muhammad I. Ismail[6], Omar Khaled[1], Tarek Erfan Ahmed[1,7], Ayatullah Gamal Abdelfattah[1,7], Eslam M.H. Ali[8], Maiy Y. Gaballah[1], Martin J. McPhillie[5], Khaled A.M. Abouzid[1], Rabah A. T. Serya[1], Maged Henary[9], Saverio Minucci[4,10], Neil P. Shah[2,*], Eman M.E. Dokla[1,*]

1 Pharmaceutical Chemistry Department, Faculty of Pharmacy, Ain Shams University, Abbassia, Cairo 11566, Egypt
2 Division of Hematology/Oncology, University of California, San Francisco, California, 94143, United States
3 Department of Pharmacology and Toxicology, Faculty of Pharmacy, Ain Shams University, Abbassia, Cairo, 11566, Egypt
4 Department of Experimental Oncology, IEO, European Institute of Oncology IRCCS, Via Adamello 16, 20139, Milan, Italy
5 School of Chemistry, University of Leeds, Leeds LS2 9JT, United Kingdom
6 Department of Pharmaceutical Chemistry, Faculty of Pharmacy, The British University in Egypt, Al-Sherouk City, Cairo-Suez Desert Road, 11837 Cairo, Egypt
7 Department of Chemistry, Georgia State University, 100 Piedmont Avenue SE, Atlanta, GA 30303, USA
8 Drug Discovery Core, Comprehensive Cancer Center, University of Virginia, Charlottesville, VA 22904, USA
9 Department of Chemistry, and Center of Diagnostics and Therapeutics, Georgia State University, 100 Piedmont Avenue SE, Atlanta, GA 30303, USA
10 Department of Biosciences, University of Milan, Milan, 20100, Italy

*Correspondence:

Eman M.E. Dokla, Pharmaceutical Chemistry Department, Faculty of Pharmacy, Ain Shams University, Abbassia, Cairo 11566, Egypt, Email: emanelawady@pharma.asu.edu.eg
Neil P. Shah, Division of Hematology/Oncology, University of California, San Francisco, California, 94143, United States, Email: Neil.Shah@ucsf.edu

†These authors have equal contributions.

Abstract

Acute myeloid leukemia (AML) is an aggressive hematological malignancy with poor survival rates in adults, posing a significant economic burden. FMS-like tyrosine kinase 3 (FLT3) mutations are linked to poor prognosis in AML and resistance to clinically approved FLT3 inhibitors. Previously, we reported a novel benzimidazole-based FLT3 inhibitor, **4ACP**, with nanomolar activities against FLT3-ITD and FLT3-TKD mutants, showing selective cytotoxicity against FLT3-ITD$^+$ AML cell lines. In this study, we synthesized 31 derivatives by modifying the 4-acetamidophenyl group and varying substituents at *N*1-phenyl and C2 positions. We identified compound **21l** (3-acetamidophenyl) as the most potent derivative (FLT3-TKD(D835Y) IC_{50} = 1.47 nM). Linking **21l** to a solvent-accessible group yielded compound **22b**, which exhibited a sub-nanomolar activity against FLT-TKD(D835Y) mutant with an IC_{50} value of 0.48 nM. Compound **22b** showed preferential antiproliferative activities against MOLM-14, MV4-11, MOLM-14-D835Y, and MOLM-14-F691L AML cell lines with IC_{50} values of 16.1 nM, 10.5 nM, 26.5 nM, and 160.3 nM, respectively. **22b** induced dose-dependent inhibition of FLT3, ERK, STAT5, and S6 phosphorylation, G0/G1 cell cycle arrest, and apoptotic cell death at low nanomolar concentrations in MOLM-14 and MOLM-14-D835Y cells. It was more selective for FLT3-dependant cell lines, showing about 80-fold selectivity towards FLT3-TKD(D835Y) over KIT, indicating relative safety and lower myelosuppression potential. The molecular dynamics study of **4ACP** and **22b** was conducted to explain the significant changes in activity resulting from subtle structural alterations. Altogether, these findings establish **22b** as a potent mutant FLT3 inhibitor, warranting further investigation and optimization to target resistant AML.

KEYWORDS

Mutant FLT3; kinase inhibitor; acute myeloid leukemia; benzimidazole; molecular dynamics

1 INTRODUCTION

Acute myeloid leukemia (AML) is a hematological malignancy characterized by abnormal proliferation and differentiation of hematopoietic cells, resulting in anemia, recurrent infections, and excessive bleeding.[1] The global incidence of AML was around 145,000 cases in 2021 with approximately 130,000 deaths.[2] Although AML is a rare malignancy, accounting for only 1% of new cases of cancer in the USA in 2024 according to SEER database, it is an aggressive cancer with a poor 5-year survival rate of 31.9% between 2014 and 2020.[3]

AML is the most frequent type of acute leukemia in adults and accounts for about 20% of cases in children.[1,4] While prognosis and survival rates are favorable in children (69%),[4] adults with AML have a poor prognosis, low five-year overall survival, and high mortality rates.[5] From an economic perspective, AML treatments are very expensive. On average, intensive induction chemotherapy costs around $198,657, consolidation chemotherapy costs around $73,428, and treatment for relapsed or refractory AML costs around $439,104.[6] Considering the aggressive nature of AML, its poor prognosis, and the significant economic burden, there is a pressing need to develop novel and cost-effective therapies to combat AML.

AML is a heterogenous disease with multiple underlying abnormalities. The most common are FMS-like tyrosine kinase 3 (FLT3) gene mutations, found in about 30% of patients and associated with poor prognosis.[7,8] The most common FLT3 mutations are internal tandem duplication (FLT3-ITD) and tyrosine-kinase domain (FLT3-TKD) mutations occurring in about 20% and 10% of AML, respectively,[9] and resulting in ligand-independent constitutive activation of FLT3 enzyme and subsequent uncontrolled cellular proliferation.[10]

Accordingly, intensive efforts have been directed towards developing selective FLT3 inhibitors to target AML.[11–16] As a result, midostaurin, gilteritinib, and recently quizartinib were approved by the FDA for AML, and another agent, crenolanib, is in late-stage clinical development (**Figure 1**).[17,18] Midostaurin, gilteritinib, and crenolanib are type I kinase inhibitors that interact with the ATP-binding site of the FLT3 enzyme in its active (DFG-in) conformation. These inhibitors do not extend into the allosteric pocket, thereby maintaining efficacy despite the presence of activation loop mutations (FLT3-TKD mutations). On the other hand, quizartinib, being a type II kinase inhibitor, extends into the allosteric back pocket of the ATP binding site, forcing the DFG motif to flip and locking the enzyme into an inactive (DFG-out) conformation. Consequently, quizartinib is susceptible to inactivation due to FLT3-TKD mutations.[14,18,19]

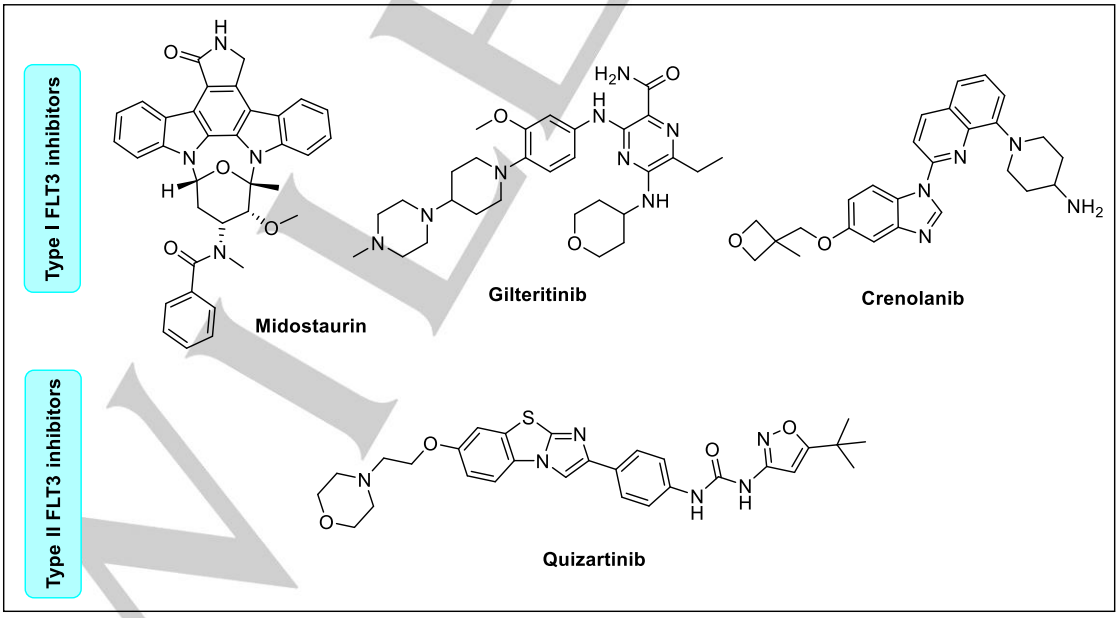

Figure 1. FDA-approved or in late-stage clinical development FLT3 inhibitors.

The emergence of resistance to clinical FLT3 inhibitors frequently occurs due to either mutations in the FLT3 enzyme or the activation of alternative pathways. Consequently, there is a significant demand for the development of novel FLT3 inhibitors.[20,21]

Guided by ligand-based design, our research group developed a benzimidazole-based FLT3 inhibitor (**4ACP**) through scaffold hopping and structure simplification of quizartinib[22] (**Figure 2**). Compared to quizartinib, **4ACP** demonstrated nanomolar inhibitory activity against both FLT3-ITD and FLT3-TKD(D835Y) mutations, whereas quizartinib lacked efficacy against FLT3-TKD mutations.[22] **4ACP** exhibited selective in vitro cytotoxic activity against FLT3-ITD$^+$ AML cell lines, while showing no activity against FLT3-ITD$^-$ AML cell lines, normal hepatocytes, and H9C2-cardiomyocytes cells, indicating a relatively safer profile. Additionally, screening **4ACP** against 17 related kinases, revealed selective enzymatic inhibition of FLT3 and low potential of synthetic lethal toxicity by exhibiting a much weaker activity against KIT enzyme.[23] **4ACP** served as a proof-of-concept compound, representing a promising candidate for further development as a FLT3 inhibitor for targeted AML therapy. In the current study, we utilized **4ACP** for further optimization and structure-activity relationship (SAR) investigation.

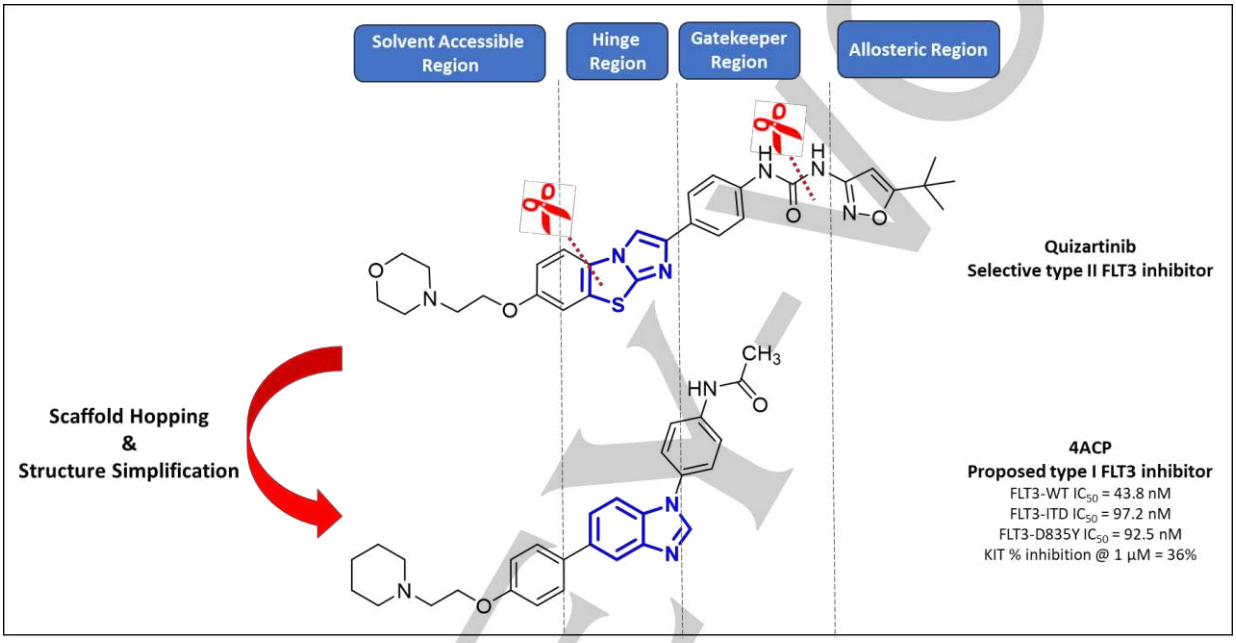

Figure 2. Design strategy for our previously reported benzimidazole-based kinase inhibitor, **4ACP**.[22]

2 RESULTS AND DISCUSSION

2.1. Design Strategy

Previously, our research group developed a novel benzimidazole-based FLT3 inhibitor (**4ACP**) to address two major limitations of quizartinib: its lack of activity against FLT3-TKD mutations and the synthetic lethal hematologic toxicity induced by potent KIT co-inhibition.[23–26] **4ACP** demonstrated potent activity against FLT3-ITD and TKD mutations while exhibiting weak activity against KIT enzyme. Based on molecular docking studies of **4ACP** and guided by its binding mode, we proposed that **4ACP** is a type I kinase inhibitor, where the benzimidazole acts as the hinge binder, the 4-acetamidophenyl group interacts with the gatekeeper region, and the 4-(2-(piperidin-1-yl)ethoxy) group extends into the solvent accessible region (**Figure 2**).[22] In the current study, we focus on exploring **4ACP**'s chemical structure and conducting SAR investigations by employing three modification approaches to improve existing interactions or explore new ones (**Figure 3**):

1. Structural morphing of the 4-acetamidophenyl group from the *N*1 into the C2 position of benzimidazole (**Scheme 1**).
2. Varying the substituents at both the *N*1-phenyl and C2 positions (**Scheme 3**-**5**).
3. Varying the 5-(4-hydroxyphenyl) position (**Scheme 3**).

Additionally, to simplify the proposed structures and minimize the synthetic efforts, we opted to remove the solvent-accessible group (i.e 4-(2-(piperidin-1-yl)ethoxy)) through primary screening, as it does not significantly affect enzymatic activity (unless designed for a specific interaction) but rather impacts cellular potency and pharmacokinetics.[27–30] To validate our approach, we synthesized and

evaluated the FLT3 inhibitory activity and cellular potency of the truncated derivative of **4ACP**; *N*-(4-(5-(4-hydroxyphenyl)-1*H*-benzimidazol-1-yl)phenyl)acetamide (**21o**, **4ACOH**). As predicted, **4ACOH** showed less than a one-fold decrease in FLT3 inhibitory activity compared to **4ACP** (42% versus 68% inhibition at 100 nM, respectively), while it exhibited a drastic decrease in antiproliferative activity against two FLT3-ITD$^+$ cell lines compared to **4ACP** (IC_{50} = 1428.0 nM and 832.0 nM versus **4ACP** IC_{50} = 46.3 nM and 65.0 nM against MOLM-14 and MV4-11, respectively) (**Figure 3** and **Table 1**). Accordingly, thirty-one derivatives were synthesized without the solvent-accessible group and evaluated for their in vitro enzymatic and cellular inhibitory activities. Next, the optimized derivative was linked to the solvent-accessible group while varying its position. Finally, the most potent derivative was further evaluated to establish its activity profile.

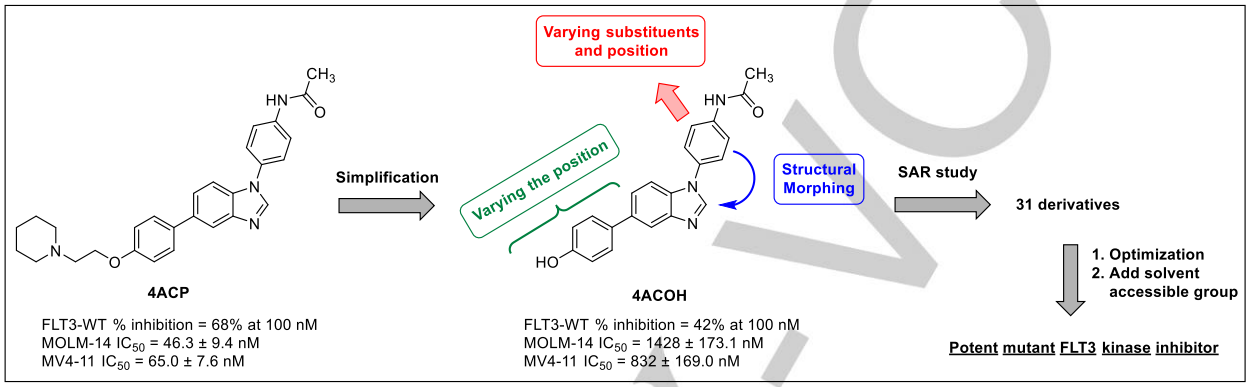

Figure 3. Workflow for SAR investigation and optimization of the benzimidazole-based kinase inhibitor, **4ACP**.

2.2. Chemistry

The designed benzimidazole derivatives were synthesized as outlined in **schemes 1**-**5** and as discussed here. In **scheme 1**, the nucleophilic aromatic substitution of 5-bromo-2-fluoro-1-nitrobenzene (**3**) with the appropriate amine derivatives (**4a**,**b**) in DMF using K_2CO_3 yielded the desired intermediates (**5a**-**b**) in excellent yields. Reduction of the nitro derivatives (**5a**-**b**) using $SnCl_2.2H_2O$ in EtOAc, followed by reacting the resulting diamines with the appropriate methanesulfonate adducts (**2a**-**b**) (obtained by the reaction of the corresponding aldehydes (**1a**-**b**) with sodium metabisulfite) in DMF furnished the desired benzimidazole intermediates (**6a**-**d**) in excellent yields. Further reduction of the intermediates (**6a**-**d**) using $SnCl_2.2H_2O$ in EtOAc and subsequent acylation using acetic anhydride in DCM yielded the acetamido intermediates (**7a**-**d**) in fair to good yields. Suzuki coupling of the bromo derivatives (**7a**-**d**) with 4-hydroxyphenylboronic acid using tetrakis(triphenylphosphine) palladium(0) and K_2CO_3 in dioxane and water yielded the desired final compounds (**8a**-**d**) in fair to good yields.

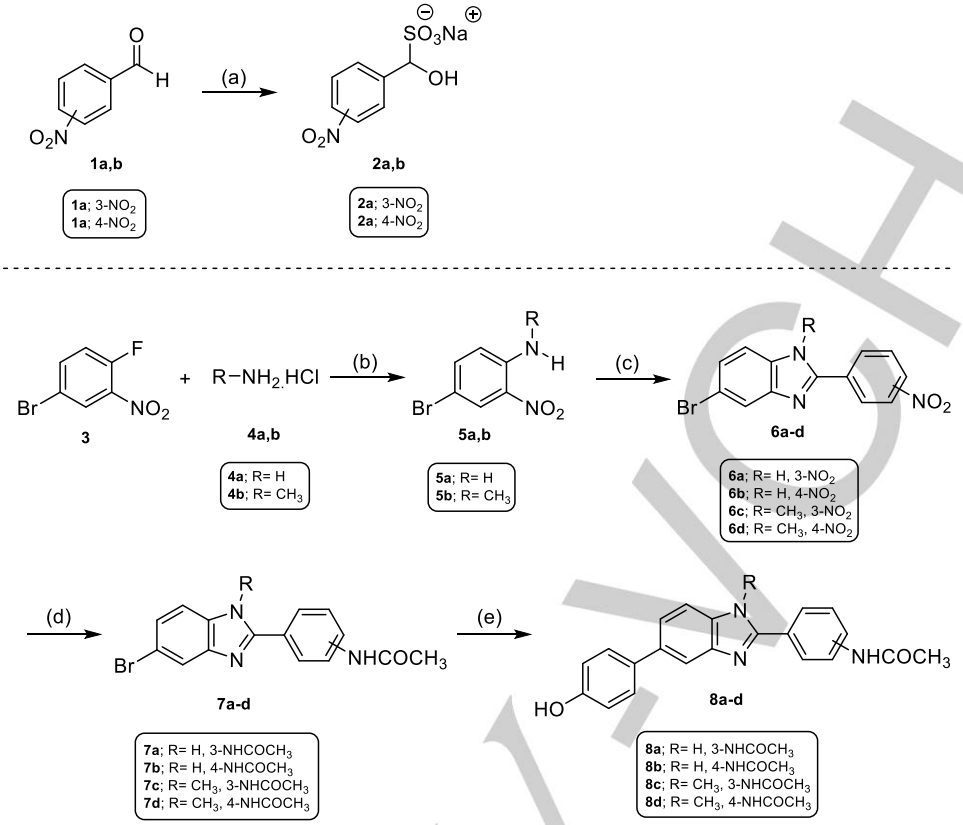

Scheme 1. Reagents and conditions: (a) $Na_2S_2O_5$, H_2O, EtOH, 0°C, 2 h, 95-98%; **(b)** K_2CO_3, DMF, 80-90°C, 16 h, 96-97%; **(c) 1.** $SnCl_2.2H_2O$, EtOAc, reflux, 12 h; **2.** sodium hydroxy (3- or 4-nitrophenyl)methanesulfonate (**2a** or **2b**), DMF, 130°C, 4 h, 89-95%, **(d) 1.** $SnCl_2.2H_2O$, EtOAc, reflux, 12 h, **2.** acetic anhydride, DCM, rt, 12 h, 61-74%; **(e)** 4-hydroxyphenylboronic acid, tetrakis(triphenylphosphine) palladium(0), K_2CO_3, dioxane/H_2O, reflux, 4 h, 49-67%.

To synthesize the final derivatives **21a**-**r** and **22a**-**e** (**scheme 3**), 5- or 4-bromo-2-fluoro-1-nitrobenzene derivatives (**3** or **17**) were substituted with the appropriate anilines (**11a**,**b**, **13**, **16a**,**b**, synthesized according to **scheme 2** or **18a**-**h**, that are commercially available) according to two methods (**scheme 3**). In **step a**, nucleophilic aromatic substitution was achieved in DMF using K_2CO_3 to give the desired intermediates (**19a**-**k**) in poor to very good yields, while in **step b**, substitution was achieved in DMF using NaH as a strong base (since the *p*-nitroaniline derivatives have an acidic amine that can be activated using NaH) to give the desired intermediates (**19l**-**n**) in fair to excellent yields. Reduction of the nitro derivatives (**19a,d**-**k**) using $SnCl_2.2H_2O$ in EtOAc yielded the corresponding diamine intermediates that were subsequently cyclized using formic acid to give the desired benzimidazole derivatives (**20a**,**d**-**k**) in fair to excellent yields. On the other hand, reduction of the nitro derivatives (**19b**,**c**,**l-n**) and subsequent cyclization by refluxing in formic acid yielded the desired benzimidazoles but as *N*-formyl derivatives, so further hydrolysis by reflux in conc. HCl to yield the corresponding amine derivatives followed by acylation using acetic anhydride in acetic acid and reflux yielded the desired benzimidazole derivatives (**20b,c**,**l**-**n**) in poor to good yields. Suzuki coupling of the bromo derivatives (**20a**-**n**) as in **scheme 1** yielded the desired compounds (**21a**-**d**,**f**,**h**-**r**) in poor to very good yields. Phenol derivatives (**21e**,**g**) were obtained in fair to good yields by hydrogenation of the corresponding benzyloxy intermediates (**21d**,**f**) using Pd/C (10%) in MeOH. Alkylation of the selected hydroxy derivatives (**21k**-**o**) with 1-(2-chloroethyl)piperidine hydrochloride in DMF using Cs_2CO_3 and KI gave the desired final compounds (**22a**-**e**) in poor to fair yields.

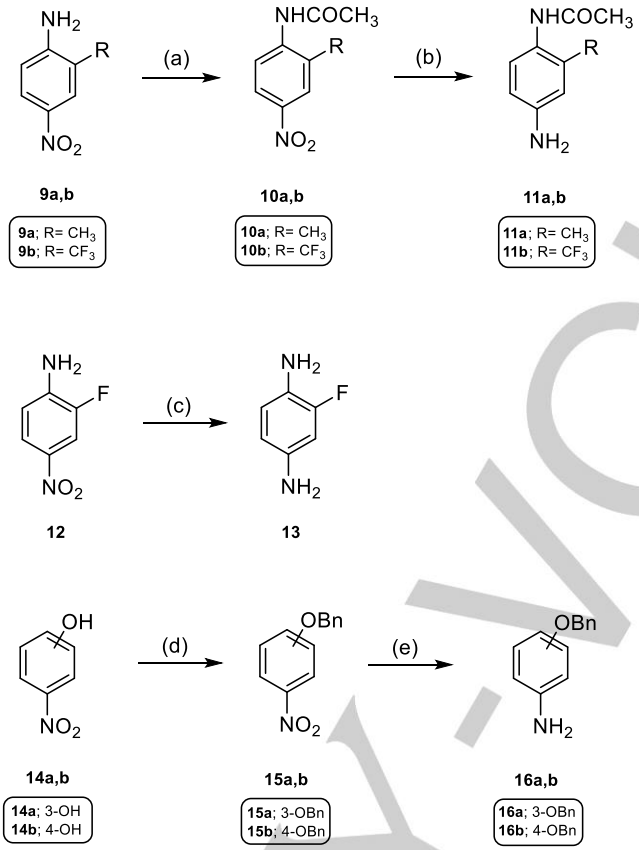

Scheme 2. Synthesis of intermediates (11a,b, 13, 16a,b). Reagents and conditions: (a) acetic anhydride, acetic acid, 80°C, 2 h, 88-95%; **(b)** $SnCl_2.2H_2O$, EtOAc, reflux, 6 h, 17-85%; **(c)** $SnCl_2.2H_2O$, EtOAc, reflux, 12 h, 74%; **(d)** benzyl bromide, K_2CO_3, DMF, rt, 12h, 95-97%; **(e)** $SnCl_2.2H_2O$, EtOAc, reflux, 6 h, 64-96%.

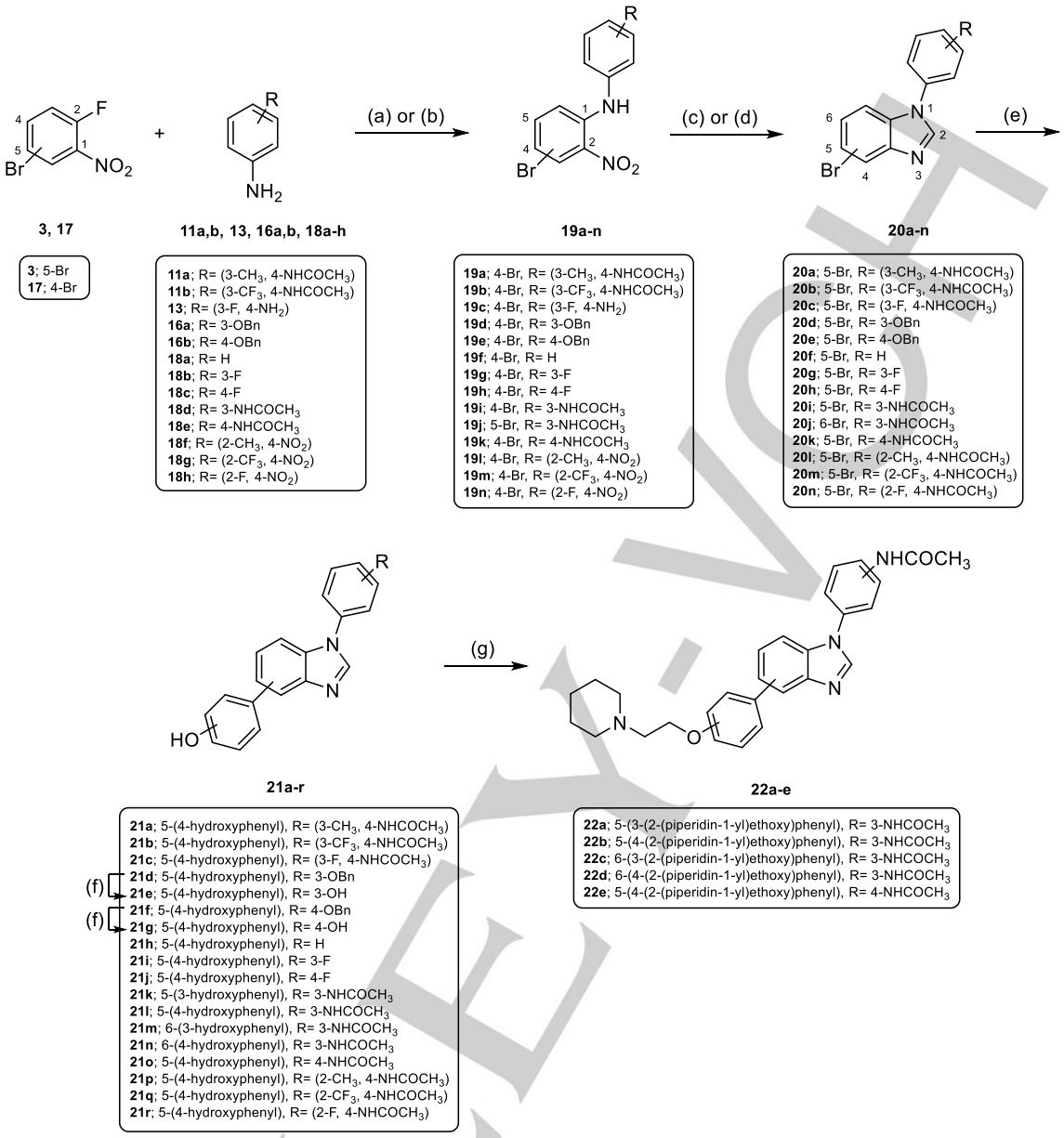

Scheme 3. Reagents and conditions: (a) 11a,b, **13**, **16a,b**, **18a-e**, K_2CO_3, DMF, 80°C, 16 h, 30-83%; **(b) 18f-h**, NaH (60% in mineral oil), DMF, 0°C, 2 h, 67-99%; **(c) 19a**,**d-k**, **1.** $SnCl_2.2H_2O$, EtOAc, reflux, 12 h, **2.** formic acid, 120°C, 1 h, 53-96%; **(d) 19b**,**c**,**l-n**, **1.** $SnCl_2.2H_2O$, EtOAc, reflux, 12 h, **2.** formic acid, 120°C, 1 h, **3.** conc. HCl, reflux, 1 h, **4.** acetic anhydride, acetic acid, 80°C, 2 h, 39-70%; **(e)** 3- or 4-hydroxyphenylboronic acid, tetrakis(triphenylphosphine)palladium(0), K_2CO_3, dioxane/H_2O, reflux, 4 h, 24-84%; **(f) 21d**,**f**, H_2, Pd/C (10%), MeOH, rt, 12h, 54-77% **(g) 21k-o**, 1-(2-chloroethyl)piperidine hydrochloride, Cs_2CO_3, KI, DMF, 80-90°C, 48 h, 26-68%.

In **scheme 4**, the desired final compound (**25**) was synthesized from the corresponding 2-nitroaniline intermediate (**19k**) by reduction using $SnCl_2.2H_2O$ in EtOAc followed by reflux with glycolic acid in 4N HCl to yield the (benzimidazol-2-yl)methanol intermediate (**23**) in poor yield. Acylation of this derivative yielded the corresponding acetamide derivative (**24**) in good yield, followed by Suzuki coupling, as in **scheme 1**, to yield the desired final compound (**25**) in poor yield.

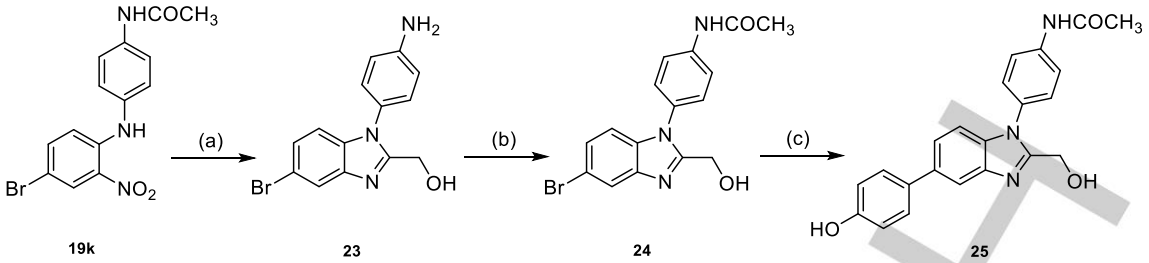

19k 23 24 25

Scheme 4. Reagents and conditions: (a) 1. $SnCl_2.2H_2O$, EtOAc, reflux, 12 h; **2.** glycolic acid (70% in water), 4N HCl, reflux, 12 h, 20%; **(b)** acetic anhydride, THF, rt, 12 h, 72%; **(c)** 4-hydroxyphenylboronic acid, tetrakis(triphenylphosphine)palladium(0), K_2CO_3, dioxane/H_2O, reflux, 4 h, 38%.

In **scheme 5**, derivatives **28a**-**n** were synthesized from the appropriate acetamide derivatives (**20i**,**k**) starting by hydrolysis using conc. HCl and reflux to yield the corresponding amine intermediates (**26a**,**b**). Carbamate and amide derivatives (**27a**-**d**) were obtained in fair to excellent yields by reacting the amine intermediates (**26a**,**b**) with ethyl chloroformate or cyclopropanecarbonyl chloride, respectively, in pyridine. Urea derivatives (**27e**-**h**) were synthesized in two steps by reacting the amine intermediates (**26a**,**b**) with triphosgene in THF to yield the isocyanate intermediates which were reacted with the appropriate amines in THF and DIPEA as a base to yield the desired derivatives (**27e**-**h**) in poor to good yields. The sulfonamide derivatives (**27i**-**l**) were synthesized by reacting the amine intermediates (**26a**,**b**) with the appropriate sulfonyl chloride derivatives in pyridine to furnish the desired sulfonamide derivatives (**27e**-**h**) in fair to excellent yields. The *N*-formyl derivatives (**27m**,**n**) were obtained in poor yields by heating the amine intermediates (**26a**,**b**) in formic acid. Finally, Suzuki coupling of these derivatives (**27a**-**n**), as in **scheme 1**, yielded the desired final compounds (**28a**-**n**) in poor to good yields.

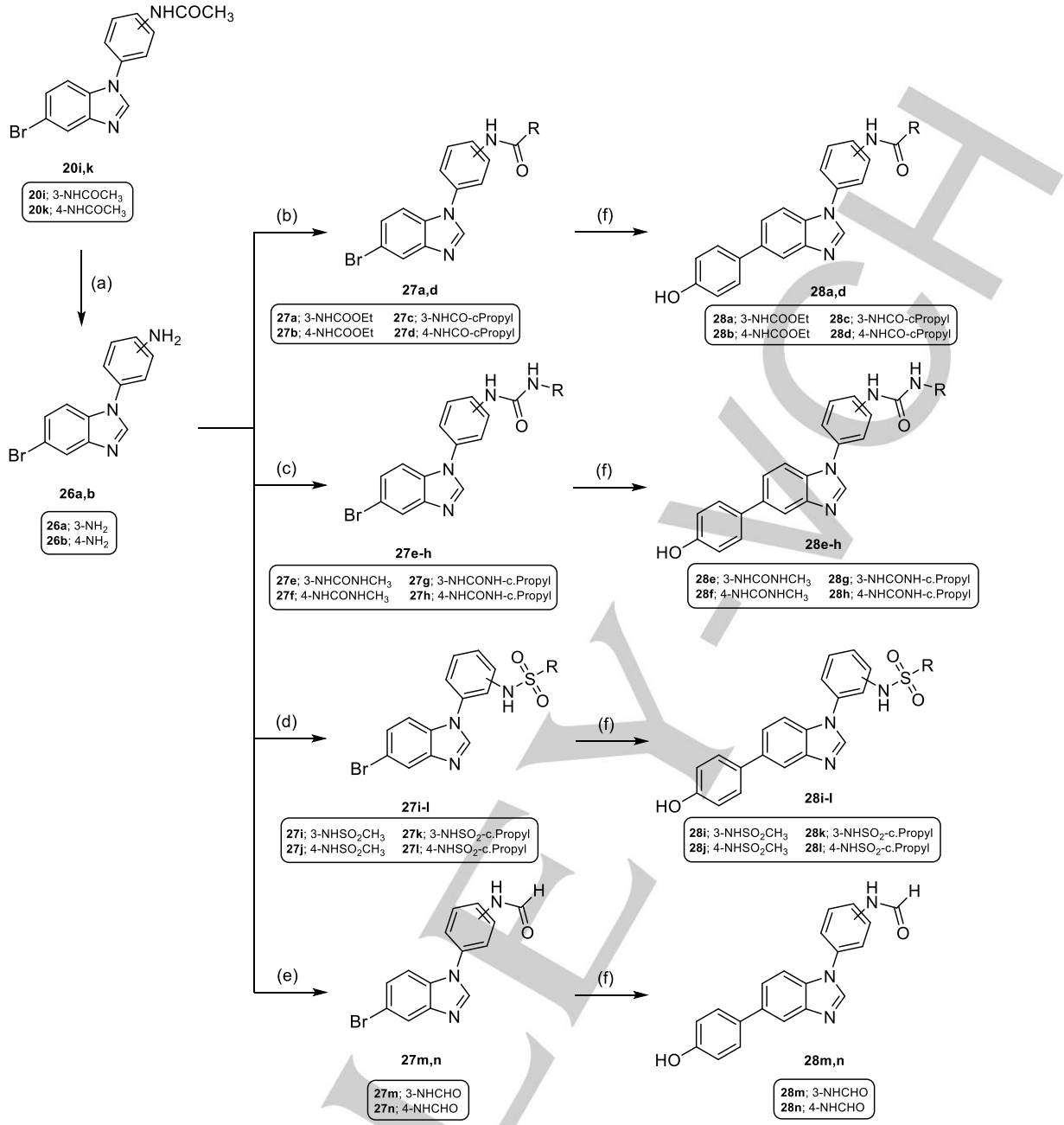

Scheme 5. Reagents and conditions: (a) conc. HCl, reflux, 1 h, 82-93%; **(b)** ethyl chloroformate or cyclopropanecarbonyl chloride, pyridine, 0°C, 4h, 53-90%; **(c) 1.** triphosgene, dry THF, reflux, 2 h, **2.** methylamine HCl or cyclopropylamine, DIPEA, THF, reflux, 24 h, 30-78%; **(d)** methanesulfonyl chloride or cyclopropanesulfonyl chloride, pyridine, 0°C, 48h, 54-95%; **(e)** formic acid, 120°C, 1 h, 21-38%; **(f)** 4-hydroxyphenylboronic acid, tetrakis(triphenylphosphine)palladium(0), K_2CO_3, dioxane/H_2O, reflux, 4 h, 19-77%

2.3. Biological activities

2.3.1. In vitro kinase assays of benzimidazole derivatives

The prognostic relevance of FLT3-TKD mutations is controversial. However, their impact on FLT3 constitutive activation and inherent resistance to type II FLT3 inhibitors, whether in the presence or absence of the FLT3-ITD mutation, warrants further research to develop potent kinase inhibitors capable of targeting these mutations.[10,31–33] To guide our optimization efforts, the designed benzimidazole derivatives were initially screened against the FLT3-WT enzyme at a 100 nM concentration using an in vitro kinase assay. Compounds showing >80% inhibition were then evaluated against FLT3-TKD(D835Y) mutant enzyme at the same concentration. Optimized derivatives showing >80% inhibition against FLT3-TKD(D835Y) mutant were further evaluated at a 20 nM concentration, and those exhibiting >50% inhibition were assessed for their IC_{50} values (**Tables 1**-**2**). Out of the 31 truncated derivatives synthesized initially, ten derivatives (**21e**, **21g**, **21l**, **28c**, **28e**-**g**, **28i**, **28k**, and **28m**) showed >80% inhibition against the FLT3-WT enzyme at a 100 nM concentration. These derivatives were further evaluated against FLT3-TKD(D835Y) mutant at the same concentration and six derivatives (**21g**, **21l**, **28e**, **28g**, **28i**, and **28m**) showed >80% inhibition. When these six derivatives were evaluated against the FLT3-TKD(D835Y) mutant at a 20 nM concentration, only four derivatives (**21l**, **28e**, **28g**, and **28m**) showed >50% inhibition and their IC_{50} were assessed. Compound **21l** (3-$NHCOCH_3$) showed the most potent inhibition with an IC_{50} value of 1.47 nM against FLT3-TKD(D835Y) mutant, while the other derivatives showed close but less potent activity (**28e**, **28g**, and **28m** IC_{50} = 12.59 nM, 13.18 nM, and 8.07 nM, respectively). Based on this data, we decided to affix the 3-$NHCOCH_3$ fragment and move into the next cycle of optimization. Next, four derivatives (**22a**-**d**) were synthesized by linking the solvent-accessible group, (2-(piperidin-1-yl)ethoxy), to **21l** while varying the position of both the phenyl and ethoxy groups. Out of these, **22b** showed the most potent activity with 99% and 82% inhibition when screened at 10 nM and 1 nM concentrations, respectively, against the FLT3-TKD(D835Y) mutant. In comparison to the two reference drugs used, gilteritinib and quizartinib, **22b** showed a more potent inhibition profile with an IC_{50} value of 0.48 nM, compared to gilteritinib's IC_{50} value of 0.72 nM, against FLT-TKD(D835Y) and IC_{50} values of 1.68 nM and 3.32 nM, compared to quizartinib's IC_{50} values of 5.72 nM and 33.93 nM, against FLT3-WT and FLT3-ITD enzymes, respectively (**Table 3**).

One of the main off-target effects of quizartinib is the inhibition of KIT kinase along with FLT3 inhibition, which results in synthetic lethal toxicity, causing severe myelosuppression due to the disruption of normal hematopoiesis.[23,34] Accordingly, compound **22b** was evaluated against KIT kinase to assess its potential for myelosuppression. Indeed, compound **22b** exhibited around 80-fold more selectivity towards the FLT3-TKD(D835Y) mutant enzyme versus KIT enzyme (KIT IC_{50} = 39.41 ± 6.84 nM), indicating its relative safety and lower potential to induce myelosuppression.

Table 1. In vitro FLT3-WT kinase inhibition and antiproliferative activities of the benzimidazole derivatives (**8a**-**d**).

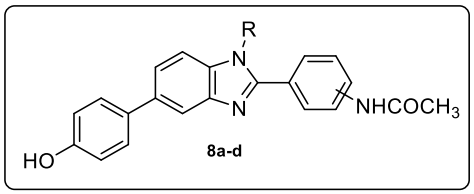

8a-d

Compound	R	-NHCOCH$_3$	FLT3-WT inhibition[a]	Cell lines	
				IC$_{50}$ (nM)[b]	
			at 100 nM	MOLM-14[c]	MV4-11[d]
8a	H	3-	15%	NT	NT
8b	H	4-	6%	NT	NT
8c	CH$_3$	3-	11%	NT	NT
8d	CH$_3$	4-	12%	NT	NT
4ACOH (21o)			42%	1428.0 ± 173.1	832.0 ± 169.0
4ACP (22e)			68%	46.3 ± 9.4	65.0 ± 7.6
Quizartinib			99%	1.1 ± 0.4	0.55 ± 0.3

[a]The kinase inhibition assays were provided by ThermoFisher Scientific. All data were obtained by double testing (average).
[b]Median inhibitory concentration (IC$_{50}$) values are expressed as mean ± SD and were based on the data obtained from triplicates of at least three independent experiments after treatment for 48 h.
[c]AML-FLT3-ITD$^+$ (heterozygous).
[d]AML-FLT3-ITD$^+$ (homozygous).

Table 2. In vitro FLT3-WT and FLT3-TKD(D835Y) kinase inhibition and antiproliferative activities of the benzimidazole derivatives (**21a**-**c**, **e**, **g**, **h**-**j**, **l**, **o**-**r**, **25**, and **28a**-**n**).

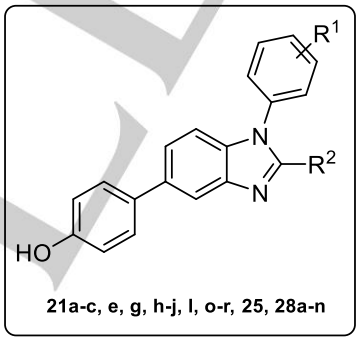

21a-c, e, g, h-j, l, o-r, 25, 28a-n

Compound	R^1	R^2	FLT3-WT inhibition	FLT3-TKD(D835Y) inhibition			Cell lines	
							IC$_{50}$ (nM)	
			at 100 nM	at 100 nM	at 20 nM	IC$_{50}$ (nM)	MOLM-14	MV4-11
21a	3-CH$_3$, 4-NHCOCH$_3$	H	31%	--	--	--	1947.5 ± 1230.9	3308.17 ± 56.1
21b	3-CF$_3$, 4-NHCOCH$_3$	H	17%	--	--	--	NT	NT
21c	3-F, 4-NHCOCH$_3$	H	26%	--	--	--	1149.5 ± 415.0	942.8 ± 86.2

21e	3-OH	H	88%	68%	--	--	236.6 ± 26.6	172.6 ± 51.3
21g	4-OH	H	89%	87%	48%	--	981.8 ± 273.3	255.3 ± 9.6
21h	H	H	71%	--	--	--	NT	NT
21i	3-F	H	29%	--	--	--	NT	NT
21j	4-F	H	44%	--	--	--	NT	NT
21l	3-$NHCOCH_3$	H	89%	97%	87%	1.47 ± 0.91	245.2 ± 33.9	227.7 ± 51.8
21p	2-CH_3, 4-$NHCOCH_3$	H	13%	--	--	--	>10,000	>10,000
21q	2-CF_3, 4-$NHCOCH_3$	H	11%	--	--	--	>10,000	>10,000
21r	2-F, 4-$NHCOCH_3$	H	19%	--	--	--	>10,000	>10,000
25	4-$NHCOCH_3$	CH_2OH	11%	--	--	--	>10,000	>10,000
28a	3-NHCOOEt	H	55%	--	--	--	NT	NT
28b	4-NHCOOEt	H	21%	--	--	--	NT	NT
28c	3-NHCO-cPropyl	H	85%	72%	--	--	471.5 ± 88.2	529.1 ± 95.7
28d	4-NHCO-cPropyl	H	11%	--	--	--	NT	NT
28e	3-$NHCONHCH_3$	H	97%	98%	79%	12.59 ± 2.16	323.3 ± 41.2	285.2 ± 55.9
28f	4-$NHCONHCH_3$	H	84%	26%	--	--	118.6 ± 21.0	66.5 ± 10.8
28g	3-NHCONH-cPropyl	H	96%	97%	64%	13.18 ± 3.59	238.3 ± 30.0	258.3 ± 55.9
28h	4-NHCONH-cPropyl	H	66%	--	--	--	NT	NT
28i	3-$NHSO_2CH_3$	H	94%	85%	42%	--	473.7 ± 57.5	407.3 ± 30.7
28j	4-$NHSO_2CH_3$	H	34%	--	--	--	NT	NT
28k	3-$NHSO_2$-cPropyl	H	96%	71%	--	--	1410.6 ± 250.5	425.3 ± 52.8
28l	4-$NHSO_2$-cPropyl	H	19%	--	--	--	NT	NT
28m	3-NHCHO	H	97%	96%	86%	8.07 ± 1.38	151.2 ± 9.8	134.5 ± 10.2
28n	4-NHCHO	H	71%	--	--	--	840.6 ± 81.4	386.9 ± 89.6
4ACOH (21o)	4-$NHCOCH_3$	H	42%	11%	--	--	1428.0 ± 173.1	832.0 ± 169.0
4ACP (22e)			68%	--	--	92.5[22]	46.3 ± 9.4	65.0 ± 7.6
Quizartinib			99%	--	--	--	1.1 ± 0.4	0.55 ± 0.3
Gilteritinib			--	--	--	0.72 ± 0.0004	7.2 ± 1.6	1.8 ± 0.5

Table 3. In vitro FLT3-TKD(D835Y), FLT3-WT, and FLT3-ITD kinase inhibition and antiproliferative activities of the benzimidazole derivatives (**22a**-**e**).

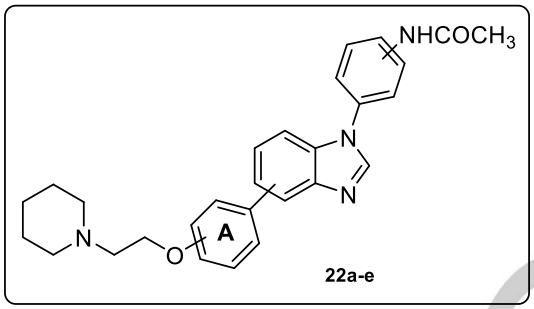

Compound	-NHCOCH$_3$	Phenyl (A)	2-(piperidin-1-yl)ethoxy	FLT3-TKD(D835Y) inhibition			FLT3-WT inhibition	FLT3-ITD inhibition	Cell lines	
									IC$_{50}$ (nM)	
				at 10 nM	at 1 nM	IC$_{50}$ (nM)	IC$_{50}$ (nM)	IC$_{50}$ (nM)	MOLM-14	MV4-11
22a	**3-**	**5-**	**3-**	91%	47%	--	--	--	98.5 ± 18.5	51.3 ± 24.8
22b	**3-**	**5-**	**4-**	99%	82%	0.48 ± 0.01	1.68 ± 0.14	3.32 ± 1.07	16.1 ± 4.3	10.5 ± 6.7
22c	**3-**	**6-**	**3-**	6%	9%	--	--	--	1484.0 ± 217.1	1188.8 ± 80.6
22d	**3-**	**6-**	**4-**	15%	6%	--	--	--	1601.3 ± 278.9	1101.3 ± 146.7
4ACP (22e)	**4-**	**5-**	**4-**	--	--	92.5[22]	43.8[22]	97.2[22]	46.3 ± 9.4	65.0 ± 7.6
Quizartinib				--	--	--	5.72 ± 1.62	33.93 ± 29.10	1.1 ± 0.4	0.55 ± 0.3
Gilteritinib				--	--	0.72 ± 0.0004	--	--	7.2 ± 1.6	1.8 ± 0.5

2.3.2. Structure Activity Relationship (SAR)

In the current study, we attempted three modification approaches (**Figure 3**) to explore and optimize **4ACP**, our previously reported FLT3 inhibitor. Starting with structural morphing of the 4-acetamidophenyl group from the *N*1 into the C2 position of benzimidazole, which might result in a modified binding mode with the gatekeeper region, four derivatives were synthesized (**8a**-**d**) and evaluated. Unfortunately, this modification resulted in a drastic decrease in activity compared to **4ACOH** (the truncated derivative of **4ACP**) when evaluated against the FLT3-WT enzyme (**Table 1**).

Next, we focused on the 4-acetamidophenyl moiety and tested the effect of adding a hydrophobic group to either the *ortho* or *meta* position, which might improve the interaction with the gatekeeper Phe691 amino acid. Accordingly, six derivatives were synthesized with a methyl, trifluoromethyl, or fluoro group at either 3- or 2-position of the 4-acetamidophenyl moiety (**21a**-**c** and **21p**-**r**, respectively). All derivatives showed lower activity compared to **4ACOH**, with the 2-substituents exhibiting a more detrimental effect on the activity than the 3-substituents (11-19% versus 17-31% inhibition against FLT3-WT at a 100 nM concentration, respectively). Removal of the 4-acetamido group (**21h**) showed slightly better activity when compared to **4ACOH** (71% versus 42% inhibition against FLT3-WT at 100 nM concentration, respectively). Next, we replaced the 4-actemaido group with a small fluoro group, where **21j** (4-F) showed similar activity while **21i** (3-F) exhibited lower activity compared to **4ACOH** (44% and 29% versus 42% inhibition against FLT3-WT at a 100 nM concentration, respectively). On the other hand, replacement of the 4-acetamido group with a small polar group such as hydroxy (**21e**: 3-OH, **21g**: 4-OH) resulted in derivatives with improved activity compared to **4ACOH** (88% and 89% versus 42% inhibition against FLT3-WT at a 100 nM concentration, respectively). So far, polar derivatives showed better activity than hydrophobic ones, so we investigated various polar functionalities at both the *para*- and *meta*-positions of the *N*-phenyl group. In general, polar substituents at the *meta*-position showed better activity than those at the *para*-position when screened against FLT3-WT at a 100 nM concentration (**21l**: *m*-NHCOCH$_3$ versus **21o**: *p*-NHCOCH$_3$, **28a**: *m*-NHCOOEt versus **28b**: *p*-NHCOOEt, **28c**: *m*-NHCO-cPropyl versus

28d: *p*-NHCO-cPropyl, **28e**: *m*-NHCONHCH$_3$ versus **28f**: *p*-NHCONHCH$_3$, **28g**: *m*-NHCONH-cPropyl versus **28h**: *p*-NHCONH-cPropyl, **28i**: *m*-NHSO$_2$CH$_3$ versus **28j**: *p*-NHSO$_2$CH$_3$, **28k**: *m*-NHSO$_2$-cPropyl versus **28l**: *p*-NHSO$_2$-cPropyl, and **28m**: *m*-NHCHO versus **28n**: *p*-NHCHO). Among these polar derivatives, *meta*-amide substituents (**21l**: *m*-NHCOCH$_3$ and **28m**: *m*-NHCHO) showed the most potent activity, followed by the *meta*-urea derivatives (**28e**: *m*-NHCONHCH$_3$ and **28g**: *m*-NHCONH-cPropyl), then the *meta*-sulfonamide derivatives (**28i**: *m*-NHSO$_2$CH$_3$ and **28k**: *m*-NHSO$_2$-cPropyl), and finally the *meta*-carbamate derivative (**28c**: *m*-NHCOOEt) when screened against FLT3-WT and FLT3-TKD(D835Y) mutant. It is noteworthy that bulky substituents such as the cyclopropyl group showed less activity than their methyl congeners in all the tested derivatives (**21l**: *m*-NHCOCH$_3$ versus **28a**: *m*-NHCO-cPropyl, **21o**: *p*-NHCOCH$_3$ versus **28b**: *p*-NHCO-cPropyl, **28e**: *m*-NHCONHCH$_3$ versus **28g**: *m*-NHCONH-cPropyl, **28f**: *p*-NHCONHCH$_3$ versus **28h**: *p*-NHCONH-cPropyl, **28i**: *m*-NHSO$_2$CH$_3$ versus **28k**: *m*-NHSO$_2$-cPropyl, **28j**: *p*-NHSO$_2$CH$_3$ versus **28l**: *p*-NHSO$_2$-cPropyl) when screened against FLT3-WT and FLT3-TKD(D835Y) mutant (**Table 2**). Finally, C-2 substitution with a hydroxymethyl group drastically lowered the activity compared to **4ACOH** (11% inhibition versus 42% inhibition against FLT3-WT at a 100 nM concentration, respectively).

Based on the previous data, out of thirty-one derivatives synthesized and evaluated, compound **21l** (*m*-NHCOCH$_3$) demonstrated the most potent activity against the FLT3-TKD(D835Y) mutant enzyme (**Table 2**). Accordingly, we opted to fix this substituent and move on to link the solvent-accessible group to this derivative while examining the effect of position variation of both the 5-phenyl and 4-ethoxy groups. Therefore, four derivatives were synthesized by varying the phenyl position at either the 5-position (**22a**,**b**) or the 6-position (**22c**,**d**) and linking the 2-(piperidin-1-yl)ethoxy moiety at either the *meta* (**22a**, **22c**) or the *para*-position (**22b**, **22d**) of the phenyl group. Placing the phenyl group at the 6-position (**22c**,**d**) had a detrimental effect on activity when screened against the FLT3-TKD(D835Y) mutant, indicating a probable steric clash with the binding site due to improper positioning of the solvent-accessible group. On the other hand, altering the position of the 2-(piperidin-1-yl)ethoxy tail from the *para*- (**22b**) to the *meta*-position (**22a**) had a less profound effect on activity and resulted in a small decline in potency (**Table 3**). The structure-activity relationship of the synthesized benzimidazole derivatives against the FLT3 kinase enzyme is summarized in **Figure 4**.

In conclusion, with respect to the parent compound, **4ACP**, a minor modification of the acetamido group from the *para* to *meta*-position (**22b**) resulted in around a 190-fold increase in activity against the FLT3-TKD(D835Y) mutant (**22b** IC_{50} = 0.48 nM; **4ACP** IC_{50} = 92.5 nM), a 25-fold increase against FLT3-WT (**22b** IC_{50} = 1.68 nM; **4ACP** IC_{50} = 43.8 nM), and a 30-fold increase against FLT3-ITD enzymes (**22b** IC_{50} = 3.32 nM; **4ACP** IC_{50} = 97.2 nM). To understand such drastic changes in activity with just a simple alteration of the chemical structure, we opted to run a molecular dynamics study to help explain this observation, which will be discussed in detail in **Section 2.4**.

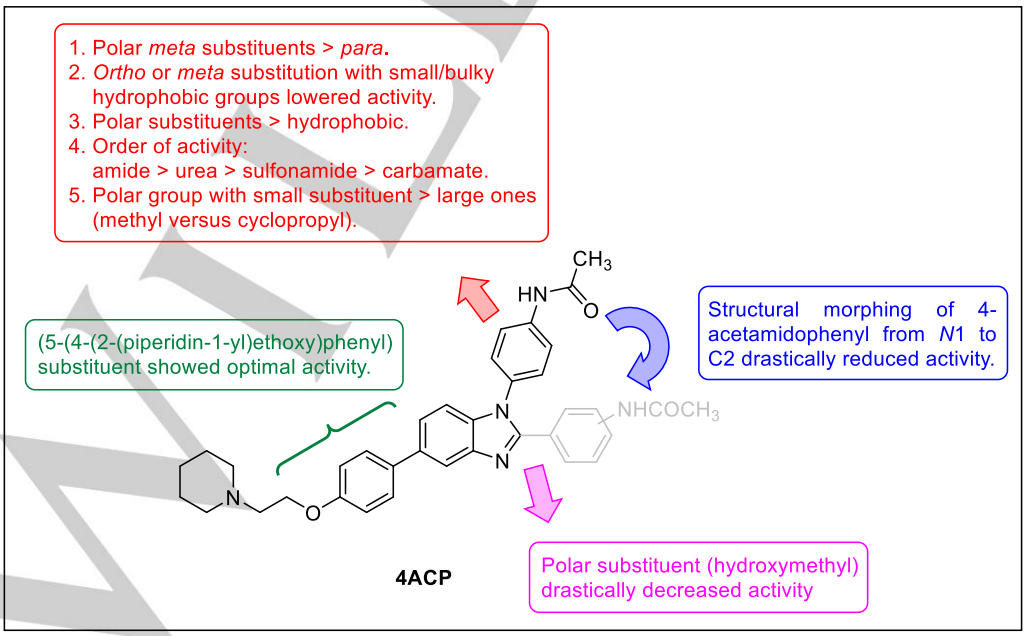

Figure 4. Structure-activity relationship for the FLT3 kinase enzyme inhibitory activities of the synthesized benzimidazole derivatives.

2.3.3. *In vitro* antiproliferative screening of benzimidazole derivatives against leukemia cell lines

Based on the FLT3-WT kinase activities of the synthesized derivatives, representative compounds were screened against two FLT3-ITD$^+$ AML cell lines, MOLM-14 and MV4-11, using gilteritinib and quizartinib as positive controls. Conforming to the FLT3 kinase activities, derivatives that demonstrated weak FLT3 enzyme inhibition exhibited poor antiproliferative activities against FLT3-ITD$^+$ AML cell lines. Compounds (**21a**, **21c**, and **21p-r**) with a hydrophobic group at either the 3- or 2-position of the 4-acetamidophenyl moiety showed weak activities against MOLM-14 and MV4-11 cell lines, with the 2-substituents (**21p-r**) having a more unfavorable effect on activity than the 3-substituents (**21a** and **21c**) (**Table 2**). In most cases, polar substituents at the *meta*-position demonstrated better antiproliferative activities than those at the *para*-position, in compliance with the FLT3 kinase enzyme activities (**21e**: *m*-OH, IC_{50} = 236.6 nM and 172.6 nM versus **21g**: *p*-OH, IC_{50} = 981.8 nM and 255.3 nM, **21l**: *m*-$NHCOCH_3$, IC_{50} = 245.2 nM and 227.7 nM versus **21o**: *p*-$NHCOCH_3$, IC_{50} = 1428.0 nM and 832.0 nM, and **28m**: *m*-NHCHO, IC_{50} = 151.2 nM and 134.5 nM versus **28n**: *p*-NHCHO, IC_{50} = 840.6 nM and 386.9 nM, against MOLM-14 and MV4-11, respectively) (**Table 2**). Derivatives linked to the solvent-accessible group (**22a-d**) were tested against FLT3-ITD$^+$ AML cell lines, compounds **22a** and **22b** demonstrated potent antiproliferative activities (**22a** IC_{50} = 98.5 nM and 51.3 nM; **22b** IC_{50} = 16.1 nM and 10.5 nM against MOLM-14 and MV4-11, respectively), while compounds **22c** and **22d** showed a drastic decrease in activity (**22c** IC_{50} = 1484.0 nM and 1188.8 nM; **22d** IC_{50} = 1601.3 nM and 1101.3 nM against MOLM-14 and MV4-11, respectively) in conformance with the FLT3 enzyme inhibition data (**Table 3**). Compound **22b** showed the most potent antiproliferative activities, with around a 3- to 7-fold improvement when compared to the parent compound **4ACP** against MOLM-14 and MV4-11, respectively. Nonetheless, **22b** was less potent than the two reference drugs used, gilteritinib and quizartinib, and further optimization is required to improve its cellular activities.

FLT3 mutations are associated with poor prognosis in AML patients and present a resistance mechanism against clinically approved FLT3 inhibitors.[9] Two important secondary mutations were identified at the FLT3-TKD D835 residue (D835Y) or the gatekeeper residue F691 (F691L). While TKD-D835Y mutation confers resistance against quizartinib but not gilteritinib, the gatekeeper F691L mutation confers resistance to both drugs.[35,36] Accordingly, we decided to examine compound **22b**'s antiproliferative activities against MOLM-14-D835Y and MOLM-14-F691L cell lines that were selected for by growth in quizartinib. Indeed, **22b** exhibited more potent activity against both cell lines compared to the parent compound, **4ACP** (**22b** IC_{50} = 26.5 nM and 160.3 nM; **4ACP** IC_{50} = 1327.4 nM and 4271.3 nM against MOLM-14-D835Y and MOLM-14-F691L, respectively). Meanwhile, **22b** was less potent than gilteritinib against both cell lines (gilteritinib IC_{50} = 7.4 nM and 26.1 nM, respectively) (**Table 4**).

To demonstrate compound **22b**'s preferential selectivity against non-FLT3 dependent leukemia cell lines, **22b** was tested against two cell lines expressing FLT3-WT, K-562 and HL-60. These two cell lines were less sensitive to compound **22b** (K-562 was around 30-46 times less sensitive, while HL-60 was 122-186 times less sensitive when compared to MOLM-14 and MV4-11, respectively), indicating **22b**'s selectivity towards FLT3-dependent cell lines (**Table 4**). Notably, the nanomolar IC_{50} observed in K-562 cells suggests potential off-target effects, which warrants further investigation.

Table 4. In vitro antiproliferative activities of **22b**, **4ACP**, and gilteritinib against two MOLM-14 mutant cell lines (MOLM-14-D835Y and MOLM-14-F691L) and two FLT3-WT cell lines (K-562 and HL-60).

Compound	Cell lines, IC_{50} (nM)			
	MOLM-14-D835Y[a]	**MOLM-14-F691L**[b]	**K-562**[c]	**HL-60**[d]
22b	26.5 ± 3.5	160.3 ± 26.9	480.5 ± 67.8	1956.5 ± 186.9
4ACP (22e)	1327.4 ± 141.3	4271.3 ± 2625.0	5078.9 ± 2875.9	>10,000
Gilteritinib	7.4 ± 2.2	26.1 ± 2.8	4012.9 ± 3480.8	1156.4 ± 117.9

[a]AML-FLT3-ITD-D835Y$^+$ (heterozygous).
[b]AML-FLT3-ITD-F691L$^+$ (heterozygous).
[c]Patient-derived CML cell line expressing FLT3-WT.
[d]Patient-derived AML cell line expressing FLT3-WT.

2.3.4. Western blot analysis of 22b effects in FLT3-ITD$^+$ MOLM-14 and MOLM-14-D835Y AML cells

FLT3-ITD mutation activates downstream signal transduction cascades, such as JAK/STAT5, Ras/Raf/MEK/ERK, and Ras/PI3K/Akt/mTOR pathways.[37,38] To confirm the effects of compound **22b** on FLT3 phosphorylation and these downstream signaling pathways, FLT3 and several mediators were examined for their total and phosphorylated levels by western blot analysis, including ERK1/2 (a MAPK signaling pathway key mediator),[39] STAT5 (a direct substrate of FLT3-ITD),[40] and S6 kinase (downstream target of mTOR).[41]

MOLM-14 and MOLM-14-D835Y cells were treated with different concentrations (0, 5, 10, 20, 40, 80, and 160 nM) of **22b** and gilteritinib, as a reference, and the cell lysates were collected after 2 hours of treatment. As expected, compound **22b** treatment resulted in a dose-dependent inhibition of FLT3, ERK, STAT5, and S6 phosphorylation without affecting their total levels in both MOLM-14 (**Figure 5A**) and MOLM-14-D835Y (**Figure 5B**) cell lines, indicating its targeted effects against FLT3. The effects of compound **22b** were observed at concentrations as low as 5 nM and demonstrated complete inhibition of phosphorylation at concentrations between 20 - 80 nM. On the other hand, gilteritinib demonstrated a more potent effect against FLT3-ITD downstream targets exhibiting complete inhibition of phosphorylation at concentrations between 10-20 nM, which aligns with the cytotoxicity data results against both AML cell lines (**Table 3**).

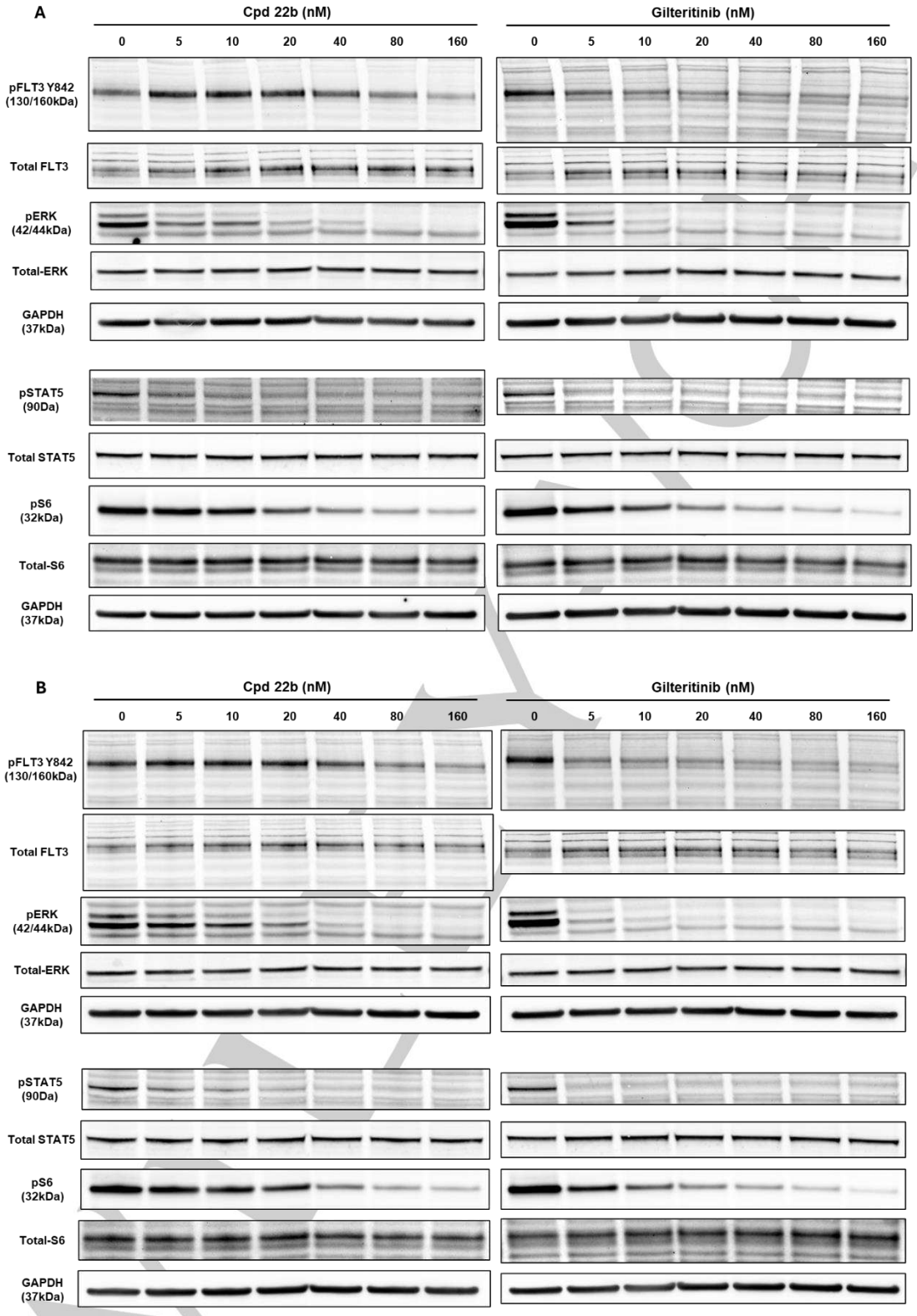

Figure 5. Western blot analysis of **22b** effects on the phosphorylation of FLT3 and FLT3 downstream signaling targets in **(A)** FLT3-ITD$^+$ MOLM-14 and **(B)** FLT3-ITD-D835Y$^+$ MOLM-14 AML cells treated with different concentrations (0 – 160 nM) of compound **22b** or gilteritinib for 2 h. DMSO was used as a vehicle control. GAPDH was used as a loading control. Each drug treatment and western blot experiment was performed three times and representative images are shown.

2.3.5. Cell cycle analysis of 22b effects in FLT3-ITD$^+$ MOLM-14 and MOLM-14-D835Y AML cells

We previously demonstrated that our parent compound **4ACP** induced a G0/G1 cell cycle arrest in two FLT3-ITD$^+$ AML cell lines, MOLM-13 and MV4-11 cells.[22] In the current work, MOLM-14 and MOLM-14-D835Y cells were treated with different concentrations (0, 5, 10, 20, 40, 80, and 160 nM) of **22b** and gilteritinib, as a reference, for 48 hours before the cells were fixed, permeabilized, stained with DAPI, and analyzed by flow cytometry for DNA content (**Figures 6** and **S1**). Compound **22b** induced a significant increase in the percentage of MOLM-14 cells in the G0/G1 phase of the cell cycle, indicating G0/G1 arrest, starting at a dose of 20 nM ($p = 0.018$ compared to untreated cells) (**Figure 6A** and **6C**). In comparison, gilteritinib's effect started at a dose of 10 nM ($p = 0.02$ compared to untreated cells) (**Figure 6B** and **6C**). This G0/G1 arrest was accompanied by a reciprocal decrease in the percentage of MOLM-14 cells in the S and G2/M2 phases of the cell cycle, starting at doses of 10 nM ($p = 0.016$) and 20 nM ($p = 0.018$) of **22b** or doses of 5 nM ($p = 0.0027$) and 10 nM ($p = 0.042$) of gilteritinib, respectively. There was also a significant increase in the percentage of MOLM-14 cells with <G0/G1 DNA content, indicating apoptosis, starting at a dose of 80 nM of **22b** ($p = 0.012$) or at a dose of 20 nM of gilteritinib ($p = 0.014$). Similarly, **22b** induced a significant increase in the percentage of MOLM-14-D835Y cells in the G0/G1 phase of the cell cycle, starting at a dose of 20 nM ($p = 0.037$ compared to untreated cells) (**Figure S1A** and **S1C**), while gilteritinib's effect started at a dose of 5 nM ($p = 0.017$ compared to untreated cells) (**Figure S1B** and **S1C**). This G0/G1 arrest was accompanied by a reciprocal decrease in the percentage of MOLM-14-D835Y cells in the S and G2/M2 phases of the cell cycle, starting at doses of 5 nM ($p = 0.0023$) and 80 nM ($p = 0.0034$) of **22b** or doses of 5 nM ($p = 0.0043$) and 10 nM ($p = 0.013$) of gilteritinib, respectively. There was also a significant increase in the percentage of MOLM-14-D835Y cells with <G0/G1 DNA content, starting at a dose of 80 nM of **22b** ($p = 0.031$) or a dose of 20 nM of gilteritinib ($p = 0.048$). Collectively, these findings indicate that **22b** induced G0/G1 cell cycle arrest in FLT3-ITD$^+$ and FLT3-ITD-D835Y$^+$ AML cell lines at low nanomolar concentrations.

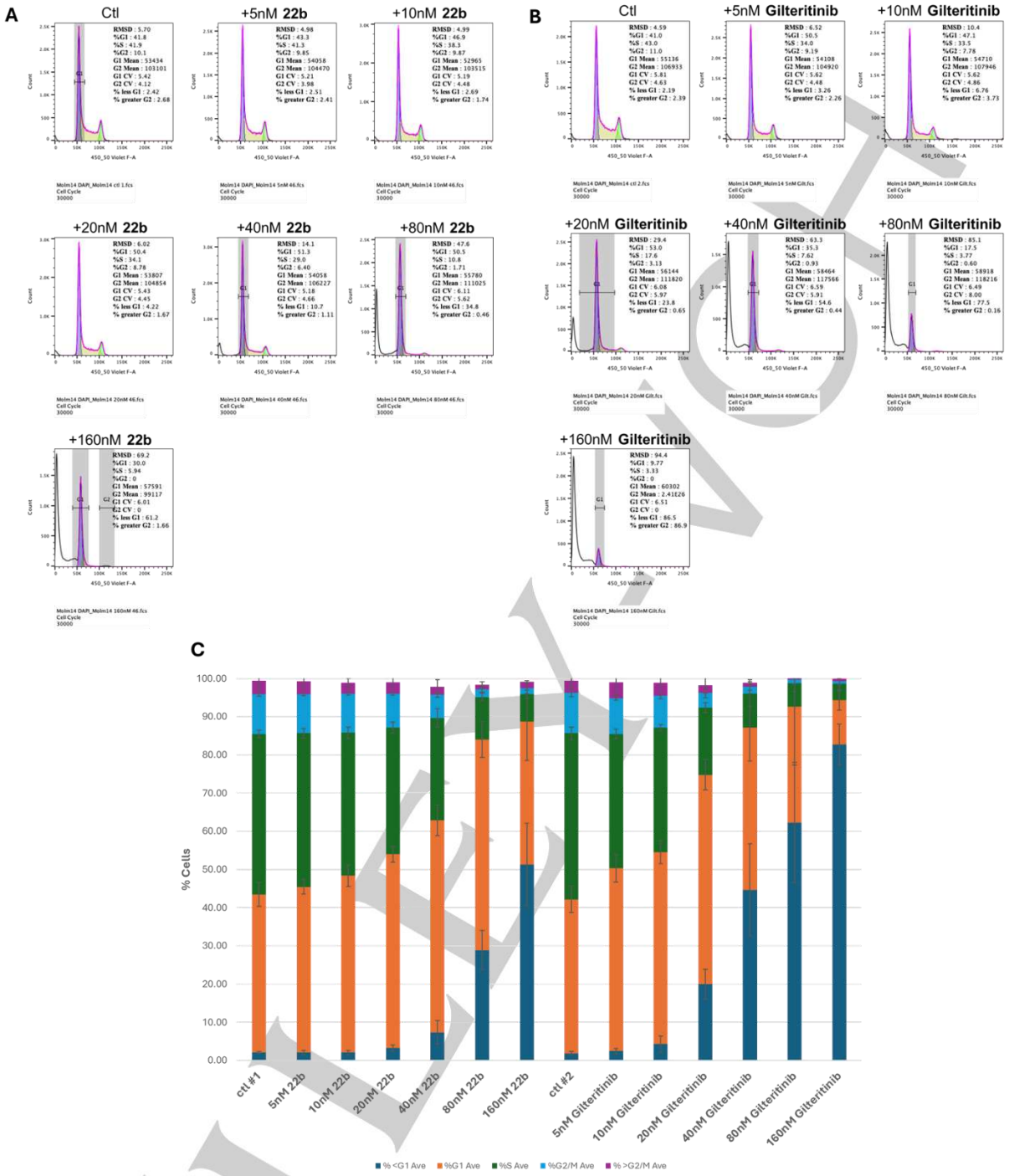

Figure 6. Cell cycle analysis of **22b** effects in FLT3-ITD$^+$ MOLM-14 AML cells. MOLM-14 cells were treated with different concentrations (0 – 160 nM) of **(A)** compound **22b** or **(B)** gilteritinib for 48 h prior to fixation, permeabilization, staining with DAPI, and flow-cytometric analysis. **(C)** Percentage of MOLM-14 cells distributed in different cell cycle phases upon treatment with the indicated concentrations of compound **22b** or gilteritinib. Sub-G1 (blue), G0/G1 phase (orange), S phase (green), G2/M phase (cyan), and >G2/M Phase (mauve). Data in **(A)** and **(B)** are representative examples of a single experiment while **(C)** represents the mean ± SD of triplicate measurements.

2.3.6. Effects of 22b on the induction of apoptosis in FLT3-ITD$^+$ MOLM-14 and MOLM-14-D835Y AML cells

We previously demonstrated that our parent compound **4ACP** induced cell death in two FLT3-ITD$^+$ AML cell lines, MOLM-13 and MV4-11.[22] In the current work, MOLM-14 and MOLM-14-D835Y cells were treated with different concentrations (0, 5, 10, 20, 40, 80, and 160 nM) of **22b** and gilteritinib, as a reference, for 48 hours. After treatment, the cells were fixed, permeabilized, stained with a FITC-conjugated anti-cleaved-caspase 3 antibody, and analyzed by flow cytometry for cleaved-caspase 3 negative (live) cells (**Figures 7** and **S2**). Compound **22b** induced a significant decrease in the percentage of cleaved-caspase 3 negative (live) MOLM-14 cells, starting at a dose of 40 nM ($p = 0.026$ compared to untreated cells) (**Figure 7A** and **7C**). In comparison, gilteritinib's effect started at a dose of 20 nM ($p = 0.013$ compared to untreated cells) (**Figure 7B** and **7C**). Similarly, **22b** induced a significant decrease in the percentage of cleaved-caspase 3 negative (live) MOLM-14-D835Y cells, starting at a dose of 80 nM ($p = 0.020$ compared to untreated cells) (**Figure S2A** and **S2C**), while gilteritinib induced such an effect starting at a dose of 40 nM ($p = 0.0072$ compared to untreated cells) (**Figure S2B** and **S2C**).

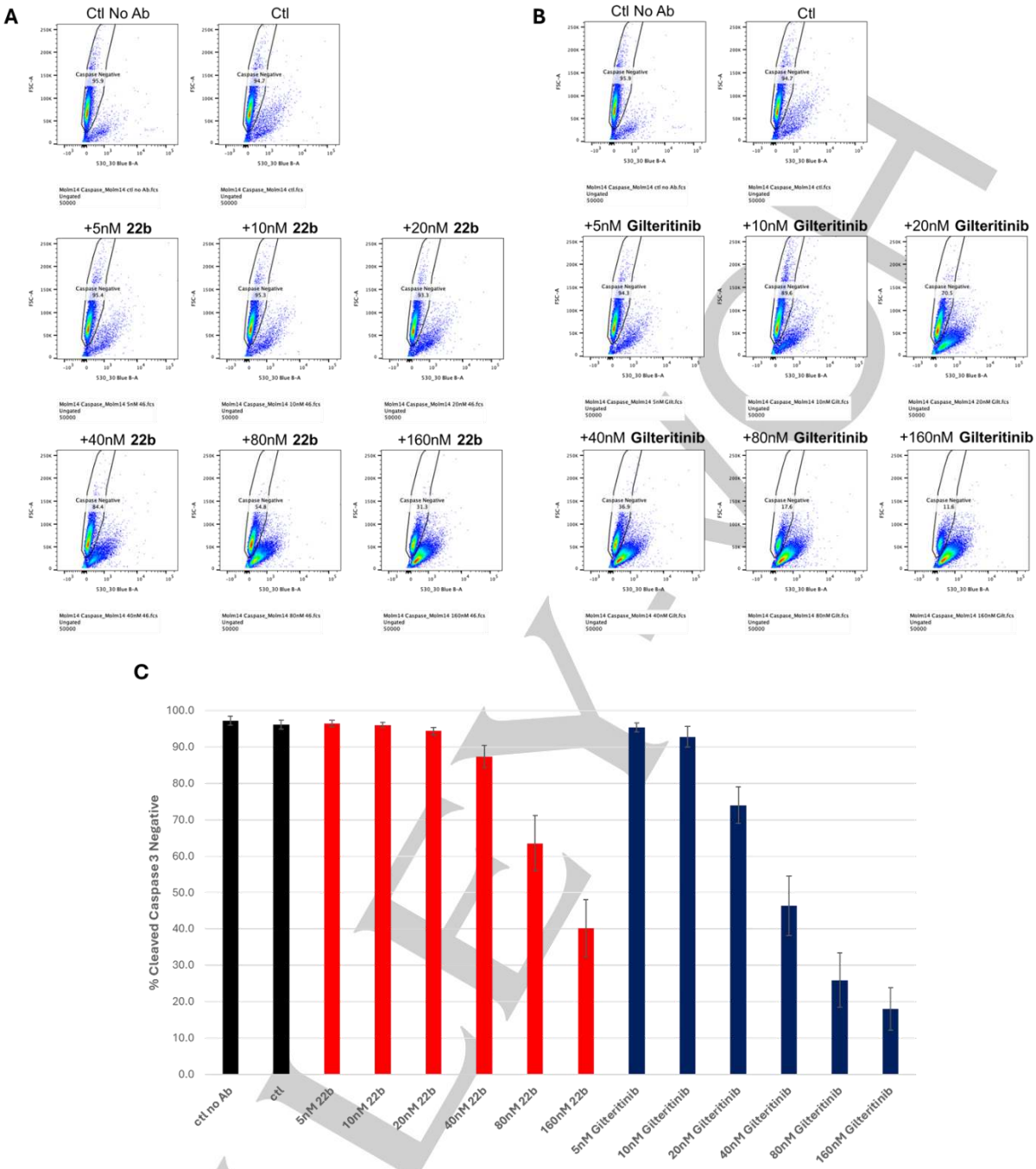

Figure 7. Effects of **22b** on the induction of apoptosis in FLT3-ITD$^+$ MOLM-14 AML cells. MOLM-14 cells were treated with different concentrations (0 – 160 nM) of **(A)** compound **22b** or **(B)** gilteritinib for 48 h prior to fixation, permeabilization, staining with a FITC-conjugated anti-cleaved-caspase 3 antibody, and flow-cytometric analysis. **(C)** Percentage of cleaved-caspase 3 negative MOLM-14 cells (live cells) upon treatment with the indicated concentrations of compound **22b** or gilteritinib. Data in **(A)** and **(B)** are representative examples of a single experiment while **(C)** represents the mean ± SD of triplicate measurements.

2.3.7. In vitro selectivity profiling of 22b against a panel of kinase enzymes

Considering the potent activity of **22b** compared to its parent compound **4ACP**, we proceeded to test **22b** against a panel of 13 kinases. This selection was based on the off-target kinases potently inhibited by quizartinib,[42] which informed our design. At a concentration of 50 nM (approximately 100-fold the IC_{50} of **22b** against the FLT-TKD(D835Y) mutant), **22b** did not exhibit more than 90% inhibition against any of the tested kinases. It showed over 80% inhibition against only two kinases, ABL1 and KDR, and demonstrated less than 80% inhibitory activity against FLT3-related kinases, including FLT1, FLT4, PDGFRα, and PDGFRβ (**Table 5**). Notably, the potent

inhibition of ABL1 may explain the observed effect on K-562 cells, as ABL1 inhibition has been shown to significantly impact the viability of K-562 cells.[43,44]

Table 5. In vitro kinase inhibition profile of **22b**.

Kinase	% Inhibition[a] at 50 nM	Kinase	% Inhibition[a] at 50 nM
ABL1	85	KDR (VEGFR2)	89
B-Raf	-2	LCK	21
CSF1R (FMS)	58	PDGFRα	74
FGFR3	38	PDGFRβ	50
FLT1 (VEGFR1)	51	RET	61
FLT4 (VEGFR3)	77	SRC	18
IGF1R	11		

[a]The kinase inhibition assays were provided by ThermoFisher Scientific. All data were obtained by double testing (average).

2.4. Molecular modeling

2.4.1. Homology modeling

Since the designed compounds are proposed to be type I inhibitors that bind to the FLT3 enzyme in an active "DFG-in" conformation, and the reported PDB structures for FLT3 represent the DFG loop in an inactive "DFG-out" conformation, a homology model for FLT3 in the "DFG-in" conformation was built based on a protocol reported by Ke et al.[45] The "DFG-out" FLT3 kinase domain 3D structure (PDB ID: **1RJB**) was used as the main template for the model creation due to its high sequence identity (93%) with the target sequence. The template (**1RJB**) lacks a loop corresponding to residues Lys649 to Ser654 and the "DFG-in" region. Therefore, a second template was needed to model these two missing parts. This was determined by conducting a protein-BLAST search against the 293-amino acid target sequence of the FLT3 Kinase domain. The search identified the colony-stimulating factor-1 receptor (CSF-1) with a "DFG-in" binding kinase inhibitor (PDB ID: **3LCD**). CSF-1 is a tyrosine kinase receptor which shares 62.7% sequence identity with the FLT3 kinase.

The FLT3 "DFG-in" kinase model was then constructed using the atomic coordinates of **1RJB** to create the protein structure and **3LCD** to model the loop corresponding to residues Lys649 to Ser654 and the activation loop's Asp729 to Ala848, containing the "DFG-in" residues Asp829-Gly831.

2.4.2. Molecular docking

The ligands, **4ACP** and **22b**, were docked into the ATP binding site of the FLT3 homology model using the previously described protocol.[22] **4ACP**'s benzimidazole retained the essential hydrogen bond with the Cys694 residue of the hinge region, while the acetamido group partially filled the hydrophobic pocket, and the 4-(2-(piperidin-1-yl)ethoxy) group acted as a solvent-accessible moiety (**Figure 8A**). **22b** showed a similar pose, forming hydrogen bonds with Lys644 of the *N*-terminal β3 strand and the DFG's Phe830 through the carbonyl acetamido group (**Figure 8B**).

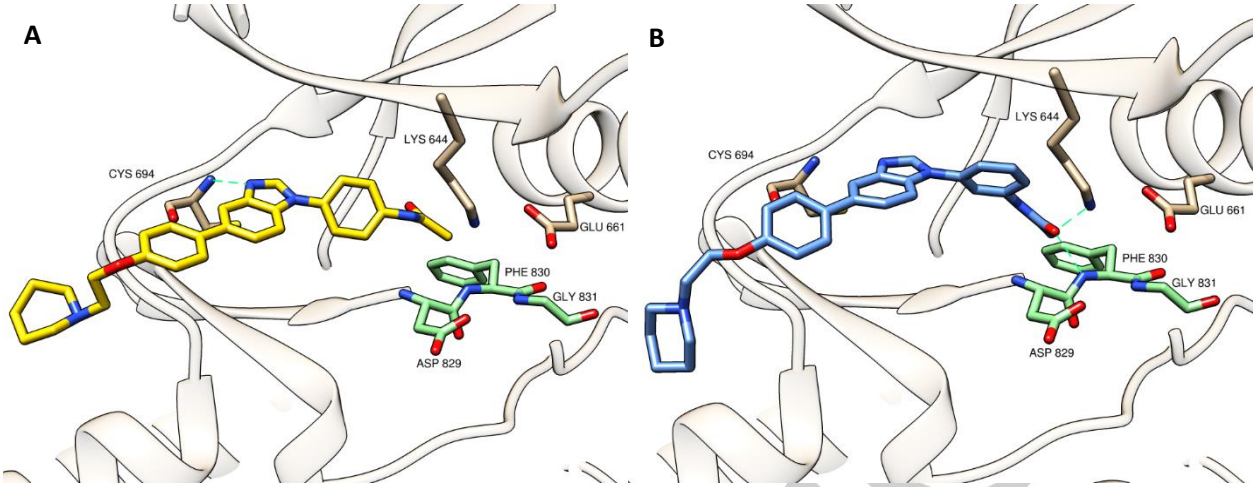

Figure 8. (A) 4ACP and **(B) 22b** binding modes within FLT3 ATP binding site. **4ACP** and **22b** are represented as yellow and blue sticks, respectively, DFG motif is displayed as green sticks, Lys644, Glu661, and Cys694 are depicted in tan color, and hydrogen bonds are shown in green dotted lines.

2.4.3. Molecular dynamics

FLT3 wildtype (WT) and D835Y mutant (Mut) structures were subjected to molecular dynamics (MD) simulations each in three states each: apo, **4ACP**-bound, and **22b**-bound. This was done to study ligand residence and the conformational changes in the binding site induced by the ligands, resulting in six simulations, each lasting 100 ns. These simulations will be referred to as Apo-WT, Apo-Mut, **4ACP**-WT, **4ACP**-Mut, **22b**-WT, and **22b**-Mut throughout the text.

Protein stability during the simulation was evaluated by calculating the protein radius of gyration (Rgyr), the root mean square deviation (RMSD), and the root mean square fluctuation (RMSF) (**Figure 9**). The radius of gyration (**Figure 9A**) indicates the compactness of the protein structure during the simulation. It remained stable around 36.5 Å throughout the simulation, indicating no major conformational changes. The root mean square deviation (**Figure 9B**) was calculated for the protein backbone atoms with respect to the starting structure and indicates protein stability during the simulation. Most structures showed stable RMSD around 2-3 Å, indicating protein stability. However, Apo-WT and **22b**-WT showed higher RMSD from 55-100 ns, which can be attributed to the flexibility of the terminal residues. The root mean square fluctuation (**Figure 9C**), which measures the average per-residue fluctuation during the simulation, indicated that the flexible regions are concentrated in the β1-β2 strands (Leu616 to Glu626) and the αC helix (Leu646 to Thr666), with RMSF > 2 Å, which sandwich the ligands within the active site. These two regions showed higher fluctuation in **4ACP**-WT which can be linked to **4ACP** leaving the binding site due to weaker binding.

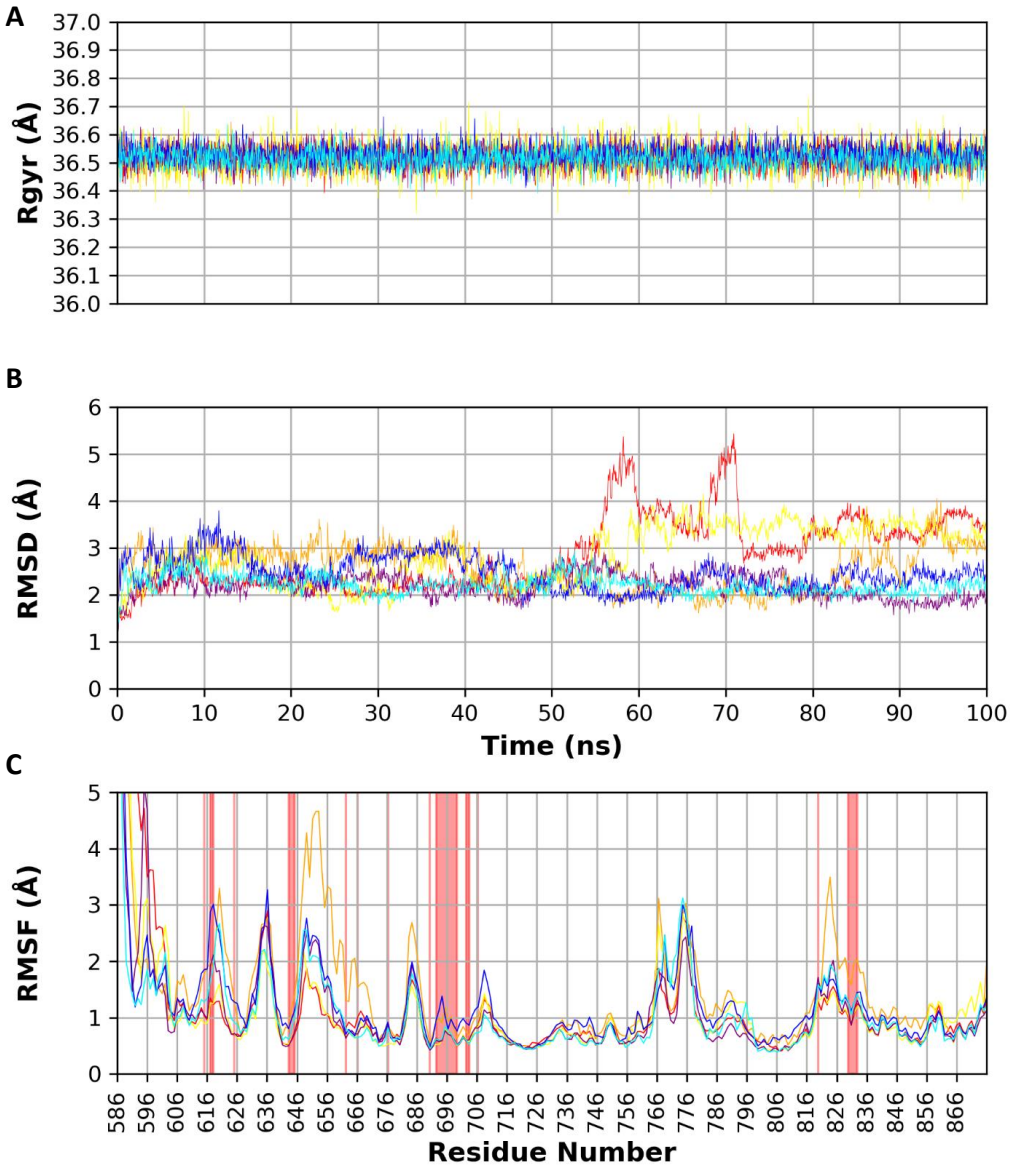

Figure 9. (A) FLT3 protein radius of gyration (Rgyr), **(B)** root mean square deviation (RMSD), and **(C)** root mean square fluctuation (RMSF) for Apo-WT (red), **4ACP**-WT (orange), **22b**-WT (yellow), Apo-Mut (purple), **4ACP**-Mut (blue), and **22b**-Mut (cyan). In **(C)** RMSF, the binding site residues are depicted by a red background.

Ligand RMSD was calculated to track the ligand trajectory during the simulation (**Figure S3A**). **4ACP** showed higher RMSD values, indicating weak binding to the protein, with an average displacement of 10 Å in the wildtype and 20 Å in the mutant proteins. In the wildtype protein, **4ACP** was displaced by 10 Å, partially leaving the binding pocket and losing the hydrogen bond between the benzimidazole nitrogen and the hinge region key amino acid Cys694. It then formed a hydrogen bond between the backbone amide hydrogen of Cys694 and the carbonyl oxygen of the ligand's amide group, as shown in **Figure 10**, which depicts the first and last simulation snapshots of the six simulation runs. This is also reflected in the hydrogen bonding interactions (**Figure S3B**), where **4ACP** lost hydrogen bonds with the protein at 40 ns through the benzimidazole nitrogen and regained it at 45 ns through the amide group. In the mutant protein, **4ACP** completely abandoned the binding pocket, losing the main hydrogen bond between the benzimidazole nitrogen and Cys694, and losing any hydrogen bond with the protein at the end of the simulation (**Figure 10D**).

On the other hand, **22b** showed lower RMSD values (3 Å average) in both proteins (**Figure S3A**), indicating longer residence time inside the binding site, which might account for its stronger binding and improved biological activity compared to **4ACP**. This is

also reflected in the hydrogen bonding pattern (**Figure S3B**), where the ligand maintained the main hydrogen bond between the benzimidazole nitrogen and Cys694 throughout the entire simulation (**Figure 10E** and **10F**).

A deeper investigation into the conformational changes induced in the binding pocket by both ligands revealed that a salt bridge between the β3 strand Lys644 and the αC helix Glu661 is a key determinant for ligand stability within the binding pocket (**Figure 10**). This salt bridge is reported to be intact in the kinase DFG-in active state.[46] At the start of the simulation, the salt bridge was present in the Apo forms (**Figure 10A** and **10B**) and both ligand-protein complexes. However, **4ACP**, with its amide group in the *para* position, disrupted the salt bridge, forcing the protein to expel it from the pocket and breaking the hydrogen bond between the benzimidazole and Cys694 in both WT and mutant proteins (**Figure 10C** and **10D**). In contrast, **22b**, with its amide group in the *meta* position, fit more easily into the back cleft guarded by these two amino acids without disrupting the salt bridge, thereby supporting the essential hydrogen bond between the benzimidazole and Cys694 (**Figure 10E** and **10F**).

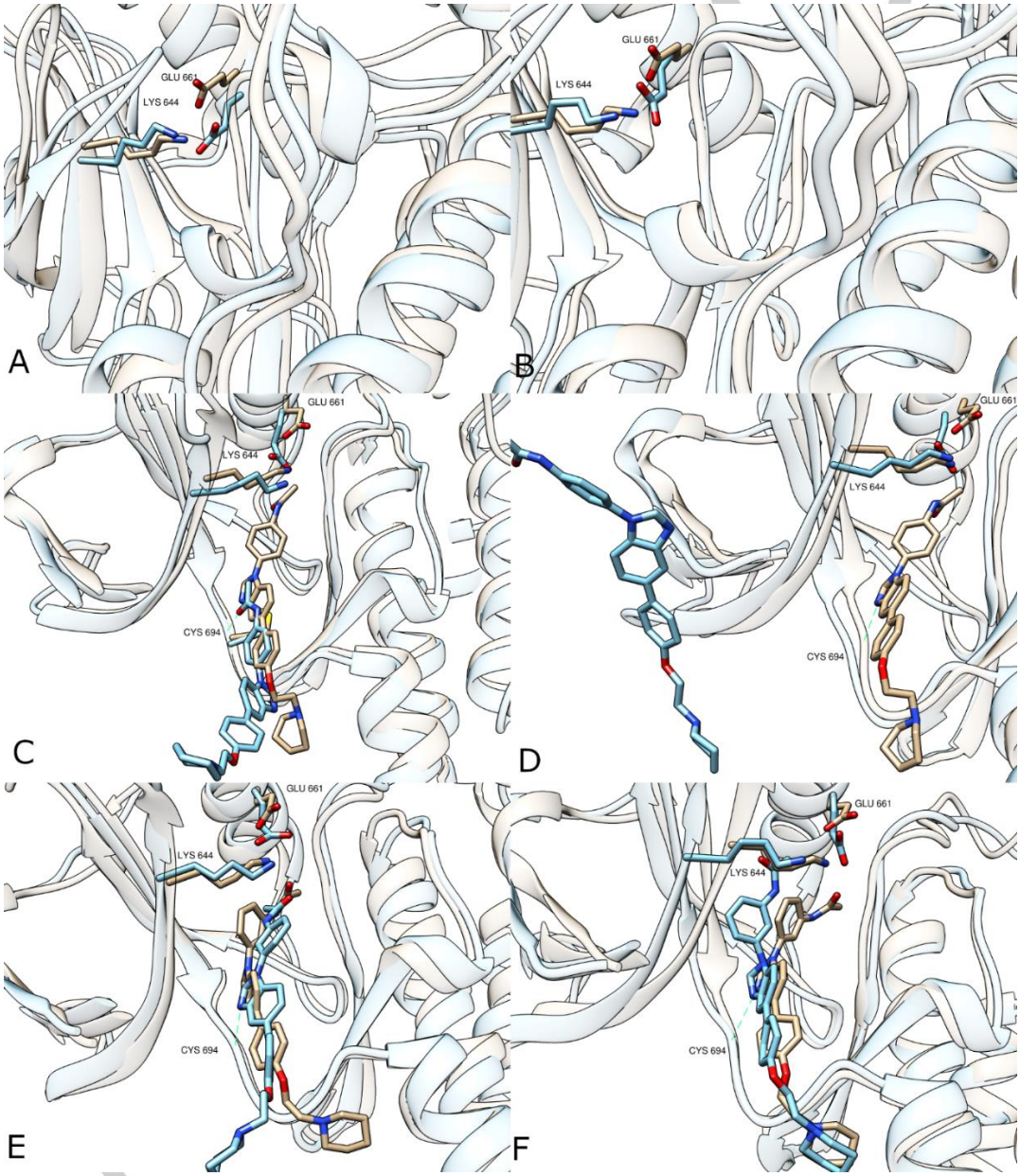

Figure 10. The first (khaki) and last (blue) snapshots of FLT3 protien in **(A)** Apo-WT, **(B)** Apo-Mut, **(C) 4ACP**-WT, **(D) 4ACP**-Mut, **(E) 22b**-WT, and **(F) 22b**-Mut. In each subfigure, the residues Lys644 and Glu661 are shown as sticks. Residues from 613-626 and hydrogen atoms are hidden for clarity.

Principal component analysis (PCA) was performed to analyze the principal movements adopted by the protein during the simulations. The 2D graphs between the first (PC1) and second (PC2) principal components are shown in **Figure 11**. Observing these graphs, it is noted that the number of clusters of **4ACP**-protein complexes is comparable to the Apo proteins, while the **22b** graphs shows one additional cluster (**Figure 11**, red circles). This reflects the different behavior of protein conformational dynamics within the two groups, indicating the different effects of **22b** binding. Additionally, the spread of MD snapshots (**Figure 11**, colored points) in the PC1-PC2 space (conformational space explored by **22b**-protein along the two first principal components) is smaller than that of **4ACP** and Apo in both WT and Mut. This suggests the conformational stability of the **22b**-protein complex, which can be attributed to the tighter binding of **22b** compared to **4ACP**. Furthermore, the latest frames of **4ACP** and Apo (90-100 ns) form a separate subcluster (**Figure 11**, blue circles), reflecting additional conformations explored at the end of the simulation. In contrast, the frames of **22b** remain within the same subclusters as the previous time scale (70-90 ns), indicating conformational stability induced by **22b** throughout the simulation. Smoothed trajectory animations projected on the first principal component (with the highest eigenvalue) of the protein heavy atoms and the ligands show the salt bridge between the β3 strand Lys644 and the αC helix Glu661 in the six simulations, with **4ACP** leaving the pocket and **22b** occupying it (**Video S1-6**).

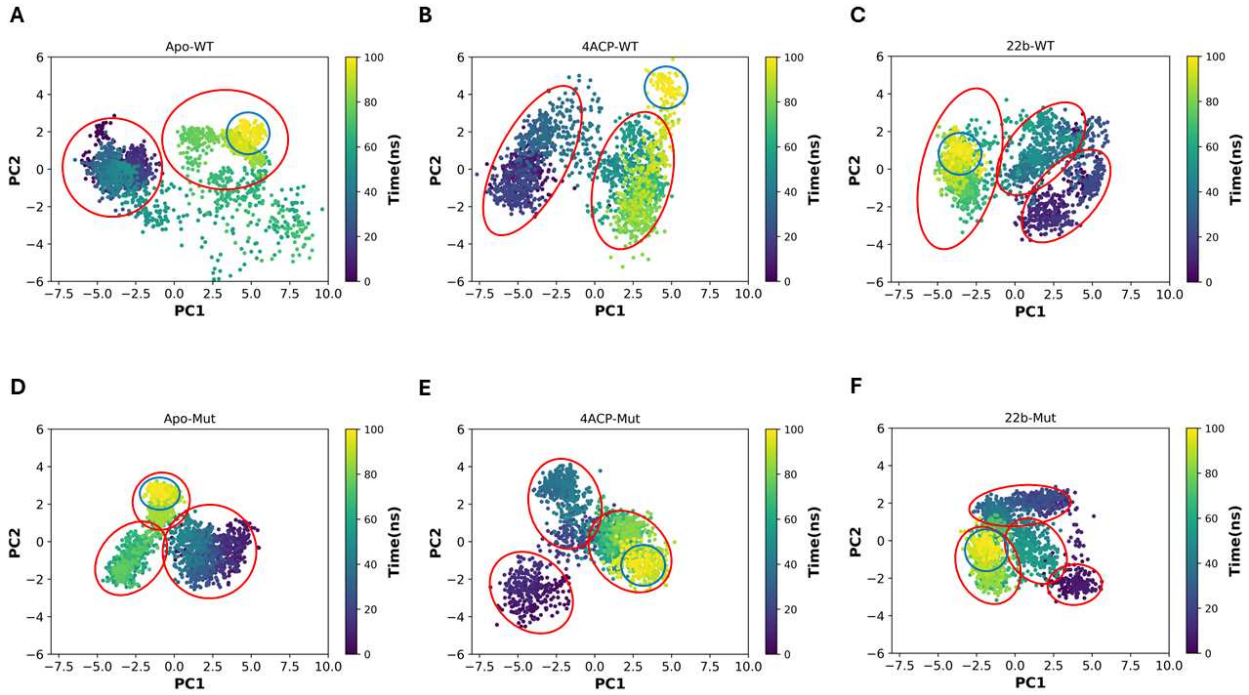

Figure 11. Principal component analysis (PCA) for FLT3 protein backbone atoms is shown for **(A)** Apo-WT, **(B) 4ACP**-WT, **(C) 22b**-WT, **(D)** Apo-Mut, **(E) 4ACP**-Mut, and **(F) 22b**-Mut. Each plot shows the 2D diagram for the first two principal components (PC1 and PC2) for every snapshot in the trajectory. Snapshots are colored according to the simulation time from 0 to 100 ns as shown in the side color bar. Red circles depict the clusters formed by the trajectory snapshots, while the blue circles indicate the last 10 ns snapshots.

3 CONCLUSION

In this study, we used the benzimidazole-based FLT3 inhibitor **4ACP** as a starting point for optimization and SAR investigation to develop potent mutant FLT3 inhibitors targeting resistant AML. We removed the solvent-accessible tail to minimize synthetic efforts and synthesized 31 derivatives by modifying the 4-acetamidophenyl group from the *N*1 to the C2 position of benzimidazole and varying the substituents at both positions. In vitro kinase assays identified compound **21l** (3-acetamidophenyl) as the most potent against the FLT3-TKD(D835Y) mutant. We then linked this derivative to the solvent-accessible group (2-(piperidin-1-yl)ethoxy) in different positions. Of the four derivatives synthesized, compound **22b** exhibited sub-nanomolar activity against FLT3-TKD(D835Y), surpassing gilteritinib and showing superior activity compared to quizartinib against FLT3-WT and FLT3-ITD enzymes. With a slight structural change (3-acetamidophenyl vs. 4-acetamidophenyl of **4ACP**), **22b** showed a 190-fold improvement in activity against FLT3-TKD(D835Y)

compared to **4ACP**. Derivatives with weak FLT3 enzyme inhibition also showed poor antiproliferative activities against MOLM-14 and MV4-11 AML cell lines. **22b** exhibited the most potent antiproliferative activity against FLT3-ITD$^+$ AML cell lines (MOLM-14 and MV4-11) and those with secondary mutations (MOLM-14-D835Y and MOLM-14-F691L), compared to **4ACP** and other derivatives. However, it was less potent than gilteritinib and quizartinib, indicating the need for further optimization to improve its cellular activities.

Western blot analysis showed that **22b** treatment resulted in dose-dependent inhibition of ERK, STAT5, and S6 phosphorylation in both MOLM-14 and MOLM-14-D835Y cell lines. Flow cytometry revealed that **22b** induced G0/G1 cell cycle arrest and apoptotic cell death in both cell lines at low nanomolar concentrations. Regarding safety and selectivity, **22b** demonstrated diminished activity against non-FLT3 dependent leukemia cell lines (K-562 and HL-60), selectively targeting FLT3-driven cell lines. It also exhibited 80-fold more selectivity towards FLT3-TKD(D835Y) versus KIT, indicating relative safety and lower potential for myelosuppression.

Molecular dynamics study revealed that **22b** showed lower RMSD, longer residence time, and more stable hydrogen bonding interactions in both wild-type and mutant FLT3 proteins. **22b**-protein complexes displayed better conformational stability, likely due to tighter binding, which may account for the improved biological activity.

In conclusion, **22b** is a promising candidate for targeting resistant AML via mutant FLT3 inhibition. Further structural optimization and pharmacokinetic and in vivo evaluations are needed to establish **22b** as a preclinical candidate for AML therapy.

4 EXPERIMENTAL

4.1 Chemistry

Chemicals and solvents were purchased from Sigma-Aldrich (Germany), Alfa Aesar (Germany), and Apollo Scientific (England) and were used as such without further purification. Reactions were followed using analytical thin layer chromatography (TLC), performed on Aluminum silica gel 60 F_{254} TLC plates, purchased from Merck, with visualization under UV light (254 nm). ^{1}H NMR spectra were determined on a Bruker Avance III HD FT NMR spectrometer operating at 9.4 T (400 MHz) or a two-channel Bruker AV-NEO NMR spectrometer operating at 11.7 T (501 MHz) in δ scale (ppm) and *J* (Hz) and referred to the deuterated solvent peak (DMSO-d_6 δ = 2.5 ppm). ^{13}C NMR spectra were determined on the two-channel Bruker AV-NEO NMR spectrometer at 126 MHz and referred to the solvent peak (DMSO-d_6 δ = 39.52 ppm). All NMR datasets were acquired at 298 K. High resolution mass spectrometry (HRMS) was carried out using a Bruker Impact II QqTOF spectrometer equipped with a VIPHESI source using electrospray ionization (ES$^+$). The purity of the final compounds was assessed by HPLC on an Agilent 1290 Infinity II Series equipped with a UV detector and a C_{18} reverse phase column eluting with an MeCN – water gradient (5-95%) and 0.1% TFA over 5 mins at a flow rate of 0.5 mL min^{-1}.

4.1.1. General procedure for the synthesis of target compounds 8a-d

Intermediates **2a**,**b** were synthesized as previously reported.[47,48] The desired final compounds **8a**-**d** were synthesized according to the following procedures [22,49–51] and is illustrated as follows.

Step (a): To a solution of 3- or 4-nitrobenzaldehyde (**1a**,**b**) (3.02 g, 20.00 mmol, 1.00 equiv) in ethanol (50 mL) was added a solution of sodium metabisulfite (2.14 g) in water (13 mL) dropwise while stirring in an ice bath. The reaction mixture was stirred at 0°C for another 2 hr then the heavy precipitate was filtered, washed with cold ethanol, and dried to yield the desired sodium hydroxy(3- or 4-nitrophenyl)methane sulfonate derivatives (**2a**,**b**) in 95-98% yield.

Step (b): A suspension of 4-bromo-1-fluoro-2-nitrobenzene (**3**) (3.00 g, 13.60 mmol, 1.00 equiv), the appropriate amine derivatives (**4a**,**b**) (15.00 mmol, 1.10 equiv), and K_2CO_3 (4.15 g, 30.00 mmol, 2.20 equiv) in DMF (20 mL) was heated at 80-90°C for 16 hr. Upon completion of the reaction as indicated by TLC, the reaction mixture was poured into ice/water, stirred for 1 hr, filtered, washed with water, and dried to yield the designated compounds (**5a**,**b**) in 96-97% yield.

Step (c): A solution of the appropriate nitro derivative (**5a**,**b**) (4.60 mmol, 1.00 equiv) and $SnCl_2.2H_2O$ (5.20 g, 23.00 mmol, 5.00 equiv) in ethyl acetate (50 mL) was refluxed for 12 hr. Upon completion of the reaction as indicated by TLC, the reaction mixture was cooled, washed with sodium bicarbonate solution (10%), brine, dried, and evaporated to give the corresponding diamine derivatives that was used as such into the following step.

A solution of the appropriate crude diamine derivative (4.30 mmol, 1.00 equiv) and sodium hydroxy(3- or 4-nitrophenyl)methanesulfonate (**2a**,**b**) (6.50 mmol, 1.50 equiv) in DMF (5 mL) was heated at 130°C for 4 hr. Upon completion of the reaction as indicated by TLC, the reaction mixture was poured into ice/water (100 mL), stirred vigorously, and the resulting solid was filtered, and dried, to yield the desired benzimidazole derivatives (**6a**-**d**) in 89-95% yield.

Step (d): A solution of the appropriate nitro derivative (**6a**-**d**) (3.00 mmol, 1.00 equiv) and $SnCl_2.2H_2O$ (3.40 g, 15.00 mmol, 5.00 equiv) in ethyl acetate (50 mL) was refluxed for 12 hr. Upon completion of the reaction as indicated by TLC, the reaction mixture was cooled, washed with sodium bicarbonate solution (10%), brine, dried and evaporated to give the corresponding amine derivatives that was used as such into the following step.

To a solution of the appropriate amine derivative (2.00 mmol, 1.00 equiv) in DCM (20 mL) was added acetic anhydride (306 mg, 284 µL, 3.00 mmol, 1.50 equiv) and the reaction mixture was stirred at room temperature for 12 hr. Upon completion of the reaction as indicated by TLC, the reaction mixture was evaporated and the resulting residue was stirred with diethyl ether, filtered, and dried to yield the desired compounds (**7a**-**d**) in 61-74% yield.

Step (e): A solution of the appropriate bromo derivative (**7a**-**d**) (0.60 mmol, 1.00 equiv) and 4-hydroxyphenylboronic acid (99 mg, 0.72 mmol, 1.20 equiv) in dioxane/water (4:1, 24 mL) was purged with nitrogen for 5 min then tetrakis(triphenylphosphine)palladium(0) (69 mg, 0.06 mmol, 0.10 equiv) and K_2CO_3 (249 mg, 1.80 mmol, 3.00 equiv) were added and the reaction was refluxed under nitrogen for 4 hr. Upon completion of the reaction as indicated by TLC, the mixture was cooled, filtered using celite, evaporated, and the resulting residue was extracted with ethyl acetate. The organic layer was dried over anhydrous Na_2SO_4, evaporated, and the resulting residue was purified by flash chromatography (DCM/MeOH) to yield the desired compounds (**8a**-**d**) in 49-67% yield.

***4.1.1.1. N*-{3-[5-(4-hydroxyphenyl)-1*H*-benzimidazol-2-yl]phenyl}acetamide (8a).** R_f = 0.30 (DCM/MeOH 9.5:0.5). Buff solid, 67% yield, **mp:** 194-196°C. **^{1}H NMR** (501 MHz, DMSO-d_6) δ 12.90 (s, 1H), 10.14 (s, 1H), 9.48 (s, 1H), 8.51 (s, 1H), 7.81 (d, *J* = 7.7 Hz, 1H), 7.72 (s, 1H), 7.66 (d, *J* = 5.7 Hz, 1H), 7.62 (d, *J* = 7.1 Hz, 1H), 7.52 (d, *J* = 8.2 Hz, 2H), 7.47 (t, *J* = 7.9 Hz, 1H), 7.43 (d, *J* = 8.3 Hz, 1H), 6.87 (d, *J* = 8.2 Hz, 2H), 2.10 (s, 3H). **HRMS** exact mass of $C_{21}H_{18}N_3O_2$ **(M+H)$^+$:** 344.1394 amu; **found:** 344.1390 amu. **HPLC purity:** 96.46%, **HPLC t_R:** 2.31 min.

***4.1.1.2. N*-{4-[5-(4-hydroxyphenyl)-1*H*-benzimidazol-2-yl]phenyl}acetamide (8b).** R_f = 0.25 (DCM/MeOH 9.7:0.3). White solid, 49% yield, **mp:** >300°C (decomp.). **^{1}H NMR** (501 MHz, DMSO-d_6) δ 12.78 (s, 1H), 10.18 (s, 1H), 9.46 (s, 1H), 8.10 (d, *J* = 8.8 Hz, 2H), 7.75 (d, *J* = 8.4 Hz, 2H), 7.69 (d, *J* = 7.5 Hz, 1H), 7.58 (s, 1H), 7.51 (d, *J* = 8.6 Hz, 2H), 7.40 (d, *J* = 7.9 Hz, 1H), 6.86 (d, *J* = 8.6 Hz, 2H), 2.09 (s, 3H). **HRMS** exact mass of $C_{21}H_{18}N_3O_2$ **(M+H)$^+$:** 344.1394 amu; **found:** 344.1392 amu. **HPLC purity:** 98.50%, **HPLC t_R:** 2.29 min.

***4.1.1.3. N*-{3-[5-(4-hydroxyphenyl)-1-methyl-1*H*-benzimidazol-2-yl]phenyl}acetamide (8c).** R_f = 0.35 (DCM/MeOH 9.7:0.3). Off-white solid, 67% yield, **mp:** >300°C (decomp.). **^{1}H NMR** (501 MHz, DMSO-d_6) δ 10.18 (s, 1H), 9.48 (s, 1H), 8.15 (s, 1H), 7.84 (d, *J* = 1.7 Hz, 1H), 7.75 (d, *J* = 7.9 Hz, 1H), 7.63 (d, *J* = 8.4 Hz, 1H), 7.54 (d, *J* = 7.8 Hz, 2H), 7.53 – 7.52 (m, 1H), 7.51 (s, 1H), 7.49 (d, *J* = 7.7 Hz, 1H), 6.87 (d, *J* = 8.6 Hz, 2H), 3.90 (s, 3H), 2.09 (s, 3H). **^{13}C NMR** (126 MHz, DMSO-d_6) δ 168.63, 156.63, 153.29, 143.10, 139.64, 135.70, 134.89, 131.87, 130.47, 129.08, 127.93 (2C), 123.65, 121.36, 120.01, 119.77, 116.06, 115.71 (2C), 110.78, 31.85, 24.09. **HRMS exact mass of** $C_{22}H_{20}N_3O_2$ **(M+H)$^+$:** 358.1550 amu; **found:** 358.1548 amu.

***4.1.1.4. N*-{4-[5-(4-hydroxyphenyl)-1-methyl-1*H*-benzimidazol-2-yl]phenyl}acetamide (8d).** R_f = 0.30 (DCM/MeOH 9.5:0.5). Off-white solid, 61% yield, **mp:** >300°C (decomp.). **^{1}H NMR** (501 MHz, DMSO-d_6) δ 10.21 (s, 1H), 9.47 (s, 1H), 7.83 (d, *J* = 2.1 Hz, 2H), 7.81 (s, 1H), 7.78 (d, *J* = 2.1 Hz, 2H), 7.60 (d, *J* = 8.4 Hz, 1H), 7.53 (d, *J* = 8.6 Hz, 2H), 7.50 (d, *J* = 6.9 Hz, 1H), 6.86 (d, *J* = 8.7 Hz, 2H), 3.88 (s, 3H), 2.11 (s, 3H). **^{13}C NMR** (126 MHz, DMSO-d_6) δ 168.73, 156.60, 153.37, 143.18, 140.60, 135.71, 134.75, 131.93, 129.85(2C), 127.92 (2C), 124.49, 121.10, 118.72 (2C), 115.88, 115.71 (2C), 110.61, 31.85, 24.15. **HRMS exact mass of** $C_{22}H_{20}N_3O_2$ **(M+H)$^+$:** 358.1550 amu; **found:** 358.1550 amu. **HPLC purity:** 98.31%, **HPLC t_R:** 2.33 min.

4.1.2. General procedure for the synthesis of intermediate compounds 11a,b, 13, and 16a,b

Intermediates **11a**,**b**, **13**, and **16a**,**b** were synthesized as previously reported[50,52,53] and is illustrated as follows.

Step (a): To a solution of the appropriate aniline (**9a**,**b**) (10.00 mmol, 1.00 equiv) in acetic acid (10 mL) was added acetic anhydride (1.53 g, 1.42 mL, 15.00 mmol, 1.50 equiv) and the reaction mixture was heated at 80°C for 2 hr. Upon completion of the reaction as

indicated by TLC, the reaction mixture was poured into ice/H_2O, and the resulting precipitate was filtered, washed with water, and dried to yield the designated compounds (**10a**,**b**) in 88-95% yield.

Step (b): A solution of the appropriate nitro derivative (**10a**-**d**) (8.00 mmol, 1.00 equiv) and $SnCl_2.2H_2O$ (9.02 g, 40.00 mmol, 5.00 equiv) in ethyl acetate (150 mL) was refluxed for 6 hr. Upon completion of the reaction as indicated by TLC, the reaction mixture was cooled, washed with sodium bicarbonate solution (10%), brine, dried and evaporated to give the desired amine derivatives (**11a**,**b**) in 17-85% yield.

Step (c): A solution of 2-fluoro-4-nitroaniline (**12**) (1.56 g, 10.00 mmol, 1.00 equiv) and $SnCl_2.2H_2O$ (11.28 g, 50.00 mmol, 5.00 equiv) in ethyl acetate (150 mL) was refluxed for 12 hr. Upon completion of the reaction as indicated by TLC, the reaction mixture was cooled, washed with sodium bicarbonate solution (10%), brine, dried and evaporated to give 2-fluorobenzene-1,4-diamine (**13**) in 74% yield.

Step (d): A suspension of *m*- or *p*-nitrophenol (2.78 g, 20.00 mmol, 1.00 equiv) and K_2CO_3 (5.53 g, 40.00 mmol, 2.00 equiv) in DMF (20 mL) was stirred at room temperature for 30 minutes, then benzyl bromide (3.59 g, 2.50 mL, 21.00 mmol, 1.05 equiv) was added dropwise over 10 minutes, and the reaction mixture was stirred at room temperature overnight. Upon completion of the reaction as indicated by TLC, the reaction mixture was poured into ice/water, stirred for 1 hr, filtered, washed with water then hexane, and dried to give the desired derivatives (**15a**,**b**) in 95-97% yield.

Step (e): A solution of the appropriate nitro derivative (**15a**-**d**) (2.29 g, 10.00 mmol, 1.00 equiv) and $SnCl_2.2H_2O$ (11.28 g, 50.00 mmol, 5.00 equiv) in ethyl acetate (150 mL) was refluxed for 6 hr. Upon completion of the reaction as indicated by TLC, the reaction mixture was cooled, washed with sodium bicarbonate solution (10%), brine, dried and evaporated to give the desired amine derivatives (**16a**,**b**) in 64-96% yield.

4.1.3. General procedure for the synthesis of target compounds 21a-r and 22a-e

The desired compounds **21a**-**r** and **22a**-**e** were synthesized according to the following procedures[22,53–55] and is illustrated as follows.

Step (a): A suspension of 4-bromo-1-fluoro-2-nitrobenzene (**3**) or 4-bromo-2-fluoro-1-nitrobenzene (**17**) (2.20 g, 10.00 mmol, 1.00 equiv), the appropriate amine derivative (**11a**,**b**, **13**, **16a**,**b**, **18a**-**e**) (11.00 mmol, 1.10 equiv), and K_2CO_3 (1.66 g, 12.00 mmol, 1.20 equiv) in DMF (20 mL) was heated at 80-90°C for 16 hr. Upon completion of the reaction as indicated by TLC, the reaction mixture was poured into ice/water, stirred for 1 hr, filtered, washed with water, and dried to yield the designated compounds (**19a**-**n**) in 30-83% yield.

Step (b): A solution of 2-substituted-4-nitroaniline derivative (**18f**-**h**) (11.00 mmol, 1.10 equiv) in DMF (20 mL) was cooled to 0°C, NaH (60% in mineral oil, 0.44 g, 11.00 mmol, 1.10 equiv) was added portion wise, and the reaction mixture was stirred at 0°C for 15 min. 4-bromo-1-fluoro-2-nitrobenzene (**3**), (2.2 g, 10.00 mmol, 1.00 equiv) in DMF (10 mL) was added dropwise and the reaction mixture was allowed to stir at room temperature for 2 hr. Upon completion of the reaction as indicated by TLC, the reaction mixture was poured into ice/H_2O, filtered, washed with water, and dried to yield the designated compounds (**19l**-**n**) in 67-99% yield.

Step (c): A solution of the appropriate nitro derivative (**19a**,**d**-**k**) (5.00 mmol, 1.00 equiv) and $SnCl_2.2H_2O$ (5.64 g, 25.00 mmol, 5.00 equiv) in ethyl acetate (50 mL) was refluxed for 12 hr. Upon completion of the reaction as indicated by TLC, the reaction mixture was cooled, washed with sodium bicarbonate solution (10%), brine, dried and evaporated to give the corresponding diamine derivatives that was used as such into the following step.

A solution of the appropriate crude diamine derivative (4.00 mmol) in formic acid (20 mL) was heated at 120°C for 1 hr. Upon completion of the reaction as indicated by TLC, the reaction mixture was cooled, diluted with cold water and neutralized with sodium carbonate solution (10%). The resulting solid was filtered and washed with diethyl ether or purified by flash chromatography to yield the designated compounds (**20a**,**d-k**) in 53-96% yield.

Step (d): The appropriate nitro/dinitro derivative (**19b**,**c**,**l**-**n**) (5.00 mmol, 1.00 equiv) was reduced using $SnCl_2.2H_2O$ and the resulting diamine/triamine was cyclized using formic acid as described previously in ***step (c)***. The resulting crude *N*-formyl derivative was refluxed in conc. HCl (15 mL) for 1 hr. Upon completion of the reaction as indicated by TLC, the reaction mixture was cooled, and sodium bicarbonate solution (10%) was added slowly to adjust to pH 9, the resulting solid was filtered, washed with water, and dried to yield the corresponding amine derivative that was used as such into the following step.

To a solution of the appropriate amine derivative obtained from the previous step (2.00 mmol, 1.00 equiv) in AcOH (10 mL) was added acetic anhydride (306 mg, 284 µL, 3.00 mmol, 1.50 equiv) and the reaction mixture was heated at 80°C for 2 hr. Upon

completion of the reaction as indicated by TLC, the reaction mixture was cooled, and sodium bicarbonate solution (10%) was added slowly to adjust to pH 9, the resulting solid was filtered, washed with water, dried, and washed with diethyl ether or purified by flash chromatography to yield the desired acetamido derivatives (**20b,c**,**l**-**n**) in 39-70% yield.

Step (e): A solution of the appropriate bromo derivative (**20a**-**n**) (0.60 mmol, 1.00 equiv) and 3- or 4-hydroxyphenylboronic acid (99 mg, 0.72 mmol, 1.20 equiv) in dioxane/water (4:1, 24 mL) was purged with nitrogen for 5 min then tetrakis(triphenylphosphine)palladium(0) (69 mg, 0.06 mmol, 0.10 equiv) and K_2CO_3 (249 mg, 1.80 mmol, 3.00 equiv) were added and the reaction was refluxed under nitrogen for 4 hr. Upon completion of the reaction as indicated by TLC, the mixture was cooled, filtered using celite, evaporated, and the resulting residue was extracted with ethyl acetate. The organic layer was dried over anhydrous Na_2SO_4, evaporated, and the resulting residue was purified by flash chromatography (DCM/MeOH or EtOAc/Hexane) to yield the desired compounds (**21a**-**d**,**f**,**h**-**r**).

***4.1.3.1. N*-{4-[5-(4-hydroxyphenyl)-1*H*-benzimidazol-1-yl]-2-methylphenyl}acetamide (21a).** R_f = 0.30 (DCM/MeOH 9.5:0.5). Off-white solid, 38% yield, **mp:** 280-283°C. **^{1}H NMR** (501 MHz, DMSO-d_6) δ 9.49 (s, 1H), 9.46 (s, 1H), 8.53 (s, 1H), 7.91 (d, *J* = 1.7 Hz, 1H), 7.68 (d, *J* = 8.5 Hz, 1H), 7.64 (d, *J* = 8.5 Hz, 1H), 7.55 (d, *J* = 2.9 Hz, 2H), 7.54 (s, 1H), 7.53 (s, 1H), 7.48 (d, *J* = 6.9 Hz, 1H), 6.86 (d, *J* = 8.6 Hz, 2H), 2.33 (s, 3H), 2.12 (s, 3H). **^{13}C NMR** (126 MHz, DMSO-d_6) δ 168.47, 156.76, 144.52, 143.75, 136.03, 135.26, 133.32, 132.46, 132.09, 131.52, 127.98(2C), 126.04, 125.21, 122.26, 121.02, 116.94, 115.73(2C), 110.94, 23.36, 17.95. **HRMS exact mass of** $C_{22}H_{20}N_3O_2$ **(M+H)$^+$:** 358.1550 amu; **found:** 358.1547 amu. **HPLC purity:** 98.42%, **HPLC t_R:** 2.24 min.

***4.1.3.2. N*-{4-[5-(4-hydroxyphenyl)-1*H*-benzimidazol-1-yl]-2-(trifluoromethyl)phenyl}acetamide (21b).** R_f = 0.35 (DCM/MeOH 9.7:0.3). White solid, 61% yield, **mp:** 254-257°C. **^{1}H NMR** (501 MHz, DMSO-d_6) δ 9.75 (s, 1H), 9.51 (s, 1H), 8.67 (s, 1H), 8.04 (s, 1H), 8.02 (d, *J* = 2.6 Hz, 1H), 7.94 (s, 1H), 7.75 (d, *J* = 8.4 Hz, 1H), 7.67 (d, *J* = 8.5 Hz, 1H), 7.58 (d, *J* = 8.4 Hz, 1H), 7.55 (d, *J* = 8.5 Hz, 2H), 6.87 (d, *J* = 8.6 Hz, 2H), 2.11 (s, 3H). **^{13}C NMR** (126 MHz, DMSO-d_6) δ 169.48, 156.83, 144.60, 143.94, 135.63, 134.76, 133.95, 132.02, 131.81, 131.36, 128.00 (2C), 127.78, 126.12 (q, $^2J_{C\text{-}F}$ = 33.9 Hz), 122.99 (q, $^1J_{C\text{-}F}$ = 274.0 Hz), 122.55, 121.50 (q, $^3J_{C\text{-}F}$ = 5.0 Hz), 117.06, 115.75 (2C), 110.78, 22.94. **HRMS exact mass of** $C_{22}H_{17}F_3N_3O_2$ **(M+H)$^+$:** 412.1265 amu; **found:** 412.1263 amu. **HPLC purity:** 98.64%, **HPLC t_R:** 2.50 min.

***4.1.3.3. N*-{2-fluoro-4-[5-(4-hydroxyphenyl)-1*H*-benzimidazol-1-yl]phenyl}acetamide (21c).** R_f = 0.30 (DCM/MeOH 9.5:0.5). Off-white solid, 35% yield, **mp:** 160-162°C. **^{1}H NMR** (501 MHz, DMSO-d_6) δ 10.07 (s, 1H), 9.50 (s, 1H), 8.54 (s, 1H), 8.35 (d, *J* = 3.8 Hz, 1H), 7.93 (s, 1H), 7.62 (d, *J* = 8.5 Hz, 1H), 7.57 (s, 1H), 7.55 (d, *J* = 8.5 Hz, 2H), 7.51 (d, *J* = 10.2 Hz, 1H), 7.46 (d, *J* = 3.4 Hz, 1H), 6.87 (d, *J* = 8.1 Hz, 2H), 2.15 (s, 3H). **^{13}C NMR** (126 MHz, DMSO-d_6) δ 169.27, 156.79, 151.83 (d, $^1J_{C\text{-}F}$ = 246.3 Hz), 144.48, 143.68, 135.44, 132.05, 131.93 (d, $^4J_{C\text{-}F}$ = 2.9 Hz), 131.42, 128.00 (2C), 127.57 (d, $^3J_{C\text{-}F}$ = 13.1 Hz), 122.42, 119.68 (d, $^3J_{C\text{-}F}$ = 7.9 Hz), 118.32, 117.05, 116.80 (d, $^2J_{C\text{-}F}$ = 21.2 Hz), 115.74 (2C), 110.65, 23.67. **HRMS exact mass of** $C_{21}H_{17}FN_3O_2$ **(M+H)$^+$:** 362.1299 amu; **found:** 362.1297 amu. **HPLC purity:** 99.67%, **HPLC t_R:** 2.32 min.

***4.1.3.4.* 4-(1-phenyl-1*H*-benzimidazol-5-yl)phenol (21h).** R_f = 0.20 (DCM/MeOH 9.8:0.2). Off-white solid, 65% yield, **mp:** >300°C (decomp.). **^{1}H NMR** (501 MHz, DMSO-d_6) δ 9.50 (s, 1H), 8.58 (s, 1H), 7.93 (d, *J* = 1.7 Hz, 1H), 7.71 (d, *J* = 7.4 Hz, 2H), 7.65 (d, *J* = 7.4 Hz, 2H), 7.63 (d, *J* = 2.8 Hz, 1H), 7.56 (d, *J* = 1.8 Hz, 2H), 7.54 (s, 1H), 7.50 (t, *J* = 7.4 Hz, 1H), 6.87 (d, *J* = 8.6 Hz, 2H). **^{13}C NMR** (126 MHz, DMSO-d_6) δ 156.79, 144.63, 143.76, 136.04, 135.37, 131.98, 131.47, 130.12 (2C), 127.99 (2C), 127.70, 123.52 (2C), 122.34, 117.00, 115.74 (2C), 110.88. **HRMS exact mass of** $C_{19}H_{15}N_2O$ **(M+H)$^+$:** 287.1179 amu; **found:** 287.1178 amu. **HPLC purity:** 99.23%, **HPLC t_R:** 2.62 min.

***4.1.3.5.* 4-[1-(3-fluorophenyl)-1*H*-benzimidazol-5-yl]phenol (21i).** R_f = 0.30 (DCM/MeOH 9.8:0.2). Buff solid, 30% yield, **mp:** 194-196°C. **^{1}H NMR** (501 MHz, DMSO-d_6) δ 10.17 (s, 1H), 9.57 (s, 1H), 9.50 (s, 1H), 8.62 (s, 1H), 8.35 (d, *J* = 1.8 Hz, 1H), 8.30 (d, *J* = 6.6 Hz, 1H), 7.93 (d, *J* = 1.7 Hz, 1H), 7.55 (d, *J* = 8.6 Hz, 2H), 7.41 (s, 1H), 6.87 (d, *J* = 2.1 Hz, 1H), 6.84 (d, *J* = 2.3 Hz, 2H).

***4.1.3.6.* 4-[1-(4-fluorophenyl)-1*H*-benzimidazol-5-yl]phenol (21j).** R_f = 0.25 (DCM/MeOH 9.8:0.2). Grey solid, 56% yield, **mp:** 280-282°C. **^{1}H NMR** (501 MHz, DMSO-d_6) δ 9.50 (s, 1H), 8.54 (s, 1H), 7.93 (d, *J* = 1.7 Hz, 1H), 7.76 (dd, *J* = 8.9, 4.8 Hz, 2H), 7.59 (d, *J* = 8.5 Hz, 1H), 7.55 (d, *J* = 1.7 Hz, 2H), 7.53 (s, 1H), 7.48 (t, *J* = 8.8 Hz, 2H), 6.87 (d, *J* = 8.5 Hz, 2H). **^{13}C NMR** (126 MHz, DMSO-d_6) δ 161.10 (d, $^1J_{C\text{-}F}$ = 245.1 Hz), 156.77, 144.45, 143.88, 135.38, 132.40 (d, $^4J_{C\text{-}F}$ = 2.9 Hz), 132.19, 131.45, 127.98 (2C), 125.94 (d, $^3J_{C\text{-}F}$ = 8.8 Hz), 122.34, 116.87 (d, $^2J_{C\text{-}F}$ = 20.5 Hz), 116.79, 115.73 (2C), 110.71. **HRMS exact mass of** $C_{19}H_{14}FN_2O$ **(M+H)$^+$:** 305.1085 amu; **found:** 305.1082 amu. **HPLC purity:** 98.89%, **HPLC t_R:** 2.70 min.

***4.1.3.7. N*-{3-[5-(4-hydroxyphenyl)-1*H*-benzimidazol-1-yl]phenyl}acetamide (21l).** R_f = 0.35 (DCM/MeOH 9.5:0.5). Light yellow solid, 80% yield, **mp:** 256-258°C. **^{1}H NMR** (501 MHz, DMSO-d_6) δ 10.29 (s, 1H), 9.51 (s, 1H), 8.57 (s, 1H), 8.05 (s, 1H), 7.93 (s,

1H), 7.84 – 7.77 (m, 1H), 7.72 (d, *J* = 13.0 Hz, 1H), 7.67 (d, *J* = 8.5 Hz, 1H), 7.59 (d, *J* = 10.2 Hz, 1H), 7.55 (d, *J* = 8.0 Hz, 2H), 7.35 (d, *J* = 8.0 Hz, 1H), 6.87 (d, *J* = 8.2 Hz, 2H), 2.10 (s, 3H). **^{13}C NMR** (126 MHz, DMSO-d_6) δ 168.83, 156.80, 144.64, 143.56, 140.72, 136.23, 135.44, 134.41, 131.83, 131.43, 130.46, 128.01 (2C), 122.36, 117.74, 117.07, 115.74 (2C), 113.47, 110.90, 24.10. **HRMS exact mass of** $C_{21}H_{18}N_3O_2$ **(M+H)$^+$:** 344.1394 amu; **found:** 344.1393 amu.

***4.1.3.8. N*-{4-[5-(4-hydroxyphenyl)-1*H*-benzimidazol-1-yl]phenyl}acetamide (21o: 4ACOH).**[22] R_f = 0.25 (DCM/MeOH 9.5:0.5). Light grey solid, 59% yield, **mp:** 293-295°C. **^{1}H NMR** (501 MHz, DMSO-d_6) δ 10.21 (s, 1H), 9.49 (s, 1H), 8.51 (s, 1H), 7.91 (d, *J* = 1.8 Hz, 1H), 7.83 (d, *J* = 8.8 Hz, 2H), 7.62 (d, *J* = 9.0 Hz, 2H), 7.59 (s, 1H), 7.54 (d, *J* = 1.8 Hz, 2H), 7.53 (d, *J* = 1.8 Hz, 1H), 6.86 (d, *J* = 8.6 Hz, 2H), 2.10 (s, 3H). **^{13}C NMR** (126 MHz, DMSO-d_6) δ 168.57, 156.76, 144.46, 143.73, 138.84, 135.25, 132.20, 131.53, 130.74, 127.98 (2C), 124.11 (2C), 122.24, 120.10 (2C), 116.92, 115.74 (2C), 110.85, 24.06. **HRMS exact mass of** $C_{21}H_{18}N_3O_2$ **(M+H)$^+$:** 344.1394 amu; **found:** 344.1396 amu.

***4.1.3.9. N*-{4-[5-(4-hydroxyphenyl)-1*H*-benzimidazol-1-yl]-3-methylphenyl}acetamide (21p).** R_f = 0.35 (DCM/MeOH 9.6:0.4). Off-white solid, 57% yield, **mp:** 166-168°C. **^{1}H NMR** (501 MHz, DMSO-d_6) δ 10.17 (s, 1H), 9.48 (s, 1H), 8.34 (s, 1H), 7.90 (s, 1H), 7.72 (s, 1H), 7.62 (d, *J* = 8.0 Hz, 1H), 7.52 (d, *J* = 8.6 Hz, 2H), 7.47 (d, *J* = 8.3 Hz, 1H), 7.35 (d, *J* = 8.5 Hz, 1H), 7.15 (d, *J* = 8.4 Hz, 1H), 6.86 (d, *J* = 8.6 Hz, 2H), 2.10 (s, 3H), 2.02 (s, 3H). **^{13}C NMR** (126 MHz, DMSO-d_6) δ 168.64, 156.70, 144.71, 143.72, 139.94, 135.11, 135.07, 133.57, 131.73, 129.19, 128.02 (2C), 127.94, 122.22, 121.12, 117.52, 116.88, 115.72 (2C), 110.58, 24.09, 17.51. **HRMS exact mass of** $C_{22}H_{20}N_3O_2$ **(M+H)$^+$:** 358.1550 amu; **found:** 358.1548 amu. **HPLC purity:** 99.45%, **HPLC t_R:** 2.33 min.

***4.1.3.10. N*-{4-[5-(4-hydroxyphenyl)-1*H*-benzimidazol-1-yl]-3-(trifluoromethyl)phenyl}acetamide (21q).** R_f = 0.35 (DCM/MeOH 9.6:0.4). Light orange solid, 24% yield, **mp:** 123-125°C. **^{1}H NMR** (501 MHz, DMSO-d_6) δ 10.58 (s, 1H), 9.48 (s, 1H), 8.34 (s, 1H), 8.32 (s, 1H), 8.01 (d, *J* = 7.1 Hz, 1H), 7.89 (s, 1H), 7.65 (d, *J* = 8.7 Hz, 1H), 7.52 (d, *J* = 8.6 Hz, 2H), 7.47 (d, *J* = 6.9 Hz, 1H), 7.14 (d, *J* = 8.4 Hz, 1H), 6.85 (d, *J* = 8.6 Hz, 2H), 2.15 (s, 3H). **^{13}C NMR** (126 MHz, DMSO-d_6) δ 169.29, 156.73, 145.18, 143.29, 140.79, 135.31, 135.07, 131.88, 131.60, 128.04 (2C), 127.09, 127.07 (q, $^2J_{C\text{-}F}$ = 30.3 Hz), 123.14, 122.87 (q, $^1J_{C\text{-}F}$ = 274.0 Hz), 122.46, 116.77, 116.70 (q, $^3J_{C\text{-}F}$ = 4.7 Hz), 115.71 (2C), 110.44, 24.15. **HRMS exact mass of** $C_{22}H_{17}F_3N_3O_2$ **(M+H)$^+$:** 412.1267 amu; **found:** 412.1265 amu. **HPLC purity:** 97.32%, **HPLC t_R:** 2.65 min.

***4.1.3.11. N*-{3-fluoro-4-[5-(4-hydroxyphenyl)-1*H*-benzimidazol-1-yl]phenyl}acetamide (21r).** R_f = 0.30 (DCM/MeOH 9.6:0.4). Light yellow solid, 42% yield, **mp:** 284-286°C. **^{1}H NMR** (501 MHz, DMSO-d_6) δ 10.43 (s, 1H), 9.49 (s, 1H), 8.44 (s, 1H), 7.94 (d, *J* = 2.3 Hz, 1H), 7.91 (d, *J* = 1.8 Hz, 1H), 7.67 (t, *J* = 8.7 Hz, 1H), 7.54 (d, *J* = 1.5 Hz, 2H), 7.52 (s, 1H), 7.50 (d, *J* = 7.3 Hz, 1H), 7.36 (d, *J* = 8.2 Hz, 1H), 6.86 (d, *J* = 8.6 Hz, 2H), 2.12 (s, 3H). **^{13}C NMR** (126 MHz, DMSO-d_6) δ 169.02, 156.76, 155.73 (d, $^1J_{C\text{-}F}$ = 247.3 Hz), 144.49, 143.76, 140.93 (d, $^3J_{C\text{-}F}$ = 10.7 Hz), 135.41, 132.93, 131.52, 128.13, 128.02 (2C), 122.41, 117.64 (d, $^3J_{C\text{-}F}$ = 12.9 Hz), 116.89, 115.72 (2C), 115.34 (d, $^4J_{C\text{-}F}$ = 3.3 Hz), 110.73, 106.85 (d, $^2J_{C\text{-}F}$ = 24.8 Hz), 24.13. **HRMS exact mass of** $C_{21}H_{17}FN_3O_2$ **(M+H)$^+$:** 362.1299 amu; **found:** 362.1300 amu. **HPLC purity:** 99.25%, **HPLC t_R:** 2.38 min.

Step (f): To a solution of the appropriate benzyloxy derivative (**21d**,**f**) (250 mg, 0.64 mmol) in MeOH (20 mL) was added Pd/C (10% w/w, 25 mg) and the reaction mixture was stirred under H_2 using a balloon overnight. Upon completion of the reaction as indicated by TLC, the mixture was filtered using celite, evaporated, and the resulting residue was purified by flash chromatography (DCM/MeOH) to yield the desired compounds (**21e**,**g**).

***4.1.3.12.* 3-[5-(4-hydroxyphenyl)-1*H*-benzimidazol-1-yl]phenol (21e).** R_f = 0.35 (DCM/MeOH 9.5:0.5). White solid, 54% yield, **mp:** 261-264°C. **^{1}H NMR** (501 MHz, DMSO-d_6) δ 10.01 (s, 1H), 9.51 (s, 1H), 8.54 (s, 1H), 7.92 (s, 1H), 7.63 (d, *J* = 8.5 Hz, 1H), 7.56 (d, *J* = 1.7 Hz, 1H), 7.54 (d, *J* = 8.6 Hz, 2H), 7.42 (t, *J* = 8.0 Hz, 1H), 7.10 (d, *J* = 8.8 Hz, 1H), 7.06 (s, 1H), 6.90 (d, *J* = 6.2 Hz, 1H), 6.87 (d, *J* = 8.6 Hz, 2H). **^{13}C NMR** (126 MHz, DMSO-d_6) δ 158.71, 156.79, 144.61, 143.66, 137.03, 135.34, 131.91, 131.48, 130.96, 128.00 (2C), 122.31, 117.00, 115.75 (2C), 114.74, 113.85, 110.97, 110.29. **HRMS exact mass of** $C_{19}H_{15}N_2O_2$ **(M+H)$^+$:** 303.1128 amu; **found:** 303.1126 amu. **HPLC purity:** 97.65%, **HPLC t_R:** 2.36 min.

***4.1.3.13.* 4-[5-(4-hydroxyphenyl)-1*H*-benzimidazol-1-yl]phenol (21g).** R_f = 0.30 (DCM/MeOH 9.5:0.5). Light violet solid, 77% yield, **mp:** 288-290°C. **^{1}H NMR** (501 MHz, DMSO-d_6) δ 9.88 (s, 1H), 9.49 (s, 1H), 8.43 (s, 1H), 7.90 (s, 1H), 7.53 (d, *J* = 8.6 Hz, 2H), 7.51 (d, *J* = 1.3 Hz, 2H), 7.46 (d, *J* = 8.7 Hz, 2H), 6.99 (d, *J* = 8.7 Hz, 2H), 6.86 (d, *J* = 8.6 Hz, 2H). **^{13}C NMR** (126 MHz, DMSO-d_6) δ 157.12, 156.72, 144.28, 143.91, 135.06, 132.66, 131.62, 127.97 (2C), 127.36, 125.41 (2C), 122.10, 116.83, 116.36 (2C), 115.73 (2C), 110.71. **HRMS exact mass of** $C_{19}H_{15}N_2O_2$ **(M+H)$^+$:** 303.1128 amu; **found:** 303.1125 amu.

Step (g): A suspension of the appropriate phenol derivative (**21k**-**o**) (206 mg, 0.60 mmol, 1.00 equiv), Cs_2CO_3 (0.39 g, 1.20 mmol, 2.00 equiv), KI (0.20 g, 1.20 mmol, 2.00 equiv), and 1-(2-chloroethyl)piperidine hydrochloride (221 mg, 1.20 mmol, 2.00 equiv)

in DMF (5 mL) was heated at 80-90°C for 48 hr. Upon completion of the reaction as indicated by TLC, the reaction mixture was poured into ice/water, stirred for 1 hr, filtered, washed with water, dried, and purified by flash chromatography (DCM/MeOH) to yield the desired derivatives (**22a**-**e**).

***4.1.3.14. N*-[3-(5-{3-[2-(piperidin-1-yl)ethoxy]phenyl}-1*H*-benzimidazol-1-yl)phenyl]acetamide (22a).** R_f = 0.35 (DCM/MeOH/NH_3 9.3:0.7:0.02). Buff solid, 63% yield, **mp:** 82-85°C. **^{1}H NMR** (501 MHz, DMSO-d_6) δ 10.29 (s, 1H), 8.61 (s, 1H), 8.07 (s, 2H), 7.70 (d, *J* = 8.5 Hz, 1H), 7.67 (d, *J* = 8.6 Hz, 1H), 7.61 (d, *J* = 8.2 Hz, 1H), 7.55 (t, *J* = 8.0 Hz, 1H), 7.39 – 7.36 (m, 1H), 7.35 (d, *J* = 3.4 Hz, 1H), 7.30 (s, 1H), 7.28 (d, *J* = 2.3 Hz, 1H), 6.92 (d, *J* = 5.6 Hz, 1H), 4.17 (t, *J* = 6.0 Hz, 2H), 2.69 (t, *J* = 6.0 Hz, 2H), 2.49 – 2.39 (m, 4H), 2.10 (s, 3H), 1.50 (p, *J* = 5.5 Hz, 4H), 1.38 (p, *J* = 5.8 Hz, 2H). **^{13}C NMR** (126 MHz, DMSO-d_6) δ 168.83, 159.04, 144.55, 143.85, 142.15, 140.73, 136.15, 135.13, 132.57, 130.47, 129.95, 122.92, 119.30, 118.13, 117.89, 117.82, 113.55, 113.34, 112.91, 110.96, 65.53, 57.45, 54.41 (2C), 25.53 (2C), 24.10, 23.89. **HRMS exact mass of** $C_{28}H_{31}N_4O_2$ **(M+H)$^+$:** 455.2442 amu; **found:** 455.2441 amu. **HPLC purity:** 99.28%, **HPLC t_R:** 2.27 min.

***4.1.3.15. N*-[3-(5-{4-[2-(piperidin-1-yl)ethoxy]phenyl}-1*H*-benzimidazol-1-yl)phenyl]acetamide (22b).** R_f = 0.30 (DCM/MeOH/NH_3 9.3:0.7:0.02). Off-white solid, 68% yield, **mp:** 158-160°C. **^{1}H NMR** (501 MHz, DMSO-d_6) δ 10.31 (s, 1H), 8.58 (s, 1H), 8.07 (s, 1H), 7.98 (s, 1H), 7.69 (d, *J* = 8.5 Hz, 1H), 7.66 (d, *J* = 8.4 Hz, 2H), 7.63 – 7.61 (m, 1H), 7.60 (d, *J* = 3.3 Hz, 1H), 7.55 (t, *J* = 8.0 Hz, 1H), 7.36 (d, *J* = 7.7 Hz, 1H), 7.04 (d, *J* = 8.4 Hz, 2H), 4.12 (t, *J* = 5.9 Hz, 2H), 2.70 (s, 2H), 2.47 (s, 4H), 2.10 (s, 3H), 1.51 (p, *J* = 5.6 Hz, 4H), 1.38 (p, *J* = 5.9 Hz, 2H). **^{13}C NMR** (126 MHz, DMSO-d_6) δ 168.82, 157.82, 144.64, 143.67, 140.73, 136.19, 134.98, 133.04, 132.04, 130.45, 128.00 (2C), 122.46, 117.83, 117.75, 117.34, 114.97 (2C), 113.48, 110.97, 65.56, 57.29, 54.35 (2C), 25.47, 24.09 (2C), 23.84. **HRMS exact mass of** $C_{28}H_{31}N_4O_2$ **(M+H)$^+$:** 455.2442 amu; **found:** 455.2442 amu. **HPLC purity:** 99.35%, **HPLC t_R:** 2.17 min.

***4.1.3.16. N*-[3-(6-{3-[2-(piperidin-1-yl)ethoxy]phenyl}-1*H*-benzimidazol-1-yl)phenyl]acetamide (22c).** R_f = 0.3 (DCM/MeOH/NH_3 9.5:0.5:0.03). Buff solid, 26% yield, **mp:** 81-83°C. **^{1}H NMR** (501 MHz, DMSO-d_6) δ 10.28 (s, 1H), 8.60 (s, 1H), 8.12 (s, 1H), 7.87 (s, 1H), 7.84 (d, *J* = 8.5 Hz, 1H), 7.62 (d, *J* = 8.4 Hz, 1H), 7.59 (d, *J* = 8.3 Hz, 1H), 7.55 (t, *J* = 7.9 Hz, 1H), 7.41 (d, *J* = 7.6 Hz, 1H), 7.35 (t, *J* = 7.8 Hz, 1H), 7.27 (s, 1H), 7.25 (s, 1H), 6.92 (d, *J* = 9.2 Hz, 1H), 4.15 (t, *J* = 5.9 Hz, 2H), 2.66 (t, *J* = 5.9 Hz, 2H), 2.43 (s, 4H), 2.09 (s, 3H), 1.48 (p, *J* = 5.6 Hz, 4H), 1.36 (q, *J* = 5.9 Hz, 2H). **^{13}C NMR** (126 MHz, DMSO-d_6) δ 168.86, 159.06, 143.84, 143.55, 142.28, 140.67, 136.16, 136.10, 133.42, 130.52, 129.98, 122.14, 120.28, 119.50, 117.82, 117.80, 113.65, 113.60, 113.03, 108.88, 65.60, 57.46, 54.43 (2C), 25.55 (2C), 24.10, 23.91. **HRMS exact mass of** $C_{28}H_{31}N_4O_2$ **(M+H)$^+$:** 455.2442 amu; **found:** 455.2443 amu. **HPLC purity:** 95.92%, **HPLC t_R:** 2.19 min.

***4.1.3.17. N*-[3-(6-{4-[2-(piperidin-1-yl)ethoxy]phenyl}-1*H*-benzimidazol-1-yl)phenyl]acetamide (22d).** R_f = 0.35 (DCM/MeOH/NH_3 9.3:0.7:0.03). Off-white solid, 33% yield, **mp:** 149-152°C. **^{1}H NMR** (501 MHz, DMSO-d_6) δ 10.30 (s, 1H), 8.56 (s, 1H), 8.07 (s, 1H), 7.82 (d, *J* = 8.4 Hz, 1H), 7.78 (s, 1H), 7.64 (d, *J* = 3.1 Hz, 2H), 7.62 (s, 1H), 7.57 (d, *J* = 2.6 Hz, 1H), 7.56 – 7.52 (m, 1H), 7.40 (d, *J* = 7.1 Hz, 1H), 7.02 (d, *J* = 8.2 Hz, 2H), 4.11 (t, *J* = 5.9 Hz, 2H), 2.69 (s, 2H), 2.46 (s, 4H), 2.09 (s, 3H), 1.50 (p, *J* = 5.6 Hz, 4H), 1.38 (q, *J* = 6.0 Hz, 2H). **^{13}C NMR** (126 MHz, DMSO-d_6) δ 168.84, 157.96, 143.56, 142.97, 140.71, 136.14, 135.99, 133.57, 133.15, 130.51, 128.20 (2C), 121.67, 120.26, 117.94, 117.84, 114.99 (2C), 113.70, 108.08, 65.55, 57.26, 54.34 (2C), 25.45, 24.11 (2C), 23.82. **HRMS exact mass of** $C_{28}H_{31}N_4O_2$ **(M+H)$^+$:** 454.2442 amu; **found:** 455.2444 amu. **HPLC purity:** 95.87%, **HPLC t_R:** 2.07 min.

***4.1.3.18. N*-[4-(5-{4-[2-(piperidin-1-yl)ethoxy]phenyl}-1*H*-benzimidazol-1-yl)phenyl]acetamide (22e: 4ACP).**[22] R_f = 0.35 (DCM/MeOH/NH_3 9.2:0.8:0.03). Off-white solid, 53% yield, **mp:** 176-178°C. **^{1}H NMR** (501 MHz, DMSO-d_6) δ 10.24 (s, 1H), 8.52 (s, 1H), 7.96 (d, *J* = 1.7 Hz, 1H), 7.84 (d, *J* = 8.3 Hz, 2H), 7.65 (s, 1H), 7.63 (d, *J* = 2.7 Hz, 2H), 7.61 (d, *J* = 2.0 Hz, 2H), 7.57 (d, *J* = 10.2 Hz, 1H), 7.03 (d, *J* = 8.5 Hz, 2H), 4.11 (t, *J* = 5.9 Hz, 2H), 2.68 (t, *J* = 5.8 Hz, 2H), 2.45 (s, 4H), 2.10 (s, 3H), 1.51 (p, *J* = 5.6 Hz, 4H), 1.43 – 1.32 (m, 2H). **^{13}C NMR** (126 MHz, DMSO-d_6) δ 168.57, 157.80, 144.46, 143.84, 138.87, 134.79, 133.11, 132.41, 130.69, 127.97 (2C), 124.11 (2C), 122.32, 120.08 (2C), 117.18, 114.96 (2C), 110.92, 65.61, 57.33, 54.38 (2C), 25.52, 24.05 (2C), 23.88. **HRMS exact mass of** $C_{28}H_{31}N_4O_2$ **(M+H)$^+$:** 455.2442 amu; **found:** 455.2441 amu. **HPLC purity:** 97.63%, **HPLC t_R:** 2.11 min.

4.1.4. General procedure for the synthesis of target compound 25

The desired compound **25** was synthesized according to the following procedures[22,51,56] and is illustrated as follows.

Step (a): A solution of *N*-(4-((4-bromo-2-nitrophenyl)amino)phenyl)acetamide (**19k**) (1.75 g, 5.00 mmol, 1.00 equiv) and $SnCl_2.2H_2O$ (5.64 g, 25.00 mmol, 5.00 equiv) in ethyl acetate (50 mL) was refluxed for 12 hr. Upon completion of the reaction as

indicated by TLC, the reaction mixture was cooled, washed with sodium bicarbonate solution (10%), brine, dried and evaporated to give the corresponding diamine derivative that was used as such into the following step.

A solution of the appropriate crude diamine derivative (1.11 g, 4.00 mmol, 1.00 equiv) and glycolic acid (70% in water, 1.74 mL, 16.00 mmol, 4.00 equiv) in 4N HCl (12 mL) was refluxed for 12 hr. Upon completion of the reaction as indicated by TLC, the reaction mixture was cooled, diluted with cold water and neutralized with sodium carbonate solution (10%). The resulting solid was filtered and purified by flash chromatography (DCM/MeOH 9.7:0.3) to yield (1-(4-aminophenyl)-5-bromo-1*H*-benzimidazol-2-yl)methanol (**23**) in 20% yield.

Step (b): To a solution of (1-(4-aminophenyl)-5-bromo-1*H*-benzimidazol-2-yl)methanol (**23**) (0.26 g, 0.82 mmol, 1.00 equiv) in THF (5 mL) was added acetic anhydride (0.13 g, 116 µL, 1.23 mmol, 1.50 equiv) dropwise and the reaction mixture was stirred at rt for 12 hr. Upon completion of the reaction as indicated by TLC, the reaction mixture was evaporated and purified by flash chromatography (DCM/MeOH 9.7:0.3) to yield *N*-(4-(5-bromo-2-(hydroxymethyl)-1*H*-benzimidazol-1-yl)phenyl)acetamide (**24**) in 72% yield.

Step (c): A solution of *N*-(4-(5-bromo-2-(hydroxymethyl)-1*H*-benzimidazol-1-yl)phenyl)acetamide (**24**) (200 mg, 0.56 mmol, 1.00 equiv) and 4-hydroxyphenylboronic acid (92 mg, 0.67 mmol, 1.20 equiv) in dioxane/water (4:1, 24 mL) was purged with nitrogen for 5 min then tetrakis(triphenylphosphine)palladium(0) (65 mg, 0.056 mmol, 0.10 equiv) and K_2CO_3 (232 mg, 1.68 mmol, 3.00 equiv) were added and the reaction was refluxed under nitrogen for 4 hr. Upon completion of the reaction as indicated by TLC, the mixture was cooled, filtered using celite, evaporated, and the resulting residue was extracted with ethyl acetate. The organic layer was dried over anhydrous Na_2SO_4, evaporated, and the resulting residue was purified by flash chromatography (DCM/MeOH) to yield the final compound (**25**).

***4.1.4.1. N*-{4-[2-(hydroxymethyl)-5-(4-hydroxyphenyl)-1*H*-benzimidazol-1-yl]phenyl}acetamide (25).** Rf = 0.30 (DCM/MeOH 9.2:0.8). Violet solid, 38% yield, **mp:** 179-180°C. **^{1}H NMR** (501 MHz, DMSO-d_6) δ 10.24 (s, 1H), 9.48 (s, 1H), 7.83 (d, *J* = 6.8 Hz, 2H), 7.81 (s, 1H), 7.51 (d, *J* = 8.3 Hz, 4H), 7.45 (d, *J* = 7.3 Hz, 1H), 7.20 (d, *J* = 8.4 Hz, 1H), 6.86 (d, *J* = 8.1 Hz, 2H), 5.52 (t, *J* = 5.7 Hz, 1H), 4.56 (d, *J* = 5.5 Hz, 2H), 2.11 (s, 3H). **^{13}C NMR** (126 MHz, DMSO-d_6) δ 168.66, 156.69, 154.26, 142.65, 139.50, 135.14, 135.12, 131.73, 130.04, 127.95 (2C), 127.14 (2C), 121.95, 119.81 (2C), 116.35, 115.72 (2C), 110.51, 55.89, 24.08. **HRMS exact mass of** $C_{22}H_{20}N_3O_3$ **(M+H)$^+$:** 374.1499 amu; **found:** 374.1498 amu.

4.1.5. General procedure for the synthesis of target compounds 28a-n

The desired final compounds **28a**-**n** were synthesized according to the following procedures[22,55,57–59] and is illustrated as follows.

Step (a): A suspension of the appropriate acetamido derivative (**20i**,**k**) (6.60 g, 20.00 mmol) in conc. HCl (100 mL) was refluxed for 1 hr. Upon completion of the reaction as indicated by TLC, the reaction mixture was cooled, and sodium bicarbonate solution (10%) was added slowly to adjust to pH 9, the resulting solid was filtered, washed with water, and dried to yield the corresponding amine derivative (**26a**,**b**) in 82-93% yield.

Step (b): A solution of the appropriate amine derivative (**26a**,**b**) (0.58 g, 2.00 mmol, 1.00 equiv) in pyridine (10 mL) was cooled to 0ºC in an ice bath, then ethyl chloroformate (0.26 g, 228 µL, 2.40 mmol, 1.20 equiv) or cyclopropanecarbonyl chloride (0.25 g, 218 µL, 2.40 mmol, 1.20 equiv) was added and the reaction mixture was stirred at rt for 4 hr. Upon completion of the reaction as indicated by TLC, the reaction mixture was evaporated, and the residue was stirred with cold water. The resulting solid was filtered, washed with water, and dried to yield the desired derivative (**27a**-**d**) in 53-90% yield.

Step (c): To a solution of the appropriate amine derivative (**26a**,**b**) (0.58 g, 2.00 mmol, 1.00 equiv) in dry THF (20 mL) was added triphosgene (0.59 g, 2.00 mmol, 1.00 equiv) and the reaction mixture was purged and refluxed under nitrogen for 2 h. Upon the reaction completion as indicated by TLC the solution was concentrated under reduced pressure. The resulting residue was dissolved in dry THF (20 mL) and DIPEA (0.52 g, 697 µl, 4.00 mmol, 2.00 equiv) was added, then methylamine hydrochloride (0.27 g, 4.00 mmol, 2.00 equiv) or cyclopropylamine (0.79 g, 962 µL, 4.00 mmol, 2.00 equiv) was added, and the reaction mixture was refluxed under nitrogen for 24 h. Upon completion of the reaction as indicated by TLC, the solution was concentrated, and the residue was purified by flash chromatography (DCM/MeOH) to give the desired derivative (**27e**-**h**) in 30-78% yield.

Step (d): A solution of the appropriate amine derivative (**26a**,**b**) (0.58 g, 2.00 mmol, 1.00 equiv) in pyridine (10 mL) was cooled to 0ºC in an ice bath, then methanesulfonyl chloride (0.28 g, 187 µL, 2.40 mmol, 1.20 equiv) or cyclopropanesulfonyl chloride (0.34 g,

245 µL, 2.40 mmol, 1.20 equiv) was added and the reaction mixture was stirred at rt for 48 hr. Upon completion of the reaction as indicated by TLC, the reaction mixture was evaporated, and the residue was stirred with cold water. The resulting solid was filtered, washed with water, and dried to yield the desired derivative (**27i**-**l**) in 54-95% yield.

Step (e): A solution of the appropriate amine derivative (**26a**,**b**) (0.58 g, 2.00 mmol, 1.00 equiv) in formic acid (10 mL) was heated at 120ºC for 1 hr. Upon completion of the reaction as indicated by TLC, the reaction mixture was cooled, diluted with cold water and neutralized with sodium carbonate solution (10%). The resulting solid was filtered and purified by flash chromatography (DCM/MeOH) to yield the designated compounds (**27m**,**n**) in 21-38% yield.

Step (f): The appropriate bromo derivative (**27a**-**n**) was coupled with 4-hydroxyphenylboronic acid as described previously in section **4.1.1.**, ***step (e)*** and the resulting residue was purified by flash chromatography (DCM/MeOH) to yield the desired compounds (**28a**-**n**).

4.1.5.1. **Ethyl {3-[5-(4-hydroxyphenyl)-1*H*-benzimidazol-1-yl]phenyl}carbamate (28a).** Rf = 0.25 (DCM/MeOH 9.7:0.3). Buff solid, 66% yield, **mp:** 234-236°C. **^{1}H NMR** (501 MHz, DMSO-d6) δ 9.97 (s, 1H), 9.50 (s, 1H), 8.56 (s, 1H), 7.93 (d, J = 1.7 Hz, 1H), 7.88 (s, 1H), 7.67 (d, J = 8.5 Hz, 1H), 7.58 (d, J = 1.8 Hz, 1H), 7.56 (s, 1H), 7.55 (s, 1H), 7.54 – 7.51 (m, 2H), 7.31 (t, J = 2.7 Hz, 1H), 6.87 (d, J = 8.6 Hz, 2H), 4.16 (q, J = 7.1 Hz, 2H), 1.26 (t, J = 7.1 Hz, 3H). **^{13}C NMR** (126 MHz, DMSO-d_6) δ 156.79, 153.61, 144.63, 143.56, 140.77, 136.38, 135.42, 131.83, 131.43, 130.52, 128.00 (2C), 127.99, 122.37, 117.07, 117.05, 115.73 (2C), 112.61, 110.90, 60.47, 14.48. **HRMS exact mass of** $C_{22}H_{20}N_3O_3$ **(M+H)$^+$:** 374.1499 amu; **found:** 374.1498 amu. **HPLC purity:** 96.02%, **HPLC t_R:** 2.77 min.

4.1.5.2. **Ethyl {4-[5-(4-hydroxyphenyl)-1*H*-benzimidazol-1-yl]phenyl}carbamate (28b).** Rf = 0.20 (DCM/MeOH 9.7:0.3). Crystalline white solid, 77% yield, **mp:** 285-287°C. **^{1}H NMR** (501 MHz, DMSO-d_6) δ 9.91 (s, 1H), 9.49 (s, 1H), 8.49 (s, 1H), 7.91 (d, *J* = 1.1 Hz, 1H), 7.71 (d, *J* = 8.9 Hz, 2H), 7.61 (d, *J* = 9.0 Hz, 2H), 7.58 (d, *J* = 0.7 Hz, 1H), 7.55 (s, 1H), 7.53 (d, *J* = 2.1 Hz, 2H), 6.86 (d, *J* = 8.6 Hz, 2H), 4.17 (q, *J* = 7.1 Hz, 2H), 1.27 (t, *J* = 7.1 Hz, 3H). **^{13}C NMR** (126 MHz, DMSO-d_6) δ 156.75, 153.60, 144.44, 143.76, 138.84, 135.21, 132.27, 131.55, 130.24, 127.98 (2C), 124.28 (2C), 122.22 (2C), 119.18, 116.91, 115.73 (2C), 110.83, 60.39, 14.50. **HRMS exact mass of** $C_{22}H_{20}N_3O_3$ **(M+H)$^+$:** 374.1499 amu; **found:** 374.1499 amu. **HPLC purity:** 98.47%, **HPLC t_R:** 2.74 min.

4.1.5.3. ***N*-{3-[5-(4-hydroxyphenyl)-1*H*-benzimidazol-1-yl]phenyl}cyclopropanecarboxamide (28c).** Rf = 0.35 (DCM/MeOH 9.6:0.4). White solid, 46% yield, **mp:** 276-278°C. **^{1}H NMR** (501 MHz, DMSO-d_6) δ 10.53 (s, 1H), 9.50 (s, 1H), 8.57 (s, 1H), 8.06 (d, *J* = 2.2 Hz, 1H), 7.93 (s, 1H), 7.67 (d, *J* = 8.5 Hz, 1H), 7.62 (d, *J* = 8.0 Hz, 1H), 7.58 (d, *J* = 1.7 Hz, 1H), 7.56 (s, 1H), 7.54 (d, *J* = 6.8 Hz, 2H), 7.35 (d, *J* = 9.1 Hz, 1H), 6.87 (d, *J* = 8.6 Hz, 2H), 1.88 – 1.74 (m, 1H), 0.85 (m, 4H). **^{13}C NMR** (126 MHz, DMSO-d_6) δ 172.16, 156.80, 144.64, 143.57, 140.72, 136.27, 135.42, 131.83, 131.44, 130.47, 128.01 (2C), 122.38, 117.80, 117.66, 117.06, 115.74 (2C), 113.55, 110.90, 14.70, 7.44 (2C). **HRMS exact mass of** $C_{23}H_{20}N_3O_2$ **(M+H)$^+$:** 370.1550 amu; **found:** 370.1547 amu. **HPLC purity:** 98.97%, **HPLC t_R:** 2.62 min.

4.1.5.4. ***N*-{4-[5-(4-hydroxyphenyl)-1*H*-benzimidazol-1-yl]phenyl}cyclopropanecarboxamide (28d).** Rf = 0.30 (DCM/MeOH 9.6:0.4). Off-white solid, 72% yield, **mp:** 194-196°C. **^{1}H NMR** (501 MHz, DMSO-d_6) δ 10.46 (s, 1H), 9.49 (s, 1H), 8.51 (s, 1H), 7.91 (d, *J* = 1.5 Hz, 1H), 7.84 (d, *J* = 8.9 Hz, 2H), 7.62 (d, *J* = 8.7 Hz, 2H), 7.59 (d, *J* = 0.7 Hz, 1H), 7.55 (s, 1H), 7.53 (d, *J* = 2.2 Hz, 2H), 6.86 (d, *J* = 8.6 Hz, 2H), 1.87 – 1.76 (m, 1H), 0.86 – 0.82 (m, 4H). **^{13}C NMR** (126 MHz, DMSO-d_6) δ 171.91, 156.76, 144.47, 143.74, 138.86, 135.24, 132.21, 131.54, 130.68, 127.98 (2C), 124.13 (2C), 122.24, 120.09 (2C), 116.93, 115.74 (2C), 110.86, 14.65, 7.39 (2C). **HRMS exact mass of** $C_{23}H_{20}N_3O_2$ **(M+H)$^+$:** 370.1550 amu; **found:** 370.1552 amu. **HPLC purity:** 95.48%, **HPLC t_R:** 2.58 min.

4.1.5.5. **1-{3-[5-(4-hydroxyphenyl)-1*H*-benzimidazol-1-yl]phenyl}-3-methylurea (28e).** Rf = 0.15 (DCM/MeOH 9.5:0.5). Buff solid, 22% yield, **mp:** 208-210°C. **^{1}H NMR** (501 MHz, DMSO-d_6) δ 9.50 (s, 1H), 8.90 (s, 1H), 8.54 (s, 1H), 7.92 (s, 2H), 7.67 (d, *J* = 8.5 Hz, 1H), 7.58 (d, *J* = 1.7 Hz, 1H), 7.55 (d, *J* = 8.6 Hz, 2H), 7.46 (t, *J* = 8.0 Hz, 1H), 7.38 (d, *J* = 8.7 Hz, 1H), 7.19 (d, *J* = 6.9 Hz, 1H), 6.87 (d, *J* = 8.6 Hz, 2H), 6.17 (q, *J* = 4.6 Hz, 1H), 2.67 (d, *J* = 4.6 Hz, 3H). **^{13}C NMR** (126 MHz, DMSO-d_6) δ 156.79, 155.81, 144.63, 143.56, 142.21, 136.29, 135.35, 131.90, 131.48, 130.28, 128.00 (2C), 122.33, 117.02, 116.56, 115.74 (2C), 115.59, 112.15, 110.97, 26.28. **HRMS exact mass of** $C_{21}H_{19}N_4O_2$ **(M+H)$^+$:** 359.1503 amu; **found:** 359.1505 amu.

4.1.5.6. **1-{4-[5-(4-hydroxyphenyl)-1*H*-benzimidazol-1-yl]phenyl}-3-methylurea (28f).** Rf = 0.25 (DCM/MeOH 9.3:0.7). Pink solid, 55% yield, **mp:** 274-276°C. **^{1}H NMR** (501 MHz, DMSO-d_6) δ 9.49 (s, 1H), 8.81 (s, 1H), 8.47 (s, 1H), 7.90 (d, *J* = 1.7 Hz, 1H), 7.64 (d, *J* = 8.9 Hz, 2H), 7.57 (d, *J* = 8.5 Hz, 1H), 7.54 (s, 1H), 7.54 (d, *J* = 1.5 Hz, 2H), 7.52 (d, *J* = 1.9 Hz, 2H), 6.86 (d, *J* = 8.6 Hz, 2H), 6.11 (q, *J* = 4.6 Hz, 1H), 2.68 (d, *J* = 4.6 Hz, 3H). **^{13}C NMR** (126 MHz, DMSO-d_6) δ 156.73, 155.78, 144.40, 143.78, 140.37, 135.13,

132.39, 131.58, 128.96, 127.97 (2C), 124.24 (2C), 122.15, 118.59 (2C), 116.88, 115.73 (2C), 110.80, 26.29. **HRMS exact mass of** $C_{21}H_{19}N_4O_2$ **(M+H)$^+$:** 359.1503 amu; **found:** 359.1503 amu. **HPLC purity:** 97.29%, **HPLC t_R:** 2.20 min.

4.1.5.7. **1-cyclopropyl-3-{3-[5-(4-hydroxyphenyl)-1*H*-benzimidazol-1-yl]phenyl}urea (28g).** Rf = 0.25 (DCM/MeOH 9.5:0.5). Buff solid, 58% yield, **mp:** 166-168°C. **^{1}H NMR** (501 MHz, DMSO-d_6) δ 9.51 (s, 1H), 8.69 (s, 1H), 8.55 (s, 1H), 7.93 (s, 1H), 7.93 (s, 1H), 7.68 (d, *J* = 8.5 Hz, 1H), 7.58 (d, *J* = 1.8 Hz, 1H), 7.55 (d, *J* = 8.5 Hz, 2H), 7.47 (t, *J* = 8.0 Hz, 1H), 7.39 (d, *J* = 6.3 Hz, 1H), 7.21 (d, *J* = 7.4 Hz, 1H), 6.87 (d, *J* = 8.6 Hz, 2H), 6.57 (d, *J* = 3.0 Hz, 1H), 2.56 (tq, *J* = 6.9, 3.5 Hz, 1H), 0.64 (dt, *J* = 6.9, 3.4 Hz, 2H), 0.43 (dt, *J* = 6.9, 3.5 Hz, 2H). **^{13}C NMR** (126 MHz, DMSO-d_6) δ 156.80, 156.02, 144.63, 143.57, 141.91, 136.27, 135.36, 131.90, 131.47, 130.27, 128.00 (2C), 122.34, 117.02, 116.82, 115.83, 115.75 (2C), 112.41, 110.97, 22.43, 6.44. **HRMS exact mass of** $C_{23}H_{21}N_4O_2$ **(M+H)$^+$:** 385.1659 amu; **found:** 385.1660 amu. **HPLC purity:** 95.24%, **HPLC t_R:** 2.47 min.

4.1.5.8. **1-cyclopropyl-3-{4-[5-(4-hydroxyphenyl)-1*H*-benzimidazol-1-yl]phenyl}urea (28h).** Rf = 0.20 (DCM/MeOH 9.5:0.5). Buff solid, 47% yield, **mp:** 244-246°C. **^{1}H NMR** (501 MHz, DMSO-d_6) δ 9.48 (s, 1H), 8.59 (s, 1H), 8.48 (s, 1H), 7.90 (d, *J* = 1.5 Hz, 1H), 7.65 (d, *J* = 8.9 Hz, 2H), 7.57 (d, *J* = 8.4 Hz, 1H), 7.54 (d, *J* = 2.7 Hz, 2H), 7.53 (s, 1H), 7.53 (d, *J* = 2.7 Hz, 2H), 6.86 (d, *J* = 8.6 Hz, 2H), 6.49 (d, *J* = 2.9 Hz, 1H), 2.57 (dq, *J* = 6.8, 3.2 Hz, 1H), 0.66 (td, *J* = 6.9, 4.8 Hz, 2H), 0.48 – 0.39 (m, 2H). **^{13}C NMR** (126 MHz, DMSO-d_6) δ 156.73, 155.97, 144.40, 143.77, 140.06, 135.14, 132.37, 131.58, 129.17, 127.97 (2C), 124.20 (2C), 122.16, 118.85 (2C), 116.89, 115.73 (2C), 110.80, 22.45, 6.45 (2C). **HRMS exact mass of** $C_{23}H_{21}N_4O_2$ **(M+H)$^+$:** 385.1659 amu; **found:** 385.1661 amu.

4.1.5.9. ***N*-{3-[5-(4-hydroxyphenyl)-1*H*-benzimidazol-1-yl]phenyl}methanesulfonamide (28i).** Rf = 0.40 (DCM/MeOH 9.6:0.4). Buff solid, 19% yield, **mp:** >300°C (decomp.). **^{1}H NMR** (501 MHz, DMSO-d_6) δ 10.13 (s, 1H), 9.51 (s, 1H), 8.60 (s, 1H), 7.94 (d, *J* = 1.8 Hz, 1H), 7.67 (d, *J* = 8.6 Hz, 1H), 7.60 (d, *J* = 8.1 Hz, 2H), 7.56 (s, 1H), 7.55 (s, 1H), 7.53 (t, *J* = 2.1 Hz, 1H), 7.43 (d, *J* = 8.4 Hz, 1H), 7.31 (d, *J* = 7.9 Hz, 1H), 6.87 (d, *J* = 8.6 Hz, 2H), 3.13 (s, 3H). **^{13}C NMR** (126 MHz, DMSO-d_6) δ 156.82, 144.66, 143.62, 140.00, 136.78, 135.51, 131.78, 131.40, 131.11, 128.02 (2C), 122.42, 118.34, 118.13, 117.08, 115.75 (2C), 113.76, 110.90, 48.62. **HRMS exact mass of** $C_{20}H_{18}N_3O_3S$ **(M+H)$^+$:** 380.1063 amu; **found:** 380.1062 amu.

4.1.5.10. ***N*-{4-[5-(4-hydroxyphenyl)-1*H*-benzimidazol-1-yl]phenyl}methanesulfonamide (28j).** Rf = 0.25 (DCM/MeOH 9.7:0.3). White solid, 27% yield, **mp:** 258-261°C. **^{1}H NMR** (400 MHz, DMSO-d_6) δ 10.05 (s, 1H), 9.51 (s, 1H), 8.52 (s, 1H), 7.92 (d, *J* = 1.7 Hz, 1H), 7.68 (d, *J* = 8.8 Hz, 2H), 7.61 (d, *J* = 8.5 Hz, 1H), 7.55 (d, *J* = 2.4 Hz, 2H), 7.53 (s, 1H), 7.44 (d, *J* = 8.8 Hz, 2H), 6.87 (d, *J* = 8.6 Hz, 2H), 3.09 (s, 3H).

4.1.5.11. ***N*-{3-[5-(4-hydroxyphenyl)-1*H*-benzimidazol-1-yl]phenyl}cyclopropanesulfonamide (28k).** Rf = 0.40 (DCM/MeOH 9.7:0.3). Buff solid, 55% yield, **mp:** 268-270°C. **^{1}H NMR** (501 MHz, DMSO-d_6) δ 10.11 (s, 1H), 9.51 (s, 1H), 8.59 (s, 1H), 7.94 (s, 1H), 7.66 (d, *J* = 8.5 Hz, 1H), 7.59 (s, 1H), 7.58 (d, *J* = 12.3 Hz, 2H), 7.55 (s, 2H), 7.43 (d, *J* = 7.9 Hz, 1H), 7.35 (d, *J* = 8.2 Hz, 1H), 6.87 (d, *J* = 8.1 Hz, 2H), 2.80 (p, *J* = 6.4 Hz, 1H), 0.99 (d, *J* = 6.6 Hz, 4H). **^{13}C NMR** (126 MHz, DMSO-d_6) δ 156.82, 144.66, 143.61, 139.99, 136.70, 135.52, 131.77, 131.38, 131.04, 128.01 (2C), 122.45, 118.70, 118.45, 117.09, 115.75 (2C), 114.22, 110.83, 29.78, 5.15 (2C). **HRMS exact mass of** $C_{22}H_{20}N_3O_3S$ **(M+H)$^+$:** 406.1220 amu; **found:** 406.1218 amu. **HPLC purity:** 98.40%, **HPLC t_R:** 2.57 min.

4.1.5.12. ***N*-{4-[5-(4-hydroxyphenyl)-1*H*-benzimidazol-1-yl]phenyl}cyclopropanesulfonamide (28l).** Rf = 0.30 (DCM/MeOH 9.7:0.3). Crystalline buff solid, 50% yield, **mp:** 258-261°C. **^{1}H NMR** (501 MHz, DMSO-d_6) δ 10.04 (s, 1H), 9.49 (s, 1H), 8.52 (s, 1H), 7.92 (d, *J* = 1.7 Hz, 1H), 7.67 (d, *J* = 8.7 Hz, 2H), 7.61 (d, *J* = 8.5 Hz, 1H), 7.55 (d, *J* = 3.4 Hz, 2H), 7.53 (s, 1H), 7.47 (d, *J* = 8.9 Hz, 2H), 6.86 (d, *J* = 8.6 Hz, 2H), 2.72 (t, *J* = 5.6 Hz, 1H), 1.00 (d, *J* = 1.6 Hz, 4H). **^{13}C NMR** (126 MHz, DMSO-d_6) δ 156.77, 144.49, 143.73, 137.87, 135.31, 132.13, 131.67, 131.50, 127.99 (2C), 124.60 (2C), 122.29, 121.19 (2C), 116.95, 115.74 (2C), 110.86, 29.72, 5.09 (2C). **HRMS exact mass of** $C_{22}H_{20}N_3O_3S$ **(M+H)$^+$:** 406.1220 amu; **found:** 406.1220 amu. **HPLC purity:** 97.81%, **HPLC t_R:** 2.52 min.

4.1.5.13. ***N*-{3-[5-(4-hydroxyphenyl)-1*H*-benzimidazol-1-yl]phenyl}formamide (28m).** Rf = 0.30 (DCM/MeOH 9.5:0.5). Buff solid, 67% yield, **mp:** 274-276°C. **^{1}H NMR** (501 MHz, DMSO-d_6) δ 10.52 (s, 1H), 9.51 (s, 1H), 8.58 (d, *J* = 6.7 Hz, 1H), 8.38 (s, 1H), 8.04 (s, 1H), 7.94 (s, 1H), 7.73 – 7.66 (m, 1H), 7.65 (d, *J* = 4.5 Hz, 1H), 7.63 – 7.59 (m, 1H), 7.56 (d, *J* = 8.1 Hz, 2H), 7.55 (s, 1H), 7.41 (d, *J* = 7.8 Hz, 1H), 6.87 (d, *J* = 8.1 Hz, 2H). **^{13}C NMR** (126 MHz, DMSO-d_6) δ 160.16, 156.81, 144.64, 143.61, 139.60, 136.36, 135.47, 131.84, 131.42, 130.69, 128.01 (2C), 122.41, 118.47, 118.09, 117.08, 115.75 (2C), 113.83, 110.85. **HRMS exact mass of** $C_{20}H_{16}N_3O_2$ **(M+H)$^+$:** 330.1237 amu; **found:** 330.1235 amu. **HPLC purity:** 96.76%, **HPLC t_R:** 2.23 min.

4.1.5.14. ***N*-{4-[5-(4-hydroxyphenyl)-1*H*-benzimidazol-1-yl]phenyl}formamide (28n).** Rf = 0.25 (DCM/MeOH 9.5:0.5). Light brown solid, 64% yield, **mp:** >300°C (decomp.). **^{1}H NMR** (501 MHz, DMSO-d_6) δ 10.46 (d, *J* = 2.0 Hz, 1H), 9.49 (s, 1H), 8.52 (s,

1H), 8.36 (d, *J* = 1.8 Hz, 1H), 7.92 (s, 1H), 7.84 (d, *J* = 8.8 Hz, 2H), 7.66 (d, *J* = 8.8 Hz, 2H), 7.61 (d, *J* = 8.5 Hz, 1H), 7.55 (d, *J* = 1.8 Hz, 2H), 7.53 (s, 1H), 6.86 (d, *J* = 8.6 Hz, 2H). **^{13}C NMR** (126 MHz, DMSO-d_6) δ 159.89, 156.76, 144.48, 143.73, 137.70, 135.28, 132.15, 131.51, 127.98 (2C), 124.28 (2C), 122.27, 120.37 (2C), 118.56, 116.94, 115.74 (2C), 110.85. **HRMS exact mass of** $C_{20}H_{16}N_3O_2$ **$(M+H)^+$:** 330.1237 amu; **found:** 330.1237 amu. **HPLC purity:** 98.71%, **HPLC t_R:** 2.16 min.

4.2 Pharmacological/biological assays

4.2.1. In vitro kinase assays

In vitro kinase enzyme assays were conducted at ThermoFisher Scientific (USA) using SelectScreen™ biochemical kinase profiling service. The enzyme assays for wild-type FLT3, FLT-TKD (D835Y mutation), KIT, ABL1, BRAF, CSF1R (FMS), FGFR3, FLT1 (VEGFR1), FLT4 (VEGFR3), IGF1R, KDR (VEGFR2), LCK, PDGFRA (PDGFR alpha), PDGFRB (PDGFR beta), RET, and SRC were performed according to the Z′-LYTE™ screening protocol and assay conditions provided by ThermoFisher Scientific (USA). Most kinase assays were conducted using the apparent Km for ATP previously determined using the Z´-LYTE assay as the ATP concentration. Exceptions include BRAF and KIT, which were assayed at 100 µM ATP, and wild-type FLT3 and FLT-TKD (D835Y mutation), which were assayed at 10 µM ATP. The FLT3-ITD enzyme assay was performed according to LanthaScreen™ Eu kinase binding assay screening protocol. Gilteritinib (Catalog. No. HY-12432) and quizartinib (Catalog. No. HY-13001) were purchased from Insight Biotechnology (UK).

4.2.2. Human cancer cell lines and cell culture

The FLT3-ITD positive patient derived AML cell lines MOLM-14 and MV4-11 were a gift from Dr. Scott Kogan (University of California, San Francisco). MOLM-14-F691L and MOLM-14-D835Y cells lines were generated by culturing parental MOLM-14 cells in media containing increasing doses of quizartinib (0.5 nM to 20 nM). Resistant cells were subcloned and Sanger sequencing performed to demonstrate that some of the clones had acquired secondary mutations within FLT3 at the F691 and D835 residues, respectively. The FLT3-ITD negative patient derived AML cell line HL-60 and patient derived CML cell line K-562 were purchased from ATCC (VA, USA). All cell lines were cultured in RPMI-1640 (Gibco, MA, USA) with 10% FBS and 1% penicillin/streptomycin/glutamine (Gibco, MA, USA). Cells were incubated at 37°C in a humidified atmosphere of 5% CO_2. Experiments were performed within 2 months of cell line thawing. Cell line authentication was performed at the University of California, Berkeley, DNA Sequencing Facility using short tandem repeat DNA profiling.

4.2.3. Cell viability assay

MOLM-14, MV4-11, MOLM-14-F691L, MOLM-14-D835Y, K-562, and HL-60 cells were plated in triplicate into 96 well plates at 1x10^5 cells/mL and exposed to 7 doses of the inhibitors (0.01 nM, 0.1 nM, 1 nM, 10 nM, 100 nM, 1 µM, and 10 µM), as well as DMSO vehicle control, at 37°C. After 48 hours, CellTiter-Glo Luminescent Cell Viability reagent (Promega, WI, USA) was added to each well and luminescence measured on a SpectraMax iD3 spectrophotometer (Molecular Devices, CA, USA). The percentage of growth for drug-treated cells versus DMSO-treated cells was calculated for each dose and graphed. IC_{50} values were calculated using a four-parameter logistics regression model (https://www.aatbio.com/tools/ic50-calculator). Each experiment was performed three times and the mean IC_{50} values and standard deviations calculated.

4.2.4. Immunoblot analysis

MOLM-14 and MOLM-14-D835Y cells, at 5x10^5 cells/mL, were exposed to compound **22b** or gilteritinib for 2 hours at 37°C at different concentrations (0, 5, 10, 20, 40, 80, and 160 nM). Cells were washed in PBS and lysed in buffer (50 mM HEPES, pH 7.4, 10% glycerol, 150 mM NaCl, 1% Triton X-100, 1 mM EDTA, 1 mM EGTA, and 1.5 mM $MgCl_2$) supplemented with protease and phosphatase inhibitors. The lysate was clarified by centrifugation, quantitated by BCA assay (Thermo Scientific, MA, USA), and

normalized to a concentration of 2 µg/µl. 30 µl of total cell lysates (60 µg) were resolved by SDS-polyacrylamide gel electrophoresis and transferred to nitrocellulose membranes. The membranes were then probed with primary antibodies purchased from Cell Signaling Technologies (MA, USA) [pFLT3 Y842 (#4577), FLT3 (#3462), pERK 1/2 T202/Y204 (#4370), ERK 1/2 (#9107), pSTAT5 Y694 (#9351), STAT5 (#9363), pS6 S235/236 (#2211), S6 (#2317), and GAPDH (#5174)] followed by secondary antibodies purchased from Licor (NE, USA). Immunoblots were then visualized by a Biorad ChemiDoc MP Imaging System (CA, USA). Each drug treatment and western blot experiment was performed three times.

4.2.5. Cell cycle analysis

MOLM-14 and MOLM-14-D835Y cells, at $2x10^5$ cells/mL, were exposed to compound **22b** or gilteritinib at 37°C at different concentrations (0, 5, 10, 20, 40, 80, and 160 nM). After 48 hours, $1x10^6$ cells were fixed in 4% paraformaldehyde for 10 minutes at room temperature, washed in cold 1X PBS, permeabilized with ice cold 100% methanol and stored at -20°C until further processing. Cells were washed with cold 1X PBS and then rehydrated in FACs Buffer (1X PBS + 4% FBS) overnight at 4°C. Cells were pelleted down and incubated in DAPI staining buffer (1X PBS + 1 µg/mL DAPI) for 30 minutes at room temperature then placed on ice in the dark until analyzed on a Becton Dickinson LSRFortessa flow cytometer (NJ, USA). The FCS files from the flow cytometer were then analyzed with FlowJo (OR, USA) using their Watson Pragmatic univariate cell cycle algorithm. Each drug treatment and flow cytometry experiment were performed three times.

4.2.6. Apoptosis assay

MOLM-14 and MOLM-14-D835Y cells, at $2x10^5$ cells/mL, were exposed to compound **22b** or gilteritinib at 37°C at different concentrations (0, 5, 10, 20, 40, 80, and 160 nM). After 48 hours, $1x10^6$ cells were fixed, permeabilized and rehydrated as described above. Cells were then pelleted down and incubated in FACs Buffer (1X PBS + 4% FBS) containing 0.5 µg Mouse BD Fc Block (#553142, BD Pharmingen, CA, USA) for 10 minutes at room temperature to prevent non-specific antibody binding. The cells were then incubated with FITC-conjugated anti-cleaved caspase 3 antibody (#559341, BD Pharmingen, CA, USA) for 60 minutes on ice in the dark. Cells were then washed with cold 1X PBS and placed on ice in the dark until analyzed on a Becton Dickinson LSRFortessa flow cytometer (NJ, USA). The FCS files from the flow cytometer were then analyzed with FlowJo (OR, USA) to determine the percentage of cells negative for cleaved-caspase 3 (live cells) under each condition. Each drug treatment and flow cytometry experiment were performed three times.

4.2.7. Statistical Analysis

All data were derived based on three independent experiments, unless stated otherwise. Student's two tailed t-test was used to calculate p-values and values less than 0.05 were considered significant.

4.3 Molecular modeling

4.3.1. Homology modeling

The homology model was developed using MODELLER software [60] through Discovery Studio® (version 2.5, Accelrys, Inc., San Diego, CA) with a medium-level optimization for the loop. NCBI NP_004110.2 reference sequence was chosen as a target sequence for FLT3 model. NCBI protein-BLAST tool[61] was used to identify a template sequence. Online quality evaluation tools, including SWISSMODEL[62] and MolProbity[63] were used to evaluate the model's quality. The D835Y mutant model was built by mutating aspartate residue to tyrosine using Dunbrack backbone-dependent rotamer library[64] implemented through UCSF Chimera 1.17.3.[65]

4.3.2. Molecular docking

Molecular docking of **4ACP** and **22b** was performed using Discovery Studio® CDOCKER protocol (version 2.5, Accelrys, Inc., San Diego, CA). The standard protein preparation procedure integrated in Accelry's Discovery Studio 2.5 was used for protein preparation step, which involved adding hydrogen atoms, calculating atomic charges, and assigning CHARMM force field parameters. The ligand was drawn using the sketching tools of Accelry's Discovery Studio. Then, it was prepared for docking by adding hydrogen atoms and partial charges using the Momany-Rone method. The binding site was defined by the residues within 10 Å distance from the co-crystallized ligand.

4.3.3. Molecular dynamics

GROMACS 2020.3 was used for molecular dynamics simulations and systems build up.[66] Each protein/protein-ligand complex was solvated in a dodecahedron box using the TIP3P explicit water model.[67] The system was then neutralized by NaCl molecules at 0.1 M concentration. Energy minimization for the system was carried out using the steepest descent algorithm setting 10 kJ/mol and 50,000 steps as convergence criteria. An NVT equilibration step followed by NPT equilibration were performed for 500 ps each at 300 K temperature and 1 atm pressure. Then, a production run was carried out for 100 ns at the NPT ensemble. Temperature coupling was implemented using the V-rescale modified Berendsen thermostat[68] for equilibration and production runs, while pressure coupling was done using the Berendsen coupling[69] and Parrinello-Rahman pressure coupling scheme[70] with 2 ps time constant for equilibration and production runs, respectively. A Verlet cutoff-scheme was used for searching neighboring atoms and Van Der Waals calculations with cutoff and switch list distances of 1.2 and 1.0 nm, respectively. Particle Mesh Ewald method[71] was used for the calculations of long-range electrostatics within 1.2 nm. Bond lengths were constrained using the LINear Constraint Solver (LINCS) algorithm.[72] CHARMM36 all-atom force field (July 2017)[73] was used for topology generation and parameter set of the protein molecules, and SwissParam server[74] was used for ligand parameterization and topology generation. Leap-frog integrator was used with a steps size of 2 fs for all simulations. Protein RMSD, RMSF and radius of gyration was calculated out using ProDy python library,[75,76] while ligand RMSD and hydrogen bonds were calculated using VMD RMSD trajectory analysis tool.[77] Covariance matrix calculation and eigenvector analysis of the principal component analysis were done using *gmx covar* and *gmx anaeig* tools of GROMACS, respectively. All analysis charts were constructed using Matplotlib python plotting library.[78] The protein-ligand figures were generated using UCSF Chimera 1.17.3.[65] The trajectory movies were generated using the gromacs *anaeig* tool and rendered using PyMOL (v 0.99rc6).

ACKNOWLEDGEMENTS

AKA was awarded a fellowship from Fondazione IEO-CCM. SNM has been awarded a PhD scholarship at University of Leeds funded by the Newton-Mosharafa Fund jointly offered by the British Council and the Ministry of Higher Education of the Arab Republic of Egypt. We thank Dr Jeanine Williams (School of Chemistry, University of Leeds) for conducting the HPLC purity determination assays. We would like to gratefully acknowledge the support of NVIDIA Corporation with the donation of the Titan Xp GPU used for molecular dynamics calculations.

CONFLICT OF INTEREST

The authors declare no competing financial interest.

SUPPLEMENTARY MATERIAL

Supplementary data to this article can be found online at https://doi.org/xxxxxxx.

REFERENCES

[1] I. De Kouchkovsky, M. Abdul-Hay, *Blood Cancer Journal* **2016**, *6*, e441–e441.
[2] Y. Zhou, G. Huang, X. Cai, Y. Liu, B. Qian, D. Li, *Biomarker Research* **2024**, *12*, 101.
[3] "Acute Myeloid Leukemia — Cancer Stat Facts," can be found under https://seer.cancer.gov/statfacts/html/amyl.html.

[4] R. V. de Morais, M. V. de Souza, K. A. de S. Silva, P. Santiago, M. C. Lorenzoni, C. F. Lorea, C. G. de C. Junior, A. N. R. Taniguchi, F. F. Scherer, M. B. Michalowski, L. E. Daudt, *J Pediatr (Rio J)* **2020**, *97*, 204–210.
[5] R. L. Siegel, K. D. Miller, N. S. Wagle, A. Jemal, *CA: A Cancer Journal for Clinicians* **2023**, *73*, 17–48.
[6] A. Forsythe, K. Sandman, *J Blood Med* **2021**, *12*, 245–255.
[7] V. Marensi, K. R. Keeshan, D. J. MacEwan, *Biochem Pharmacol* **2021**, *183*, 114348.
[8] N. Daver, R. F. Schlenk, N. H. Russell, M. J. Levis, *Leukemia* **2019**, *33*, 299–312.
[9] H. Kiyoi, N. Kawashima, Y. Ishikawa, *Cancer Sci* **2020**, *111*, 312–322.
[10] V. E. Kennedy, C. C. Smith, *Front Oncol* **2020**, *10*, 612880.
[11] A. I. Antar, Z. K. Otrock, E. Jabbour, M. Mohty, A. Bazarbachi, *Leukemia* **2020**, *34*, 682–696.
[12] Y. Zhong, R.-Z. Qiu, S.-L. Sun, C. Zhao, T.-Y. Fan, M. Chen, N.-G. Li, Z.-H. Shi, *J Med Chem* **2020**, *63*, 12403–12428.
[13] L. Tong, X. Li, Y. Hu, T. Liu, *Future Med Chem* **2020**, *12*, 961–981.
[14] Z. Wang, J. Cai, J. Cheng, W. Yang, Y. Zhu, H. Li, T. Lu, Y. Chen, S. Lu, *J Med Chem* **2021**, *64*, 2878–2900.
[15] B. Acharya, D. Saha, D. Armstrong, N. R. Lakkaniga, B. Frett, *RSC Med. Chem.* **2022**, *13*, 798–816.
[16] C. Negotei, A. Colita, I. Mitu, A. R. Lupu, M.-E. Lapadat, C. E. Popovici, M. Crainicu, O. Stanca, N. M. Berbec, *J Clin Med* **2023**, *12*, 6429.
[17] A. K. Abdel-Aziz, E. M. E. Dokla, M. K. Saadeldin, *Critical Reviews in Oncology/Hematology* **2023**, *191*, 104139.
[18] N. Alaa El-Deen, E. M. E. Dokla, M. Y. Jaballah, K. Abouzid, R. A. Serya, *Egyptian Journal of Chemistry* **2023**, *67*, 529–553.
[19] D. Capelli, D. Menotti, A. Fiorentini, F. Saraceni, A. Olivieri, *Cancers (Basel)* **2022**, *14*, 4315.
[20] G. Ghiaur, M. Levis, *Hematol Oncol Clin North Am* **2017**, *31*, 681–692.
[21] T. J. L. Lang, F. Damm, L. Bullinger, M. Frick, *Cancers (Basel)* **2023**, *15*, 4573.
[22] E. M. E. Dokla, A. K. Abdel-Aziz, S. N. Milik, M. J. McPhillie, S. Minucci, K. A. M. Abouzid, *Bioorg Med Chem* **2022**, *56*, 116596.
[23] A. A. Warkentin, M. S. Lopez, E. A. Lasater, K. Lin, B.-L. He, A. Y. Leung, C. C. Smith, N. P. Shah, K. M. Shokat, *Elife* **2014**, *3*, e03445.
[24] T. Aikawa, N. Togashi, K. Iwanaga, H. Okada, Y. Nishiya, S. Inoue, M. J. Levis, T. Isoyama, *Oncotarget* **2020**, *11*, 943–955.
[25] L. Fletcher, S. K. Joshi, E. Traer, *Cancer Manag Res* **2020**, *12*, 151–163.
[26] A. Galanis, M. Levis, *Haematologica* **2015**, *100*, e77–e79.
[27] L. N. Johnson, *Quarterly Reviews of Biophysics* **2009**, *42*, 1–40.
[28] R. M. Miller, J. Taunton, *Methods Enzymol* **2014**, *548*, 93–116.
[29] P. Wu, T. E. Nielsen, M. H. Clausen, *Trends Pharmacol Sci* **2015**, *36*, 422–439.
[30] R. Roskoski, *Pharmacol Res* **2016**, *103*, 26–48.
[31] Y. Chen, Y. Pan, Y. Guo, W. Zhao, W. T. Ho, J. Wang, M. Xu, F.-C. Yang, Z. J. Zhao, *Stem Cell Investigation* **2017**, *4*, 48.
[32] L. M. Jones, K. Melgar, L. Bolanos, K. Hueneman, M. M. Walker, J.-K. Jiang, K. M. Wilson, X. Zhang, J. Shen, F. Jiang, P. Sutter, A. Wang, X. Xu, G. J. Tawa, S. B. Hoyt, M. Wunderlich, E. O'Brien, J. P. Perentesis, D. T. Starczynowski, C. J. Thomas, *J Clin Invest* **n.d.**, *130*, 2017–2023.
[33] J.-S. Ahn, H.-J. Kim, *Blood Res* **2022**, *57*, 32–36.
[34] A. Galanis, M. Levis, *Blood* **2013**, *122*, 3846–3846.
[35] D. Capelli, D. Menotti, A. Fiorentini, F. Saraceni, A. Olivieri, *Cancers* **2022**, *14*, 4315.
[36] M. Ruglioni, S. Crucitta, G. I. Luculli, G. Tancredi, M. L. Del Giudice, S. Mechelli, S. Galimberti, R. Danesi, M. Del Re, *Critical Reviews in Oncology/Hematology* **2024**, *201*, 104424.
[37] C. Choudhary, C. Brandts, J. Schwable, L. Tickenbrock, B. Sargin, A. Ueker, F.-D. Böhmer, W. E. Berdel, C. Müller-Tidow, H. Serve, *Blood* **2007**, *110*, 370–374.
[38] L. S. Steelman, S. L. Abrams, J. Whelan, F. E. Bertrand, D. E. Ludwig, J. Bäsecke, M. Libra, F. Stivala, M. Milella, A. Tafuri, P. Lunghi, A. Bonati, A. M. Martelli, J. A. McCubrey, *Leukemia* **2008**, *22*, 686–707.
[39] Y.-J. Guo, W.-W. Pan, S.-B. Liu, Z.-F. Shen, Y. Xu, L.-L. Hu, *Exp Ther Med* **2020**, *19*, 1997–2007.
[40] K. Okada, A. Nogami, S. Ishida, H. Akiyama, C. Chen, Y. Umezawa, O. Miura, *Oncotarget* **2017**, *9*, 8870–8886.
[41] R. Kraaijvanger, K. Seldenrijk, E. Beijer, J. Damen, J. L. Wilson, T. Weichhart, J. C. Grutters, M. Veltkamp, *Cells* **2021**, *10*, 3545.
[42] P. P. Zarrinkar, R. N. Gunawardane, M. D. Cramer, M. F. Gardner, D. Brigham, B. Belli, M. W. Karaman, K. W. Pratz, G. Pallares, Q. Chao, K. G. Sprankle, H. K. Patel, M. Levis, R. C. Armstrong, J. James, S. S. Bhagwat, *Blood* **2009**, *114*, 2984–2992.
[43] C. Busch, T. Mulholland, M. Zagnoni, M. Dalby, C. Berry, H. Wheadon, *Cell Commun Signal* **2023**, *21*, 342.
[44] T.-A.-T. Phan, K.-K.-H. Ngo, T.-C.-T. Nguyen, T.-T. Mai, H.-D. Nguyen, T.-T. Duong, L.-P. Tran, T.-T. Duong, T.-K.-C. Huynh, E. V. Koroleva, Z. V. Ignatovich, A. L. Ermolinskaya, H.-P. Nguyen, T.-H.-A. Nguyen, A.-K. Ton, T.-H. Do, T.-K.-D. Hoang, *RSC Adv* **2025**, *15*, 4458–4471.
[45] Y.-Y. Ke, V. K. Singh, M. S. Coumar, Y. C. Hsu, W.-C. Wang, J.-S. Song, C.-H. Chen, W.-H. Lin, S.-H. Wu, J. T. A. Hsu, C. Shih, H.-P. Hsieh, *Scientific Reports* **2015**, *5*, 11702.
[46] V. Modi, R. L. Dunbrack, *Proceedings of the National Academy of Sciences* **2019**, *116*, 6818–6827.
[47] Y. K. Yoon, M. A. Ali, A. C. Wei, T. S. Choon, R. Ismail, *European Journal of Medicinal Chemistry* **2015**, *93*, 614–624.
[48] A. Shaukat, H. M. Mirza, A. H. Ansari, M. Yasinzai, S. Z. Zaidi, S. Dilshad, F. L. Ansari, *Med Chem Res* **2013**, *22*, 3606–3620.
[49] C. Kim, K. Lee, G. Lee, T. Jin, Y.-H. Lee, J.-H. Ryou, J. Brenneman, S. U. Kang, *N2-Phenylpyrimidine-2,4-Diamine Compounds, and Preparation Methods and Methods of Use Thereof*, **2022**, WO2022208454A1.
[50] E. M. E. Dokla, N. S. Abutaleb, S. N. Milik, E. A. E. A. Kandil, O. M. Qassem, Y. Elgammal, M. Nasr, M. J. McPhillie, K. A. M. Abouzid, M. N. Seleem, P. Imming, M. Adel, *Eur J Med Chem* **2023**, *247*, 115040.
[51] E. M. E. Dokla, N. S. Abutaleb, S. N. Milik, D. Li, K. El-Baz, M.-A. W. Shalaby, R. Al-Karaki, M. Nasr, C. D. Klein, K. A. M. Abouzid, M. N. Seleem, *European Journal of Medicinal Chemistry* **2020**, *186*, 111850.
[52] A. P. Patel, M. M. Shaikh, K. K. Gurjar, K. H. Chikhalia, *Res Chem Intermed* **2021**, *47*, 2049–2061.
[53] A. K. Chakraborti, S. V. Chankeshwara, *J Org Chem* **2009**, *74*, 1367–1370.
[54] R. D. Hamprecht, A. D. Hartmann, E. D. Klauke, I. D. Hammann, H. P. D. Roessler, W. Brandes, *1-Arylamino-2,4-Dinitronaphthaline, Verfahren Zu Ihrer Herstellung Sowie Ihre Verwendung Als Schaedlingsbekaempfungsmittel*, **1978**, DE2708440A1.
[55] N. Vicker, X. Su, D. Ganeshapillai, A. Purohit, M. J. Reed, B. V. L. Potter, *Inhibitors of 11-Beta-Hydroxy Steroid Dehydrogenase Type 1 and Type 2*, **2004**, WO2004037251A1.

[56] D. Valdez-Padilla, S. Rodríguez-Morales, A. Hernández-Campos, F. Hernández-Luis, L. Yépez-Mulia, A. Tapia-Contreras, R. Castillo, *Bioorganic & Medicinal Chemistry* **2009**, *17*, 1724–1730.
[57] S. N. Milik, A. K. Abdel-Aziz, D. S. Lasheen, R. A. T. Serya, S. Minucci, K. A. M. Abouzid, *European Journal of Medicinal Chemistry* **2018**, *155*, 316–336.
[58] E. M. E. Dokla, A. K. Abdel-Aziz, S. N. Milik, A. H. Mahmoud, M. K. Saadeldin, M. J. McPhillie, S. Minucci, K. A. M. Abouzid, *Bioorg Chem* **2021**, *117*, 105451.
[59] Z. Chen, G. Liu, S. Pu, S. H. Liu, *Dyes and Pigments* **2017**, *143*, 409–415.
[60] A. Šali, T. L. Blundell, *Journal of Molecular Biology* **1993**, *234*, 779–815.
[61] E. W. Sayers, E. E. Bolton, J. R. Brister, K. Canese, J. Chan, D. C. Comeau, R. Connor, K. Funk, C. Kelly, S. Kim, T. Madej, A. Marchler-Bauer, C. Lanczycki, S. Lathrop, Z. Lu, F. Thibaud-Nissen, T. Murphy, L. Phan, Y. Skripchenko, T. Tse, J. Wang, R. Williams, B. W. Trawick, K. D. Pruitt, S. T. Sherry, *Nucleic Acids Research* **2022**, *50*, D20–D26.
[62] A. M. Waterhouse, G. Studer, X. Robin, S. Bienert, G. Tauriello, T. Schwede, *Nucleic Acids Research* **2024**, *52*, W318–W323.
[63] C. J. Williams, J. J. Headd, N. W. Moriarty, M. G. Prisant, L. L. Videau, L. N. Deis, V. Verma, D. A. Keedy, B. J. Hintze, V. B. Chen, S. Jain, S. M. Lewis, W. B. Arendall III, J. Snoeyink, P. D. Adams, S. C. Lovell, J. S. Richardson, D. C. Richardson, *Protein Science* **2018**, *27*, 293–315.
[64] M. V. Shapovalov, R. L. Dunbrack, *Structure* **2011**, *19*, 844–858.
[65] E. F. Pettersen, T. D. Goddard, C. C. Huang, G. S. Couch, D. M. Greenblatt, E. C. Meng, T. E. Ferrin, *Journal of Computational Chemistry* **2004**, *25*, 1605–1612.
[66] M. J. Abraham, T. Murtola, R. Schulz, S. Páll, J. C. Smith, B. Hess, E. Lindahl, *SoftwareX* **2015**, *1–2*, 19–25.
[67] P. Mark, L. Nilsson, *J. Phys. Chem. A* **2001**, *105*, 9954–9960.
[68] G. Bussi, D. Donadio, M. Parrinello, *The Journal of Chemical Physics* **2007**, *126*, 014101.
[69] H. J. C. Berendsen, J. P. M. Postma, W. F. van Gunsteren, A. DiNola, J. R. Haak, *The Journal of Chemical Physics* **1984**, *81*, 3684–3690.
[70] M. Parrinello, A. Rahman, *Journal of Applied Physics* **1981**, *52*, 7182–7190.
[71] T. Darden, D. York, L. Pedersen, *The Journal of Chemical Physics* **1993**, *98*, 10089–10092.
[72] B. Hess, H. Bekker, H. J. C. Berendsen, J. G. E. M. Fraaije, *Journal of Computational Chemistry* **1997**, *18*, 1463–1472.
[73] J. Huang, A. D. MacKerell Jr, *Journal of Computational Chemistry* **2013**, *34*, 2135–2145.
[74] V. Zoete, M. A. Cuendet, A. Grosdidier, O. Michielin, *Journal of Computational Chemistry* **2011**, *32*, 2359–2368.
[75] A. Bakan, L. M. Meireles, I. Bahar, *Bioinformatics* **2011**, *27*, 1575–1577.
[76] A. Bakan, A. Dutta, W. Mao, Y. Liu, C. Chennubhotla, T. R. Lezon, I. Bahar, *Bioinformatics* **2014**, *30*, 2681–2683.
[77] W. Humphrey, A. Dalke, K. Schulten, *Journal of Molecular Graphics* **1996**, *14*, 33–38.
[78] J. D. Hunter, *Computing in Science & Engineering* **2007**, *9*, 90–95.

Entry for the Table of Contents

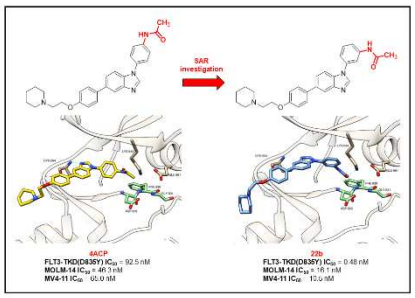

Acute myeloid leukemia (AML), often driven by FLT3 mutations, has poor survival rates. We developed a benzimidazole-based FLT3 inhibitor, **4ACP**, and synthesized 36 derivatives. Compound **22b** exhibited sub-nanomolar activity against FLT3-TKD(D835Y) mutants and showed preferential cytotoxicity towards FLT3-dependent AML cells. It induced FLT3 inhibition, cell cycle arrest, and apoptosis at low nanomolar concentrations, demonstrating high selectivity and potential for further development.